

Eastern Kentucky University

Encompass

Online Theses and Dissertations

Student Scholarship

January 2020

Structural Investigation On The Thermal Degradation Of Aqueous Amines In Post-Combustion Co₂ Capture

Jeffrey Alexander Laub
Eastern Kentucky University

Follow this and additional works at: <https://encompass.eku.edu/etd>

 Part of the [Physical Chemistry Commons](#)

Recommended Citation

Laub, Jeffrey Alexander, "Structural Investigation On The Thermal Degradation Of Aqueous Amines In Post-Combustion Co₂ Capture" (2020). *Online Theses and Dissertations*. 663.
<https://encompass.eku.edu/etd/663>

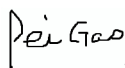
This Open Access Thesis is brought to you for free and open access by the Student Scholarship at Encompass. It has been accepted for inclusion in Online Theses and Dissertations by an authorized administrator of Encompass. For more information, please contact Linda.Sizemore@eku.edu.

STRUCTURAL INVESTIGATION ON THE THERMAL DEGRADATION OF AQUEOUS AMINES
IN POST-COMBUSTION CO₂ CAPTURE

BY

JEFFREY ALEXANDER LAUB

THESIS APPROVED:




Chair, Advisory Committee



Member, Advisory Committee



Member, Advisory Committee



Dean, Graduate School

STATEMENT OF PERMISSION TO USE

In presenting this thesis in partial fulfillment of the requirements for a Master of Science degree at Eastern Kentucky University, I agree that the Library shall make it available to borrowers under rules of the Library. Brief quotations from this document are allowable without special permission, provided that accurate acknowledgements of the source are made. Permission for extensive quotation from or reproduction of this document may be granted by my major professor. In [his/her] absence, by the Head of Interlibrary Services when, in the opinion of either, the proposed use of the material is for scholarly purposes. Any copying or use of the material in this document for financial gain shall not be allowed without my written permission.

Signature:

X 

Date: 4/8/2020

STRUCTURAL INVESTIGATION ON THE THERMAL DEGRADATION OF AQUEOUS AMINES
IN POST-COMBUSTION CO₂ CAPTURE

BY

JEFFREY ALEXANDER LAUB

Submitted to the Faculty of the Graduate School of
Eastern Kentucky University
in partial fulfillment of the requirements for the degree of

MASTER OF SCIENCE

2020

© Copyright by JEFFREY ALEXANDER LAUB 2020
All Rights Reserved.

DEDICATION

In loving memory of my grandparents, Silas Young Jr. and Carolyn Stidham Young.

ACKNOWLEDGEMENTS

First, I would like to recognize and thank Dr. Jeffrey W. Laub (my father) and Lynn Dillard from Central Virginia Community College for their assistance with repairing the metal containment vessels used for this research.

To the Eastern Kentucky University's Department of Chemistry for use of facilities, access to instrumentation, and for providing chemicals used for this research. Also, to Mary Lamar for ordering and delivering the chemicals.

To Dr. Judy Jenkins and Joseph Bequette for their assistance with the operation of the JEOL ECS-400 nuclear magnetic resonance (NMR) instrument.

To Dr. Pei Gao (research advisor), Dr. Buchang Shi (committee member), and Dr. Donghui Quan (committee member) for their consistent support and encouragement throughout the duration of this research. A special thanks to Dr. Pei Gao for the opportunity to perform this research and for the constant support, dedication, and time spent to help ensure the research was accomplished and to answer or solve any questions or problems that arose.

Finally, I would like to thank my parents for their constant support and encouragement throughout my time at Eastern Kentucky University, especially during the performance of this research.

ABSTRACT

One of the major issues concerning the increase in global temperature is with the elevating levels of CO₂ in the atmosphere. Combustion of fossil fuels in power plants is a leading contributor to the elevated anthropogenic CO₂ concentration. To help alleviate this issue, the investigation of aqueous amines being implemented for the capture of CO₂ in the post-combustion carbon capture (PCCC) in power plants has been a growing interest to chemists. One of the concerns with aqueous amines, is their ability to thermally degrade. Thermal degradation is a prominent aspect for the loss of aqueous amines during the stripper process in powerplants. The focus of this research was to investigate the structural effect on the thermal degradation of aqueous amines. The method for this investigation involved the degradation of a 30 wt% amine solution loaded with a 0.4 ratio of moles CO₂/moles of amine, over a one-week span at 125, 135, and 145°C. After which, the degraded species were analyzed using high-performance liquid chromatography (HPLC) and nuclear magnetic resonance (NMR). A computational analysis using the B3LYP functional for the thermodynamics of CO₂ binding to aqueous amines was attempted and compared to the results acquired from HPLC and NMR experimentation to help quantify the favorability of thermal degradation based on the structure of certain amines.

TABLE OF CONTENTS

| | |
|---|----|
| Chapter 1. Introduction | 1 |
| 1.1 Climate Change and the Greenhouse Effect..... | 1 |
| 1.2 CO ₂ as a Direct Indicator of the Greenhouse Effect | 3 |
| 1.3 Sequestering of Post-Combustion CO ₂ using Aqueous Amines..... | 5 |
| 1.4 Aqueous Amines and CO ₂ Absorption | 7 |
| 1.4.1 Primary and Secondary Amines..... | 8 |
| 1.4.2 Tertiary Amines..... | 11 |
| 1.5 Thermal Degradation of Aqueous Amines..... | 13 |
| 1.6 Research Objectives..... | 18 |
| Chapter 2. Experimental Methods and Computational Details | 19 |
| 2.1 Aqueous Amines Chosen for Study..... | 19 |
| 2.2 Thermal Degradation | 20 |
| 2.2.1 Sample Preparation | 20 |
| 2.2.2 Thermal Degradation of Prepared Samples..... | 21 |
| 2.3 Nuclear Magnetic Resonance (NMR)..... | 23 |
| 2.3.1 Sample Preparation | 23 |
| 2.3.2 Analysis | 24 |
| 2.3.3 Theory | 25 |
| 2.3.4 Objectives..... | 27 |
| 2.4 High-Performance Liquid Chromatography (HPLC) | 28 |
| 2.4.1 Dilutions | 28 |

| | |
|--|----|
| 2.4.2 Analysis | 30 |
| 2.4.3 Theory | 31 |
| 2.4.4 Objectives..... | 33 |
| 2.5 Computational Details | 33 |
| 2.5.1 Avogadro and the Universal Force Field | 33 |
| 2.5.2 Gaussian 09 with GaussView | 37 |
| 2.5.3 DFT, B3LYP, Basis Set, and Thermochemistry in Gaussian 09 | 38 |
| 2.5.4 Objectives..... | 40 |
| Chapter 3. Degraded Solutions and NMR Evaluation | 42 |
| 3.1 Thermal Degradation Solution Appearances and Descriptions..... | 42 |
| 3.1.1 Sample Appearances..... | 42 |
| 3.1.2 Sample Descriptions | 43 |
| 3.2 NMR Analysis | 46 |
| 3.2.1 Overview | 46 |
| 3.2.2 ¹ H and ¹³ C analysis | 46 |
| 3.3 Summary of Key Results..... | 51 |
| Chapter 4. HPLC Concentrations of Each Amine and Kinetics Study on MEA, MDEA, and PZ..... | 53 |
| 4.1 Introduction | 53 |
| 4.2 Experimental..... | 53 |
| 4.2.1 Monoethanolamine | 53 |
| 4.2.2 1-Amino-2-propanol | 56 |

| | |
|---|----|
| 4.2.3 Ethylenediamine | 58 |
| 4.2.4 (3-aminopropyl)trimethoxysilane | 60 |
| 4.2.5 2-(Butylamino)ethanol..... | 63 |
| 4.2.6 Methyldiethanolamine | 67 |
| 4.2.7 Piperazine..... | 71 |
| 4.3 Thermal Degradation Activation Energy..... | 73 |
| 4.3.1 Monoethanolamine | 74 |
| 4.3.2 Methyldiethanolamine | 76 |
| 4.3.3 Piperazine..... | 77 |
| 4.4 Conclusions | 78 |
| Chapter 5. Computational Investigation..... | 80 |
| 5.1 Introduction | 80 |
| 5.2 Computational Analysis | 81 |
| 5.2.1 Computational Results..... | 81 |
| 5.3 Conclusions from Computational Results..... | 81 |
| Chapter 6. Theoretical Degradation Products and Reaction Pathways | 83 |
| 6.1 Introduction | 83 |
| 6.2 Theoretical Thermal Degradation Reaction Pathways | 84 |
| 6.2.1 1-Amino-2-propanol | 84 |
| 6.2.2 Ethylenediamine | 85 |
| 6.2.3 (3-aminopropyl)trimethoxysilane | 87 |
| 6.2.4 2-(Butylamino)ethanol..... | 88 |

| | |
|--|-----|
| 6.2.5 Methyldiethanolamine | 89 |
| 6.3 Conclusions | 90 |
| Chapter 7. Conclusions and Future Directions | 91 |
| 7.1 Summary of Key Results from this Study..... | 91 |
| 7.2 Future Directions | 94 |
| References | 96 |
| Appendix A. NMR Spectra for MEA | 101 |
| Appendix B. NMR Spectra for 1A2P..... | 103 |
| Appendix C. NMR Spectra for EN..... | 105 |
| Appendix D. NMR Spectra for 3APT..... | 108 |
| Appendix E. NMR Spectra for 2BAE | 110 |
| Appendix F. NMR Spectra for MDEA | 112 |
| Appendix G. NMR Spectra for PZ..... | 114 |

LIST OF TABLES

| | |
|--|----|
| Table 2-1. List of Aqueous Amines Chosen for this Research. ²⁵ | 19 |
| Table 2-2. Reference Letter for Each Degraded Sample. | 22 |
| Table 2-3. Concentrations of the Diluted Pure Amines..... | 29 |
| Table 4-1. Thermal Degradation Activation Energies as well as their Associated Slope and Reaction Order for MEA, MDEA, and PZ. | 74 |
| Table 5-1. Summary of Computational Results for ϵ_{bind} , $\Delta_r H$, and $\Delta_r G$ | 81 |

LIST OF FIGURES

Figure 1-1. Average global temperature change from 1880-2019 with a key describing the colors that represent specific time frames, Reproduced from References (1) and (2). (Sources: (1) GISTEMP Team, 2019: *GISS Surface Temperature Analysis (GISTEMP), version 4*. NASA Goddard Institute for Space Studies. Dataset accessed 2019-12-29 at <https://data.giss.nasa.gov/gistemp/> and (2) Lenssen, N., G. Schmidt, J. Hansen, M. Menne, A. Persin, R. Ruedy, and D. Zyss, 2019: Improvements in the GISTEMP uncertainty model. *J. Geophys. Res. Atmos.* **124**, 12, 6307-6326.)..... 1

Figure 1-2. Demonstration of the greenhouse effect, where the solid blue color represents C, green is F, white is H, red is O, and yellow is S, and make up the greenhouse gasses: CO₂, SF₆, and CH₄. The linear molecule on the far right with the red and blue shading represents N₂O. Reproduced from Reference (5). (Source: Photo courtesy of Barb Deluisi, NOAA, Boulder, Colorado, USA (<http://esrl.noaa.gov/gmd/>)) 3

Figure 1-3. Seasonal concentration of CO₂ from December 2018-December 2019. Reproduced from Reference (6). (Source: Data provided by NOAA ESRL Global Monitoring Division, Boulder, Colorado, USA (<http://esrl.noaa.gov/gmd/>))..... 4

Figure 1-4. Demonstration of the increase in CO₂ concentration since 1980. Reproduced from Reference (6). (Source: Data provided by NOAA ESRL Global Monitoring Division, Boulder, Colorado, USA (<http://esrl.noaa.gov/gmd/>))..... 5

Figure 1-5. Typical Absorber-stripper system for the sequestering of post-combustion CO₂.^{4, 11,17-19} 7

| | |
|---|----|
| Figure 1-6. Probable reactions that could occur between CO ₂ and H ₂ O during CO ₂ absorption into an amine solution. ²²⁻²⁵ | 9 |
| Figure 1-7. Zwitterion intermediate production with MEA and CO ₂ . ^{22-23,25-28} | 10 |
| Figure 1-8. Zwitterion deprotonation with MEA to form MEA carbamate and protonated MEA. ^{22-23,25-28} | 10 |
| Figure 1-9. Typical CO ₂ absorption reaction for MEA produced MEA carbamate and protonated MEA. ^{4,22-32} | 11 |
| Figure 1-10. Reaction pathway for the absorption of CO ₂ by MDEA. ^{4,21,33-36} | 12 |
| Figure 1-11. Proposed thermal degradation reactions of MEA produced by reference (4). ^{4,25} | 15 |
| Figure 1-12. Proposed thermal degradation pathways for PZ produced by reference (39). ^{25,39} | 17 |
| Figure 2-1. Steel vessel used for housing the aqueous amine solutions loaded with CO ₂ for thermal degradation. | 21 |
| Figure 2-2. JEOL ECS-400 NMR instrument used for this research at Eastern Kentucky University in Richmond, KY..... | 24 |
| Figure 2-3. Agilent 1260 Infinity II HPLC instrument used for this research at Eastern Kentucky University in Richmond, KY..... | 30 |
| Figure 3-1. Starting on the left and going right the amines are: MEA, 1A2P, EN, 3APT, 2BAE, MDEA, PZ. A.) The stock solutions of CO ₂ loaded amines before degradation. B.) Degradation at 125°C. C.) Degradation at 135°C. D.) Degradation at 145°C. | 42 |

| | |
|--|----|
| Figure 3-2. ^1H and ^{13}C NMR data acquired for MEA and its degraded samples. MEA is labelled, and the letters indicate the degraded sample. | 47 |
| Figure 3-3. ^1H and ^{13}C NMR data acquired for 1A2P and its degraded samples. 1A2P is labelled, and the letters indicate the degraded sample. | 47 |
| Figure 3-4. ^1H and ^{13}C NMR data acquired for EN and its degraded samples. EN is labelled, and the letters indicate the degraded sample. | 48 |
| Figure 3-5. ^1H and ^{13}C NMR data acquired for 3APT and its degraded samples. 3APT is labelled, and the letters indicate the degraded sample. | 48 |
| Figure 3-6. ^1H and ^{13}C NMR data acquired for 2BAE and its degraded samples. 2BAE is labelled, and the letters indicate the degraded sample. | 49 |
| Figure 3-7. ^1H and ^{13}C NMR data acquired for MDEA and its degraded samples. MDEA is labelled, and the letters indicate the degraded sample. | 49 |
| Figure 3-8. ^1H and ^{13}C NMR data acquired for PZ and its degraded samples. PZ is labelled, and the letters indicate the degraded sample. | 50 |
| Figure 4-1. Calibration Curve for MEA..... | 54 |
| Figure 4-2. Demonstration of the concentration of MEA after degradation at different temperatures..... | 54 |
| Figure 4-3. Calibration Curve for 1A2P..... | 56 |
| Figure 4-4. Demonstration of the concentration of 1A2P after degradation at different temperatures..... | 57 |
| Figure 4-5. Calibration Curve for EN..... | 58 |

| | |
|--|----|
| Figure 4-6. Demonstration of the concentration of EN after degradation at different temperatures..... | 58 |
| Figure 4-7. Insufficient calibration curve for 3APT..... | 61 |
| Figure 4-8. Calibration curve for 3APT. | 61 |
| Figure 4-9. Demonstration of the concentration of 3APT after degradation at different temperatures..... | 62 |
| Figure 4-10. Calibration curve for 2BAE. | 64 |
| Figure 4-11. Demonstration of the concentration of 2BAE after degradation at different temperatures..... | 64 |
| Figure 4-12. Calibration curve for MDEA..... | 68 |
| Figure 4-13. Demonstration of the concentration of MDEA after degradation at different temperatures..... | 68 |
| Figure 4-14. Calibration curve for PZ..... | 71 |
| Figure 4-15. Demonstration of the concentration of PZ after degradation at different temperatures..... | 72 |
| Figure 5-1. Reaction system used for the computational investigation. MEA is used as the example..... | 80 |
| Figure 6-1. Thermal degradation reactions for 1A2P produced by reference (40). ^{25,40} | 84 |
| Figure 6-2. Theoretical thermal degradation reactions for EN. ²⁵ | 85 |
| Figure 6-3. Continued theoretical thermal degradation reactions for EN. ²⁵ | 86 |
| Figure 6-4. Theoretical thermal degradation reactions for 3APT. ²⁵ | 87 |
| Figure 6-5. Theoretical thermal degradation reactions for 2BAE. ²⁵ | 88 |

| | |
|---|-----|
| Figure 6-6. Continued theoretical thermal degradation reactions for 2BAE. ²⁵ | 88 |
| Figure 6-7. Theoretical thermal degradation reactions for MDEA. ²⁵ | 89 |
| Figure 7-1. Structural representation for the thermal stability of the amines used in this study. ²⁵ | 93 |
| Figure A-1. DEPT-90 NMR data acquired for MEA and its degraded samples. MEA is labelled, and the letters indicate the degraded sample. | 101 |
| Figure A-2. DEPT-135 NMR data acquired for MEA and its degraded samples. MEA is labelled, and the letters indicate the degraded sample. | 102 |
| Figure A-3. ¹⁵ N NOE NMR data acquired for MEA and its degraded samples. MEA is labelled, and the letters indicate the degraded sample. | 102 |
| Figure B-1. DEPT-90 NMR data acquired for 1A2P and its degraded samples. 1A2P is labelled, and the letters indicate the degraded sample. | 103 |
| Figure B-2. DEPT-135 NMR data acquired for 1A2P and its degraded samples. 1A2P is labelled, and the letters indicate the degraded sample. | 104 |
| Figure B-3. ¹⁵ N NOE NMR data acquired for 1A2P and its degraded samples. 1A2P is labelled, and the letters indicate the degraded sample. | 104 |
| Figure C-1. DEPT-90 NMR data acquired for EN and its degraded samples. EN is labelled, and the letters indicate the degraded sample. | 105 |
| Figure C-2. DEPT-135 NMR data acquired for EN and its degraded samples. EN is labelled, and the letters indicate the degraded sample. | 106 |
| Figure C-3. ¹⁵ N NOE NMR data acquired for EN and its degraded samples. EN is labelled, and the letters indicate the degraded sample. | 107 |

| | |
|---|-----|
| Figure D-1. DEPT-90 NMR data acquired for 3APT and its degraded samples. 3APT is labelled, and the letters indicate the degraded sample. | 108 |
| Figure D-2. DEPT-135 NMR data acquired for 3APT and its degraded samples. 3APT is labelled, and the letters indicate the degraded sample. | 109 |
| Figure D-3. ¹⁵ N NOE NMR data acquired for 3APT and its degraded samples. 3APT is labelled, and the letters indicate the degraded sample. | 109 |
| Figure E-1. DEPT-90 NMR data acquired for 2BAE and its degraded samples. 2BAE is labelled, and the letters indicate the degraded sample. | 110 |
| Figure E-2. DEPT-135 NMR data acquired for 2BAE and its degraded samples. 2BAE is labelled, and the letters indicate the degraded sample. | 111 |
| Figure E-3. ¹⁵ N NOE NMR data acquired for 2BAE and its degraded samples. 2BAE is labelled, and the letters indicate the degraded sample. | 111 |
| Figure F-1. DEPT-90 NMR data acquired for MDEA and its degraded samples. MDEA is labelled, and the letters indicate the degraded sample. | 112 |
| Figure F-2. DEPT-135 NMR data acquired for MDEA and its degraded samples. MDEA is labelled, and the letters indicate the degraded sample. | 113 |
| Figure F-3. ¹⁵ N NOE NMR data acquired for MDEA and its degraded samples. MDEA is labelled, and the letters indicate the degraded sample. | 113 |
| Figure G-1. DEPT-90 NMR data acquired for PZ and its degraded samples. PZ is labelled, and the letters indicate the degraded sample. | 114 |
| Figure G-2. DEPT-135 NMR data acquired for PZ and its degraded samples. PZ is labelled, and the letters indicate the degraded sample. | 115 |

Figure G-3. DEPT-135 NMR data acquired for PZ and its degraded samples. PZ is
labelled, and the letters indicate the degraded sample. 115

Chapter 1. Introduction

1.1 Climate Change and the Greenhouse Effect

Since 1880, the global average temperature has been tracked by the Goddard Institute for Space Studies (GISS) from the National Aeronautics and Space Administration (NASA) by using weather reports from the past and data collected from the ocean to have increased by approximately 0.8°C causing climate change.^{1,2} The increase in seasonal average change in the global temperature from 1880-2019 is demonstrated by Figure 1-1.^{1,2} While there are multiple contributions towards the

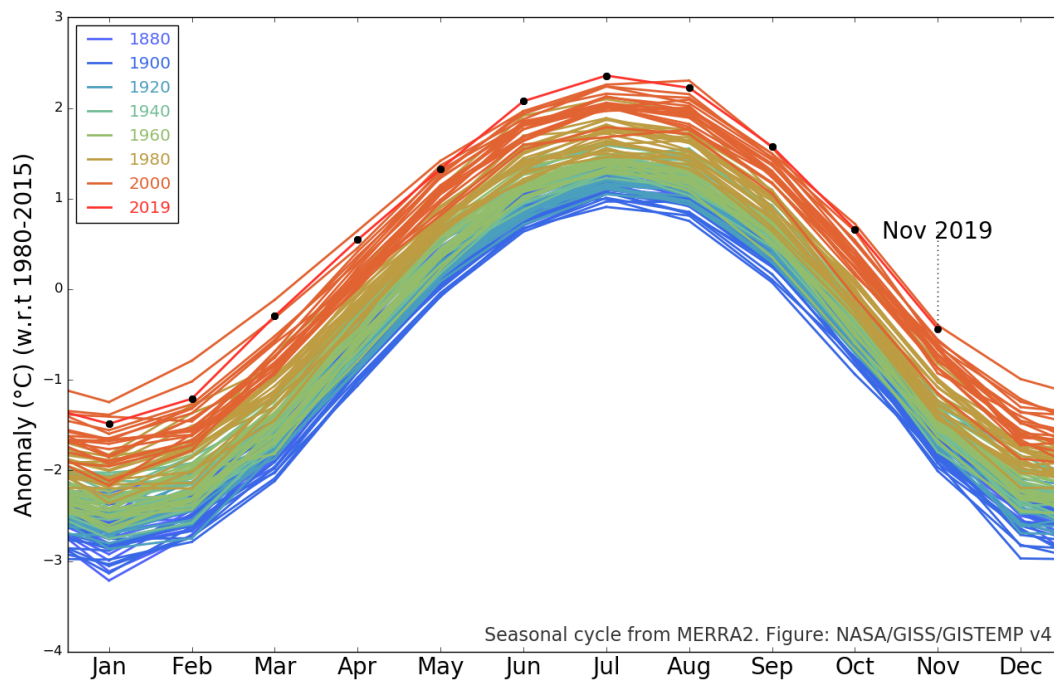


Figure 1-1. Average global temperature change from 1880-2019 with a key describing the colors that represent specific time frames, Reproduced from References (1) and (2). (Sources: (1) GISTEMP Team, 2019: *GISS Surface Temperature Analysis (GISTEMP), version 4*. NASA Goddard Institute for Space Studies. Dataset accessed 2019-12-29 at <https://data.giss.nasa.gov/gistemp/> and (2) Lenssen, N., G. Schmidt, J. Hansen, M. Menne, A. Persin, R. Ruedy, and D. Zyss, 2019: Improvements in the GISTEMP uncertainty model. *J. Geophys. Res. Atmos.* **124**, 12, 6307-6326.)

increase in global temperature, one of the major components is the presence of greenhouse gases into the troposphere.^{3,4}

Greenhouse gases are gases that possess a net dipole moment allowing the gas molecules to absorb infrared radiation (IR) with a wavelength range of 10^{-6} - 10^{-3} m. The absorbed radiation can cause vibrational or rotational motions of a gas molecule.³ Because of this, greenhouse gases can absorb heat from the earth and then reradiate some of the warmth back to the Earth and other atmospheric gases such as N_2 and O_2 (Figure 1-2), creating what is known as the *greenhouse effect*.⁴⁻⁵

The major greenhouse gases include: water (H_2O), carbon dioxide (CO_2), methane (CH_4), and nitrous oxide (N_2O).^{3,4} Not including H_2O , the National Oceanic and Atmospheric Administration's (NOAA) Earth System Research Laboratory's (ESRL) Global Monitoring System (GMS) provides the current concentration of CO_2 , CH_4 , and N_2O as 410.27 ppm, 1863.6 ppb, and 331.9 ppb respectively.⁶⁻⁸ Although these are the major greenhouse gases, halocarbons and sulfur hexafluoride (SF_6) are also present in the troposphere the current concentration of 10.07 ppt.^{3,9} The concentration of greenhouse gases plays a major role in the absorption of heat. For example, CH_4 is approximately 24 times more effective at absorbing IR than CO_2 , however, CO_2 is more

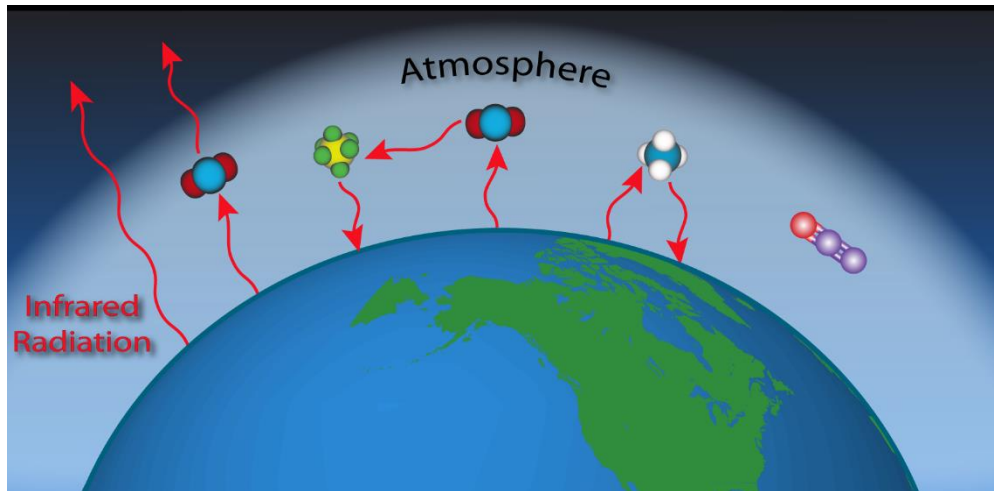


Figure 1-2. Demonstration of the greenhouse effect, where the solid blue color represents C, green is F, white is H, red is O, and yellow is S, and make up the greenhouse gasses: CO₂, SF₆, and CH₄. The linear molecule on the far right with the red and blue shading represents N₂O. Reproduced from Reference (5). (Source: Photo courtesy of Barb Deluise, NOAA, Boulder, Colorado, USA (<http://esrl.noaa.gov/gmd/>))

abundant as a greenhouse gas due to anthropogenic sources, and accounts for 7.5% of the greenhouse effect.³

1.2 CO₂ as a Direct Indicator of the Greenhouse Effect

One of the major contributions towards the rising average global temperature is due to the emissions of CO₂ by the combustion of fossil fuels.^{3,4,10-15} It can be demonstrated that the average global temperature has a direct dependence on the concentration of CO₂ in the atmosphere; a comparison between Figure 1-1 and Figure 1-3 demonstrates how the altering seasonal concentrations of CO₂ and the global average temperature are related.¹⁰ It is important to note that the variations from month-to-month, when comparing CO₂ concentration to temperature, could be due to Figure 1-3 being data at the Mauna Loa Observatory, while Figure 1-1 is of the global average temperature. Regardless, it is demonstrated that the CO₂ concentration is

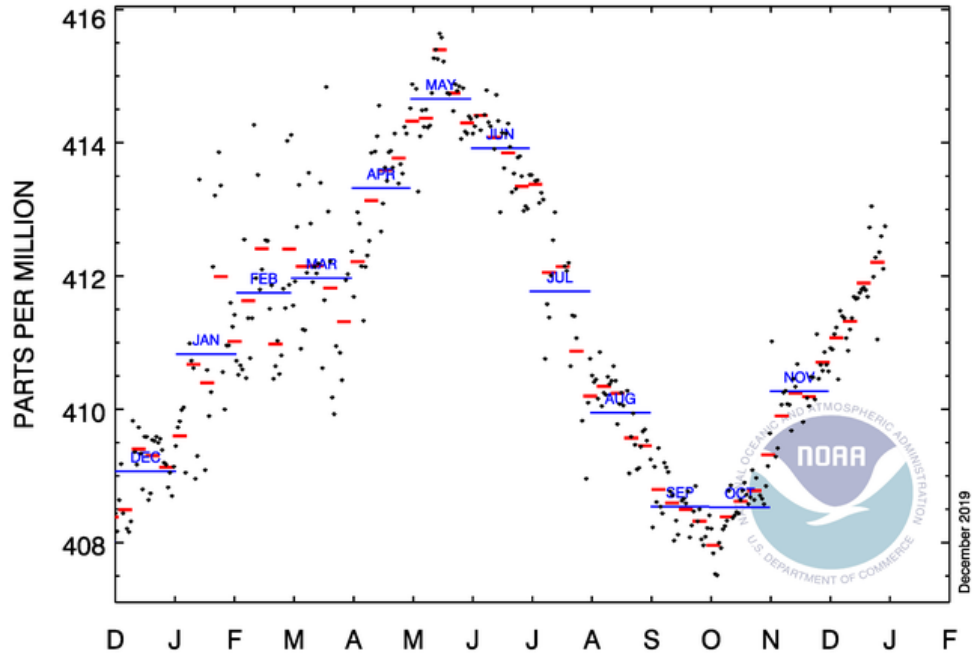


Figure 1-3. Seasonal concentration of CO₂ from December 2018-December 2019. Reproduced from Reference (6). (Source: Data provided by NOAA ESRL Global Monitoring Division, Boulder, Colorado, USA (<http://esrl.noaa.gov/gmd/>))

directly related to the increase in global temperature.¹⁰ Figure 1-4 also demonstrates the direct relation of the increase in CO₂ on the global temperature. As the concentration of CO₂ increased, so has the global temperature.

The data demonstrated by Figures 1-3 and 1-4 was collected by the Mauna Loa Observatory. The observatory is positioned upon the slopes of the Mauna Loa volcano in Hawaii because, the bare lava that surrounds the slopes allows the accurate determination of CO₂ concentration in the surrounding area.¹⁶ The bare lava means little-to-no soil and vegetation that can serve as CO₂ sinks. Due to this, if a baseline measurement of the air in the area is measured, any fluctuation in CO₂ could be readily detected.¹⁶

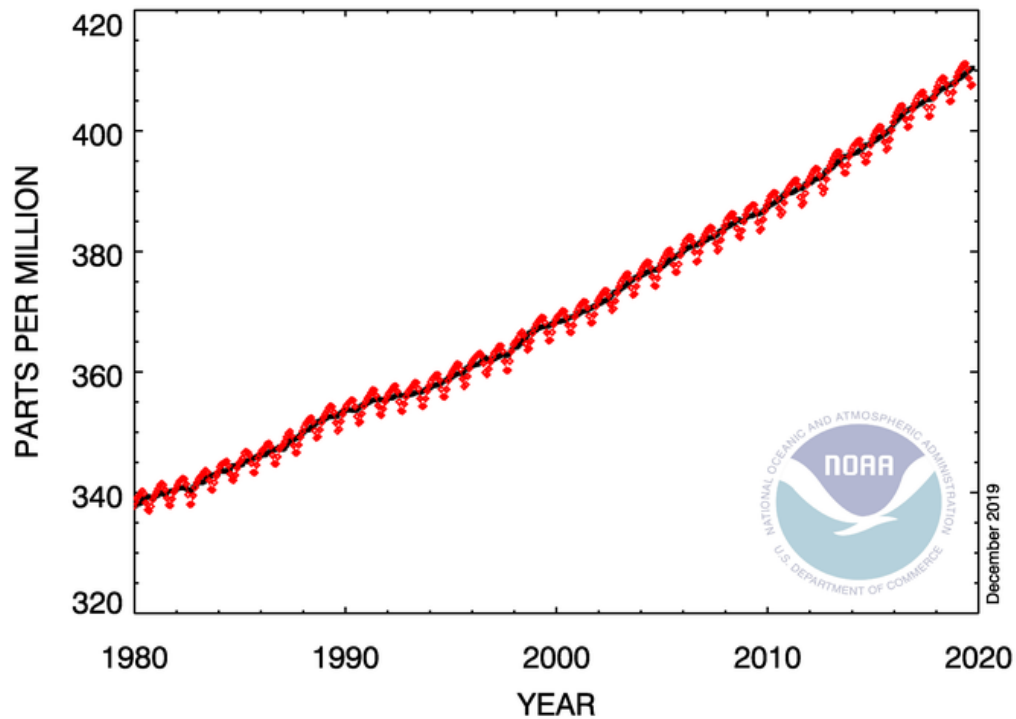


Figure 1-4. Demonstration of the increase in CO₂ concentration since 1980. Reproduced from Reference (6). (Source: Data provided by NOAA ESRL Global Monitoring Division, Boulder, Colorado, USA (<http://esrl.noaa.gov/gmd/>))

CO₂ can absorb IR due to the different vibrational modes, one stretching mode (asymmetric) and two bending modes (out-of-plane and in-plane bending).³ Therefore, IR spectroscopy can be used to accurately determine the CO₂ concentration in the sample due to the fact that the greater the CO₂ concentration, the more IR that will be absorbed.¹⁶

1.3 Sequestering of Post-Combustion CO₂ using Aqueous Amines

While there are multiple techniques proposed towards sequestering CO₂ from flue gas in power plants, the use of aqueous amines seems to be the most auspicious technique.¹¹ This technique is based on the same technology used for natural gas sweetening, and is able to be performed by retrofitting existing power plants.¹⁰ With

this process, monoethanolamine (MEA) is the benchmark solvent, and the discussion on the sequestration process will be described using temperatures correlated with MEA (absorber at approximately 40-50°C and stripper at approximately 100-140°C).^{4,11} It is important to note that the temperatures used for the absorber and stripper varies based on the specific amine solvent and its thermal stability.⁴

Flue gas containing CO₂, N₂, and O₂ are brought to the absorber-desorber (stripper) system.^{4,11} It is important to note that flue gas contains NO_x and SO_x particulates, however, these should be removed prior to entering the absorber-stripper system by a pretreatment of the flue gas.^{4,17} The absorber-stripper system is demonstrated by Figure 1-5. Using Figure 1-5, the flue gas enters from the bottom of the absorber, and flows through the amine solvent in an ascending fashion, while the amine solvent is flowing in a descending manner.^{4,11} With the opposing currents, a packing material is also present inside of the absorber, which ensures the two phases meet.^{4,18-19} It was estimated that with a properly designed absorber column, the efficiency for the removal of CO₂ could range anywhere between 70-99%.¹⁷

After the amine solvent absorbs CO₂, the CO₂-rich solvent flows into the stripper at a much higher temperature, where the temperature is dependent on the thermal stability of the CO₂-rich solvent.^{4,11,17-19} The temperature needs to be high enough to be able to remove CO₂ from the CO₂-rich solvent. Steam from the power plant is used to heat up the regenerated solvent in the stripper, and consequently, this is the most expensive part of the absorber-stripper system due to high energy consumption.¹¹ The heat exchanger, demonstrated by Figure 1-5, heats up the CO₂-

rich solvent before it enters the stripper. This is accomplished by allowing the steam collected in the power plant to heat up the CO₂ rich solvent, removing CO₂, which becomes CO₂-lean solvent that will then flow back into the absorber through the heat exchanger which will not only heat up the CO₂-rich solvent as it enters the stripper but also cool down the CO₂-lean solvent as it returns to the absorber.¹⁸

Upon the regeneration of the CO₂-lean solvent, the CO₂ and H₂O gas produced leaves through the top of the stripper. The H₂O can be removed, and pure CO₂ is then compressed and stored for future use.^{4,11} The CO₂-lean solvent then flows to the heat exchanger, and the cooled solvent is brought back to the absorber for further usage.^{4,11,17-18}

1.4 Aqueous Amines and CO₂ Absorption

Here, the evaluation of the different amines, or alkanolamines, including the coordination, CO₂ capture mechanisms, and structural effects is discussed. Primary and

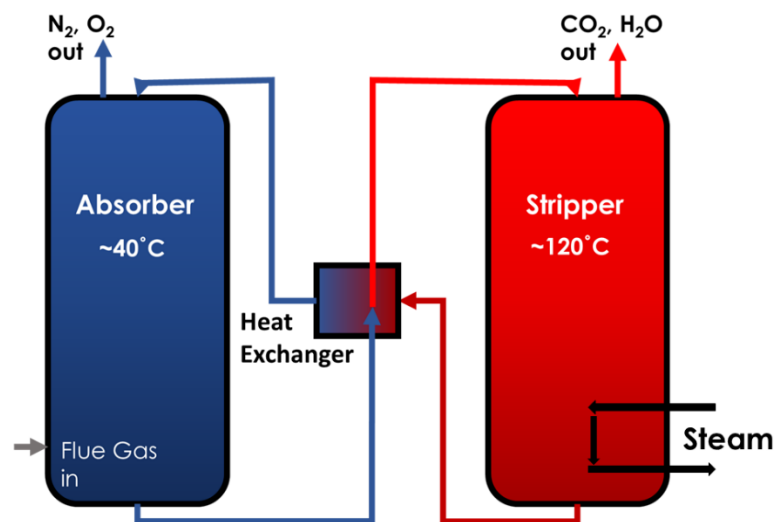


Figure 1-5. Typical Absorber-stripper system for the sequestering of post-combustion CO₂.^{4, 11,17-19}

secondary amines are given a section together due to their similar behaviors during CO₂ capture, however the differences between the two will be addressed. The overall characterization of amines is demonstrated in section 1.4.1, however, this same reasoning can be used to describe tertiary amines. The differences being in the absorption of CO₂, and coordination.

1.4.1 Primary and Secondary Amines

Like the coordination of substituted carbons, amine groups are specified according to how many carbons are attached to the nitrogen atom. A primary amine is an amine that contains two hydrogen atoms and one substituent, which is typically an alkyl group.²⁰ Likewise, a secondary amine has two substituents and a single hydrogen atom.²⁰ Treating the substituent as an alkyl group, the amine and the substituent(s) would have a σ bond due to the amine possessing sp^3 hybridized orbitals.²⁰ However, this is the case only when the arrangement of the nitrogen and its substituents is pyramidal. There are cases in which the substituted amine could take on a planar arrangement, changing from an sp^3 arrangement to an sp^2 hybridization, such as in arylamines and amides.²⁰

The aqueous amines can range in concentrations (experimental concentrations found as low as 3 wt% and as high as 40 wt%), however, as an example, MEA is typically used as 30 wt%.^{4,21} It was demonstrated that too much amine in the solution could cause harm to the absorber-stripper system by corrosion, thus, a threshold concentration for each aqueous amine must be determined to avoid damage and

solvent degradation.⁴ Also, upon experimental comparisons for the energy required for CO₂ absorption between 20 wt% and 30 wt% MEA, the 30 wt% solution required 28% less energy for the absorption.⁴ This information is important when other amines are being considered for CO₂ absorption, demonstrating that different concentrations should be tested to determine the best fit that requires the least amount of energy and will not increase corrosion or solvent degradation.⁴

Before the analysis of CO₂ absorption by primary and secondary amines, the reactions between H₂O with CO₂ should be demonstrated as they can occur concurrently during CO₂ absorption into the aqueous amine solution, and these possibilities are shown by Figure 1-6. The reactions demonstrated by Figure 1-6 are

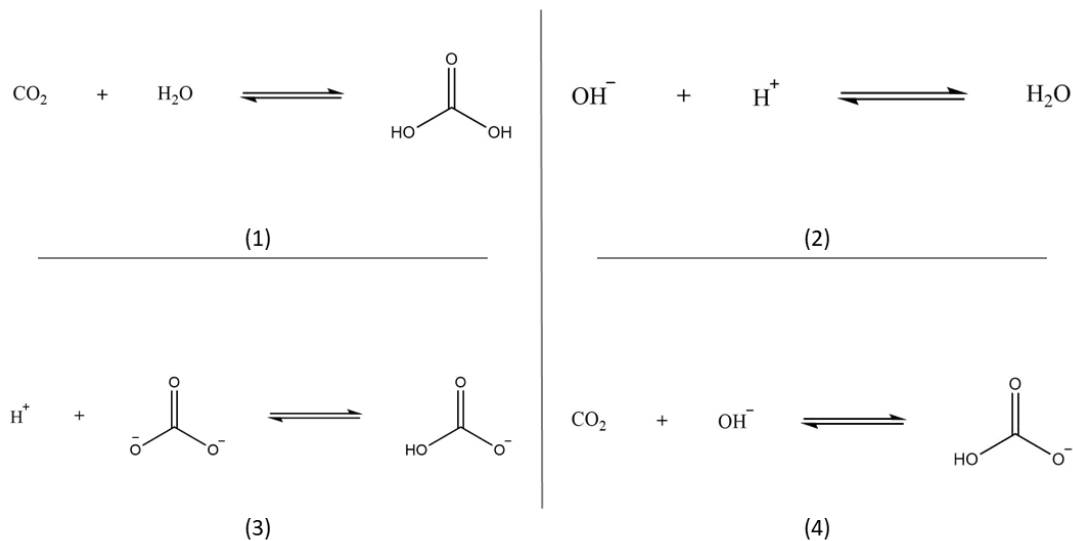


Figure 1-6. Probable reactions that could occur between CO₂ and H₂O during CO₂ absorption into an amine solution.²²⁻²⁵

more important for the reactions dealing with tertiary amines, due to the lack of hydrogen on the nitrogen atom, and will be discussed further in section 1.4.2, but it is

important to recognize the other reactions that can occur during the absorption of CO₂.

For the analysis of CO₂ absorption with aqueous amines, MEA will be used as the example. While MEA is a primary amine, secondary amines absorb CO₂ in the same

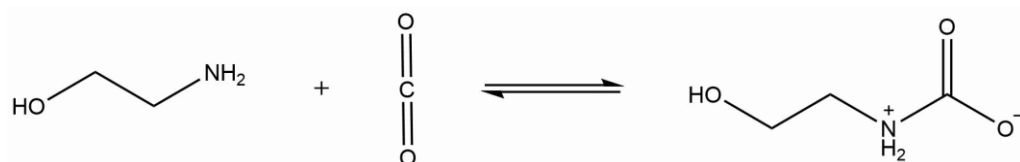


Figure 1-7. Zwitterion intermediate production with MEA and CO₂.^{22-23,25-28}

process. However, the first mechanism of the CO₂ absorption, that has been extensively studied with MEA, includes the production of a zwitterion intermediate.²²⁻

^{23,26-28} The zwitterion production has been determined as the rate-determining step, and is demonstrated by Figure 1-7.²⁸ The zwitterion then undergoes deprotonation to form carbamate and protonated MEA with the presence of other MEA molecules demonstrated by Figure 1-8.²² The free MEA involved in the reaction demonstrated by Figure 1-8, acquires the proton from the zwitterion, to produce MEA carbamate and



Figure 1-8. Zwitterion deprotonation with MEA to form MEA carbamate and protonated MEA.^{22-23,25-28}

the deprotonated MEA. In many cases, the reaction in Figure 1-8 is demonstrated by the nucleophilic attack by MEA to CO₂, specifically, attacking the carbon.⁴ While the MEA carbamate species is in equilibrium with bicarbonate and MEA, this reaction will be excluded, but it is important to understand the side reactions that could occur.⁴

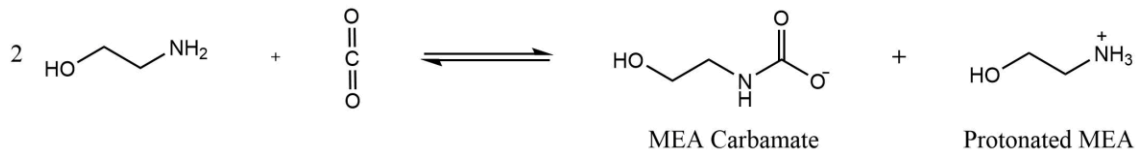


Figure 1-9. Typical CO₂ absorption reaction for MEA produced MEA carbamate and protonated MEA.^{4,22-32}

Figure 1-9 demonstrates the overall reaction, in terms of the ionic species, for the CO₂ absorption by MEA, which can be applied to other primary and secondary amines.

With the reaction mechanisms for the absorption of CO₂ by MEA, the absorption capacity must also be evaluated, as it is dependent upon the structure of the amine.^{22,29} It was determined that sterically hindered amines have a higher CO₂ absorption capacity due to the formation of bicarbonate as opposed to carbamate, much like the reactions demonstrated by Figure 1-6.^{4,22,29} Carbamates are more stable and as a result, require more energy to release the captured CO₂ and regenerate the amine.^{4,29} While sterically hindered amines have a higher CO₂ absorption capacity, non-sterically hindered amines have faster reaction kinetics.^{4,29} A general relationship can be used to explain this phenomenon: CO₂ absorption capacity is proportional to the ability of an amine to form carbamate (more carbamate formation, less absorption capacity), which is dependent on the structure of the amine.^{4,29}

1.4.2 Tertiary Amines

Tertiary amines behave similarly to sterically hindered primary and secondary amines, in terms of CO₂ absorption, and have similar hybridizations that were demonstrated in section 1.4.1.²⁰ Since, much of the information presented in section

1.4.1 can be related to tertiary amines, this section is going to outline the major differences of tertiary amines from primary and secondary amines, especially that of CO₂ absorption capacity and the reaction mechanism of CO₂ absorption.

The reaction mechanism for CO₂ absorption by tertiary amines is demonstrated by N-methyldiethanolamine (MDEA), one of the most researched tertiary amine for

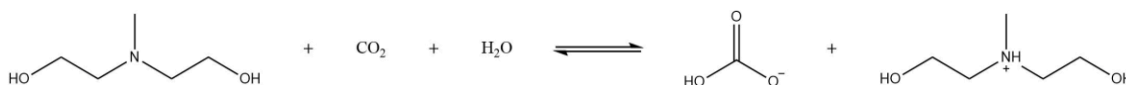


Figure 1-10. Reaction pathway for the absorption of CO₂ by MDEA.^{4,21,33-36}

CO₂ absorption, by Figure 1-10. In the reaction demonstrated by Figure 1-10, the base-catalytic hydration of CO₂ by MDEA forms bicarbonate and protonated MDEA.^{4,34} The reactions shown in Figure 1-6, demonstrates the production of bicarbonate that would occur in this reaction. The role of the tertiary amines for CO₂ absorption is for the hydrolysis of CO₂, which is possible due to tertiary amines, such as MDEA, not possessing a hydrogen bond with nitrogen.^{4,21} Primary and secondary amines have at least one hydrogen bond with the nitrogen, allowing the formation of stable carbamates, whereas tertiary amines allow the formation of unstable bicarbonate.^{4,33}

Due to the formations of bicarbonate with tertiary amines, the regeneration of the tertiary amine requires less energy than it would if a primary or secondary amine was used with the production of a carbamate.^{21,33-36} However, tertiary amines are less reactive than an unhindered primary and secondary amine.^{21,33-36} Thus, it is a trade-off; more efficient regeneration, but slow and inefficient CO₂ absorption.

1.5 Thermal Degradation of Aqueous Amines

As mentioned in section 1.3, CO₂ is released by heating the CO₂-rich solvent in the stripper portion of the absorber-stripper system to regenerate the amine solution, which will cause the thermal degradation of amines at high temperature.^{4,37-42} During thermal degradation, imidazolidones, ureas, aldehydes, oxazolidones, amine dimers, amine trimers, polymeric and cyclic compounds are all possible products for the degradation of an aqueous amine.^{4,37,39} For unhindered primary and secondary amines, the production of polymeric compounds was determined to be the main pathway.⁴ Regardless of the product formed, thermal degradation reduces the CO₂ capacity of regenerated amine solutions, increases the energy required for amine regeneration, and could cause fouling and foaming which may produce a hazard to the system due to the volatility of some degradation products.^{4,38,42}

Before the demonstration and discussion of two examples of degradation for the primary amine MEA and secondary amine piperazine (PZ), general trends have been observed based on the study of the amine structure that effect thermal degradation. While steric hindrance of the amines effects the CO₂ absorption capacity of amines, it also effects the thermal degradation of amines.⁴⁰ Sterically hindered amines would have a lower degradation rate compared to unhindered amines due to the formation of bicarbonate and unstable carbamates, as opposed to the stable carbamates formed with unhindered amines.⁴⁰ In a study conducted with aminosilicone carbamates and temperature, it was determined that high temperature and CO₂ loadings led to more thermal degradation.⁴¹ The same conclusions were also

demonstrated in a study on PZ, where an increase in temperature demonstrated an increase in the degradation rate, and that with higher CO₂ loadings, more degradation occurred. However, the degradation rate was demonstrated to reach a plateau with different CO₂ loading ratios up to a ratio of 0.4 mol CO₂/mol PZ.³⁸⁻³⁹ Thus, while a higher CO₂ loading does enhance the thermal degradation, there is a possibility, when comparing PZ to other amines, that other amines could possess a threshold CO₂ where the thermal degradation rate can decrease once above this threshold.³⁹ Since, Freeman et al. demonstrated that with a CO₂ loading above 0.4 mol CO₂/mol PZ, the thermal degradation rate rapidly decreased, which could be explained by the existence of lower amounts of reactive species present and with the presence of bicarbonate.³⁸⁻

39

The possible degradation pathways for MEA will be discussed first and is demonstrated by Figure 1-11. Reaction (1), demonstrated by Figure 1-11 (when referring to the different reactions from Figure 1-11 henceforth will be denoted by the numbered reaction), is the capture of CO₂ by MEA to form MEA carbamate.⁴ It is then possible, at high temperatures, that instead of the release of CO₂, an OH group and an H atom from the other OH groups could be released, and the molecule can undergo intramolecular cyclization to produce oxazolidine-2-one (OZD) demonstrated by (2).⁴ The produced OZD is then subject to ring opening reactions with an MEA molecule.⁴ The amine group of MEA could nucleophilically attack the carbon adjacent to the oxygen, to produce N-(2-hydroxyethyl)ethylenediamine (HEEDA) demonstrated by (3).⁴ Following HEEDA, HEEDA can then capture CO₂ demonstrated by (4).⁴ Upon amine

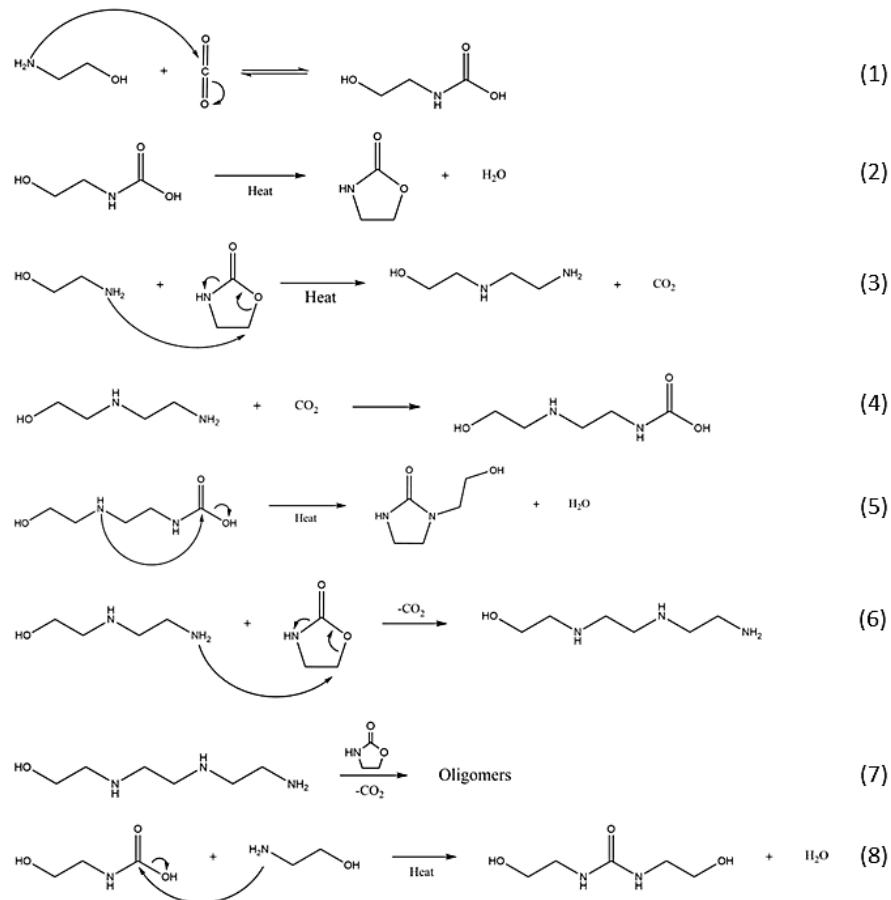


Figure 1-11. Proposed thermal degradation reactions of MEA produced by reference (4).^{4,25}

regeneration, the HEEDA carbamate could then undergo an intramolecular cyclization, similar to the formation of OZD, to form hydroxyethylimidazolidone (HEIA) demonstrated by (5).⁴ HEEDA also has the capability to nucleophilically attack the thermal degradation product OZD, to form N-(2-hydroxyethyl) diethylenetriamine (HEDETA) and releasing CO_2 demonstrated by (6).⁴ It is important to note that HEEDA was found to be the most abundant degradation species, accounting for approximately 50% of the MEA loss at 145°C .⁴ The pathways demonstrated by (2)-(6) could be repeated to form oligomers demonstrated by (7) until completion.⁴ Finally, the MEA carbamate species can undergo a thermal degradation pathway other than the

intramolecular cyclization. The MEA that could still be present after CO₂ absorption, could act as a nucleophile and attack the carbonyl carbon of the MEA carbamate to produce N,N'-bis (2-hydroxyethyl)urea (BHEU) demonstrated by (8).⁴ It is important to note that BHEU was found to be the second most abundant species, followed by HEIA, OZD, and HEDETA.^{4,37} On the basis of urea formation, an increased abundance of urea species could be effected by having a higher concentration of carbamates, lower water concentrations, and higher temperatures, which could explain why BHEU was the second most abundant species found at 145°C.^{1,41}

With piperazine, the CO₂ absorption reaction would follow that of MEA, producing PZ carbamate and a protonated PZ.³⁸ However, unlike the thermal degradation of MEA, it was proposed that the first thermal degradation product for PZ occurs by the nucleophilic attack by PZ on one of the α -carbons of a protonated PZ species, in a ring opening reaction to produce 1-[2-((2-aminoethyl)amino)ethyl] piperazine (AEAEPZ) demonstrated by reaction (1) in Figure 1-12 (just like with the description of the thermal degradation pathway for MEA, when referring to a specific reaction from Figure 1-12, on the reaction number will be presented).³⁹ Following the production of AEAEPZ, AEAEPZ could capture CO₂ to be in an equilibrium with urea AEAPZ (2).³⁹ The AEAPZ species could then be protonated, as demonstrated by (3), and have two different pathways it could undergo due to the nucleophilic attack by PZ (4-5).³⁹ In (4), the PZ attacks an adjacent carbon to the protonated amino functional, in a way that would produce 1,1'-(1,2-ethanediyl)bis-piperazine (PEP) and ethylenediamine (EN).³⁹ The other pathway, (5), PZ attacks an adjacent carbon to protonated amino

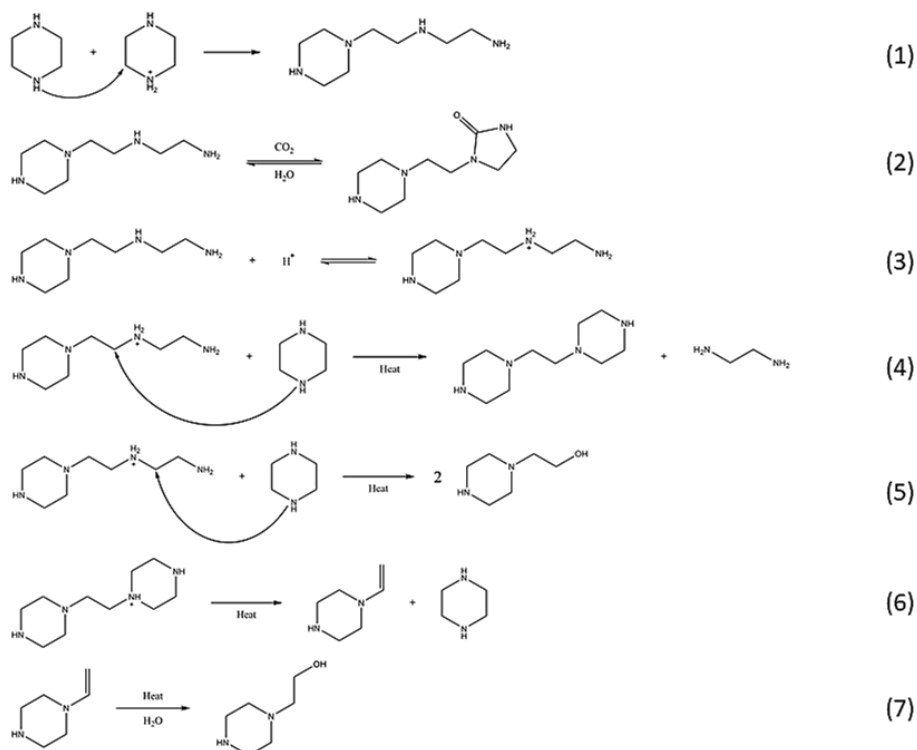


Figure 1-12. Proposed thermal degradation pathways for PZ produced by reference (39).^{25,39}

functional in a way that would produce N-(2-aminoethyl)piperazine (AEP).³⁹ The final two reactions being used for the discussion of the thermal degradation of PZ (6-7), involves Hofmann elimination and anti-Markovnikov hydration.³⁹ For (6), protonated PEP undergoes Hofmann elimination to produce 1-ethenylpiperazine and PZ.³⁹ Sequentially, 1-ethenylpiperazine could undergo anti-Markovnikov hydration to produce N-(2-hydroxyethyl)piperazine (HEP).³⁹

While Figure 1-11 and Figure 1-12 demonstrate proposed thermal degradation pathways for MEA and PZ, the thermal degradation pathway and species for MEA and PZ are not limited to those demonstrated. However, the proposed pathways described

are the main reaction pathways likely to occur during thermal degradation of the two species.

1.6 Research Objectives

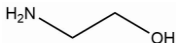
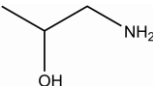
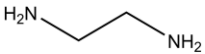
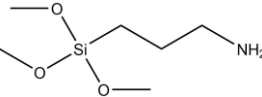
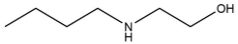
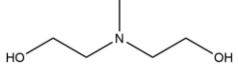
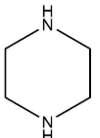
The overarching goal for this research is to determine how the structure of aqueous amines affects thermal degradation. Unlike many of the thermal degradation studies, this research is set to compare seven different aqueous amines all at the same concentration, CO₂ loading, and degraded under the same conditions, to compare the extent of degradation based on different functional groups and structure. The standard is MEA, and the other aqueous amines will be compared to the results from MEA in this research. While other studies give an idea about how structure could affect thermal degradation based, the uniformity between the aqueous amines being used will help develop a better understanding for how much of an extent the structure plays on thermal degradation, instead of focusing on the CO₂ loading. In doing so, this information could help in the development of a better suited amine for CO₂ capture. To achieve this, ¹H, ¹³C, DEPT-90, DEPT-135, and ¹⁵N nuclear Overhauser effect (NOE) nuclear magnetic resonance (NMR), high-performance liquid chromatography (HPLC), and Gaussian09, a computational software, were utilized.

Chapter 2. Experimental Methods and Computational Details

2.1 Aqueous Amines Chosen for Study

Seven aqueous amines were chosen for this research and are listed in Table 2-1.

Table 2-1. List of Aqueous Amines Chosen for this Research.²⁵

| Amine | Structure | Source | Purity (%) |
|---|--|----------------------|------------|
| Monoethanolamine (MEA) |  | Alfa Aesar | ≥99 |
| DL-1-Amino-2-propanol (1A2P) |  | Acros Organics | 94 |
| Ethylenediamine (EN) |  | Fisher Chemical | ≥99 |
| (3-aminopropyl)trimethoxysilane (3APT) |  | Alfa Aesar | 97 |
| 2-(Butylamino)ethanol (2BAE) |  | Aldrich Chemistry | ≥98 |
| N-Methyldiethanolamine (MDEA) |  | Aldrich Chemistry | ≥99 |
| Piperazine (PZ) |  | Oakwood Chemical | 99 |

2.2 Thermal Degradation

2.2.1 Sample Preparation

For the preparation of the aqueous amine solutions with CO₂, the targeted concentration was 30 wt% and a CO₂ loading ratio of 0.4 mol CO₂/mol amine was desired, as these are conventional parameters used for MEA in industrial practices.⁴ To accomplish this, each amine was individually added to a separate flask on a balance and 18.2 MΩ Milli-Q H₂O dispensed from a Q-pod manufactured by Millipore, was added to each solution to achieve an approximate concentration of 30 wt%. The following are the measured concentrations of each aqueous amine prepared: 30.8143 wt% MEA, 30.0343 wt% 1A2P, 30.0378 wt% EN, 30.1837 wt% 3APT, 30.1984 wt% 2BAE, 29.7817 wt% MDEA, and 29.7704 wt% PZ.

For the loading of CO₂, multiple calculations were accomplished to determine the amount of time required to bubble the CO₂ through the amine solution. The first step was to determine how much volume of CO₂ gas would need to be bubbled to produce the ratio 0.4 mol CO₂/mol amine. Since, the mass of the amine being used was known, the mass was converted to moles and the moles of CO₂ required was calculated for each amine using the ratio. The ideal gas law was then used with laboratory temperature and pressure during the time the sample was loaded. It is important to note that PZ started as a solid, and in order to dissolve, required heating around 25-30°C for the amount that was used for this research. Highly pure CO₂ from the Scott-Gross Company, Inc. was then bubbled into the solution by a mass flow

controller (GFC) from AALBORG at a rate of 0.5 L/min. The amount of time required for CO₂ bubbling was found by inverting the rate and then multiplying it by the volume of CO₂ to satisfy the targeted ratio. Each solution was capped and sealed with Parafilm "M" from American National Can until needed.

2.2.2 Thermal Degradation of Prepared Samples

Metal cylinders made of 316 steel with a length of 6.16" and width 1.00" and



Figure 2-1. Steel vessel used for housing the aqueous amine solutions loaded with CO₂ for thermal degradation.

HY-LOK 316 HML and 316 HBC 1/2" sealing caps were used as sample containment vessels. One end of the steel vessels was welded shut, leaving the other open for sample injection and vessel sealing, demonstrated by Figure 2-1. It is important to note that the threads of the metal vessel were wrapped with 1/2"x260" polytetrafluoroethylene (PTFE) Megatape designed for gas and water lines to prevent leaking.

Approximately 5 mL of each sample was individually measured out and placed in separate steel vessels. The steel vessels were then tightly sealed and placed in a VWR gravity convection oven with vacuum capabilities for thermal degradation. The pre-weighed samples were kept stagnant for one week at each temperature of 125°C,

135°C, and 145°C. After degradation, the samples were weighed and any sample with $\geq 2.5\%$ weight loss was excluded. However, it must be noted that the MEA sample degraded at 125°C gained a small amount of mass (0.09342%), which could have resulted from leftover waste in the oven from previous trials that leaked and went unnoticed during measurements. There are other possible sources for this error, however, due to the small mass change, the sample was believed to be viable and 5.324 g of the degraded MEA sample was transferred and collected for future measurements.

Each degraded solution was capped, sealed with Parafilm “M,” and placed in a refrigerator which held its temperature around 4.8°C to prevent further degradation. Table 2-2 demonstrates the labels associated with each degraded sample for referencing. Sample S is not included as it was a confirmation test of MEA at 145°C.

Table 2-2. Reference Letter for Each Degraded Sample.

| Amine | Temperature (°C) | | |
|-------|------------------|-----|-----|
| | 125 | 135 | 145 |
| MEA | A | E | I |
| 1A2P | B | F | L |
| EN | C | G | J |
| 3APT | D | H | K |
| 2BAE | M | P | T |
| MDEA | N | Q | U |
| PZ | O | R | V |

2.3 Nuclear Magnetic Resonance (NMR)

2.3.1 Sample Preparation

The degraded amine samples and parent amines for NMR analysis were prepared by loading NMR tubes that were approximately 7.10'' long, with about 1 cm of degraded solution and approximately 4 cm of deuterated chemical and capped on the open end. For samples that were highly concentrated, less than 1 cm of degraded sample was added, with the deuterated chemical added to have a total of 4 cm, however, slightly more deuterated chemical was added for further dilution of the sample if necessary. For all the samples except for those containing PZ, deuterium oxide from Acros Organics containing 99.8 atom % D, was used as the solvent. For the PZ samples, chloroform-d from Acros Organics containing 99.8 atom % D was used as the solvent as it demonstrated better dissolution capabilities for PZ compared to deuterium oxide at room temperature. It should be noted, that if a sample was prepared for NMR analysis and was unable to be analyzed the day of preparation, the sample was stored in a refrigerator around 4.8°C until analysis could be accomplished.

With each sample, except for the parent amines, water was present after degradation. A technique was used to try and remove the water, by evaporation of the water under a vacuum in a gravity convection oven at approximately 40°C, but this proved to further degrade the sample. Thus, the NMR samples were prepared with unaltered degraded species.

2.3.2 Analysis

After the preparation of samples, the samples were individually placed in an autosampler attached to the JEOL ECS-400 NMR instrument with multiple nuclei analysis capabilities demonstrated by Figure 2-2. With this NMR, ^1H , ^{13}C , DEPT-90, DEPT-135, and ^{15}N NOE was accomplished. The NMR probe was preset with an LF1 tune of 2681, an LF1 match of 3549, and the coarse at A, which allowed the analysis of ^1H , ^{13}C , DEPT-90, and DEPT-135. For ^1H NMR, the instrument operated at a frequency of 399.78 MHz, and for the analysis containing ^{13}C , the frequency was 100.53 MHz. However, for ^{15}N analysis, the LF1 tune was set to 5274, the LF1 Match to 4179, and the coarse was changed to C on the external dials of the NMR probe. The frequency used for ^{15}N NOE analysis was 40.51 MHz.



Figure 2-2. JEOL ECS-400 NMR instrument used for this research at Eastern Kentucky University in Richmond, KY.

2.3.3 Theory

For this discussion, the general theory for how NMR works will be introduced, as well as the theory behind the distortionless enhancement by polarization transfer (DEPT) and ^{15}N nuclear Overhauser effect (NOE). The nuclides and their natural abundance used for this research were; ^1H (99.9885%), ^{13}C (1.07%), and ^{15}N (0.368%).⁴³

NMR takes advantage of quantum mechanical and classical mechanical models by altering the intrinsic angular momentum of nuclei.⁴³ To begin, each nuclei will possess a nuclear spin angular momentum value, I , and a nuclear magnetic moment, μ .⁴³ For this specific research, $I=1/2$, is the nuclear spin angular momentum value for all of the nuclei used for analysis.⁴³ In assessing the nuclear magnetic moment, the analogy of a planet in the solar system with a nuclei is a useful technique, although, is not accurate relative to the actual occurrence. The imagery, which is a classical mechanical approach, is the spinning of nuclides about its μ -axis, while the nuclides also undergo a precession about, for the case of a magnetic, like NMR, the magnetic field B_0 .⁴³ The μ -axis is simply the vector of the net intrinsic angular momentum of each nuclei.⁴³

Moving into the magnetic field and the electrons, NMR takes full advantage of the different electron orientations; α and β . For α electrons, the quantum number, m , also referred to as electron spin, is denoted $m=1/2$, while β electrons have $m=-1/2$. This is important, as each electron will be in a different energy level, dependent on the m . With $I=1/2$, there will be two different energy levels, with α electrons occupying the

lowest energy state, and β the highest. The differences in the energy fields can be demonstrated by equation 2-1,

$$\Delta E = \left(\frac{h\gamma}{2\pi}\right) B_0 \quad (2-1)$$

where h is Planck's constant and γ is the nuclei specific magnetogyric ratio.⁴³ Equation 2-1 also demonstrates the proportionality between the energy change, ΔE , and magnetic field strength, B_0 . Each nuclei requires a specific radiofrequency that matches the required ratio for resonance of, $\frac{\gamma}{2\pi}$, to allow the transition of an electron in the lower energy state to the higher energy state.⁴³ For example, a ^1H nuclei would require a radiofrequency of 300 MHz.⁴³

For the acquisition of data by free induction decay (FID), the sample is pulsed quickly by a strong radiofrequency.⁴³ The excited nuclei would then precess about the direction of the magnetic field (z-axis), which would create a current that can be recorded.⁴³

After excitation, relaxation would occur, which effects the FID read-out.⁴³ Relaxation, is the occurrence of the excited nuclei returning to an equilibrium nuclear spin magnetization.⁴³ There are two different types of relaxations; longitudinal spin, or spin-lattice, and spin-spin.⁴³ Longitudinal spin relaxation is described by the Boltzmann distribution for the excited nuclides about the z-axis to re-establish equilibrium, while spin-spin relaxation deals with the xy-axes nuclides and is described by these nuclides approaching zero.⁴³ Spin-spin relaxation has a direct effect on the readout acquired by NMR.⁴³ Shorter FIDs and broader peaks are due to a faster spin-spin relaxation, and vice-versa.⁴³

Distortionless enhancement by polarization transfer (DEPT) uses the theory of NMR for analysis, however, it can determine the amount of hydrogens bonded to a ^{13}C nuclei.⁴³ The difference, is the variable proton pulse angle which can determine whether a -CH, -CH₂, -CH₃, or -C- groups is present.⁴³ The proton pulse angles used for this experiment, and are two of the most common DEPT analysis was DEPT-90 and DEPT-135 where the 90 and 135 represent angles.

The nuclear Overhauser effect (NOE) allows the determination of the proton environment around a specific nuclei.⁴³ For this research, ^{15}N NOE was used to evaluate the protons that are close to the nitrogen group(s). This is accomplished by cross-relaxation which is based on dipolar interactions between spins.⁴³ Using ^{15}N also allows the intensity to increase considerably with the presence of ^1H , without the need for ^{15}N doping due to the very low abundance of ^{15}N isotopes .⁴³

2.3.4 Objectives

The original objective for NMR analysis was to acquire spectral data that could be used to help with the structural determination of the degraded species with the results acquired from ion chromatography (IC), comparisons to be made between the parent amine and the degraded samples, and the comparison of ^1H and ^{13}C NMR spectra for a single species at the different degradation temperatures with the results acquired from HPLC. However, since the IC was unavailable for this research, the first original objective was discarded, but the last two were retained. The data that was to be used for comparisons with IC (^{15}N , Dept-90, and Dept-135) are included in this work

with the hope of future evaluation of the species present after degradation of the seven amines at varying temperatures.

2.4 High-Performance Liquid Chromatography (HPLC)

2.4.1 Dilutions

Stock samples of 30 wt% for the seven amines were prepared for dilution to enable the construction of a calibration curve. These sample must be produced exclusive from those already produced, to have 30 wt% solutions that did not contain CO₂ so that the concentration of the base amine in the degraded solution could be accurately determined. Beginning with the stock 30 wt% solutions, 100x dilutions by mass were accomplished for each solution for the first concentration for analysis. For example, 0.1109 g of 30 wt% MEA had 10.0279 g of 18.2 MΩ H₂O added to have approximately a 100x dilution factor. The dilution factor did not have to be exact, however, the concentrations of each were necessary to maintain and record for the successful construction of a calibration curve for each amine. The 30 wt% amines were then diluted by a further factor of 2x (total dilution factor of stock concentration by 200), 5x (500), 8x (800), and 10x (1000). The concentrations of each sample used for analysis with HPLC to produce a calibration curve is demonstrated by Table 2-3. It is important to note that the concentration of amine for the diluted solutions was determined by multiplying the mass of the 30 wt% solution measured by the concentration (0.30400 for MEA for example) to determine the mass of the MEA in the

homogeneous solution and then divided it by the mass summation of the 18.2 MΩ H₂O and then converting to wt%.

Table 2-3. Concentrations of the Diluted Pure Amines.

| Amine | Stock (wt%) | 100x (wt%) | 200x (wt%) | 500x (wt%) | 800x (wt%) | 1000x (wt%) |
|-------|----------------|---------------|---------------|---------------|---------------|----------------|
| MEA | 30.400 | 0.3336 | 0.148 | 0.0589 | 0.0375 | 0.0253 |
| 1A2P | 30.362 | 0.3247 | 0.158 | 0.0557 | 0.0378 | 0.0275 |
| EN | 30.461 | 0.3427 | 0.124 | 0.0576 | 0.0362 | 0.0331 |
| 3APT | 30.014 | 0.3154 | 0.138 | 0.0529 | 0.0389 | 0.0256 |
| 2BAE | 29.728 | 0.3339 | 0.127 | 0.0604 | 0.0373 | 0.0296 |
| MDEA | 30.087 | 0.3159 | 0.161 | 0.0603 | 0.0385 | 0.0297 |
| PZ | 30.388 | 0.3880 | 0.175 | 0.0604 | 0.0356 | 0.0300 |

For the dilution of the degraded amine solutions, an initial dilution of 100x was accomplished, exactly like the preparations with the 30 wt% amine solutions. If the sample was still too concentration, a similar dilution factor would be applied, stepwise, until the solution was dilute enough for HPLC analysis.

Demonstrated by Table 2-3, as the dilution factor got larger, the significant figures dropped, and the dilution become more difficult, as the dilutions were made inside of the containment vessels for storage. These vessels could only hold between 20-25 g of H₂O making the dilutions require very small portions of sample for dilution. After the dilution of each sample, each were sealed with Parafilm and placed in a refrigerator at approximately 4.8°C until analysis was conducted.

2.4.2 Analysis

For HPLC analysis, the procedure used in the dissertation research by Huang was used for this research as it was proven to work well.⁴ After the preparation of samples, the samples were individually placed in a small vial specifically designed to fit in the autosampler of an Agilent 1260 Infinity II HPLC instrument demonstrated by Figure 2-3. The mobile phase mixture was produced with 90.0 mL 18.2 MΩ H₂O, 10.0 mL methanol, and about two small drops of formic acid, where more of the same quantity was produced as needed. The methanol and formic acid used were redistributed by the Eastern Kentucky University chemical storage facility. A Polaris 3μm C₁₈-A 50 × 3.0 mm column was used with the reverse phase Agilent 1260 Infinity II HPLC. As with previous research, the flow rate was set to 0.3 mL/min and the injection



Figure 2-3. Agilent 1260 Infinity II HPLC instrument used for this research at Eastern Kentucky University in Richmond, KY.

volume at 5 μ L. The total run time that was used for this research was 10 min, with the column temperature being that of room temperature during the time of operation.

2.4.3 Theory

The general idea for how a reversed-phase HPLC works, is by the entrance of a polar mobile phase by a pump which will push the mobile phase to the injection port where the analyte is injected. At this point, the analyte and the mobile phase will pass through a nonpolar column, which leads to the separation of the analyte. The column, while more detail will be explained in this section, is housed in a column oven, allowing the temperature to be increased if necessary. The separated species is then brought to a detector, a photodiode array detector for this discussion, and the intensity versus retention time chromatogram for the separated analyte is displayed.

It was mentioned that there is a column oven associated with the reversed-phase HPLC. By using the column oven, it can reduce the pressure needed to push the mobile phase and analyte through the column by decreasing the viscosity of the solvent, decrease the retention time, and increase the flow rate.⁴⁴ However, if reproducible retention times are required for comparisons, the heating of the column is not advised.⁴⁴

With the column itself, the inside of the column has a microporous silica coating.⁴⁴ Attached to the silica coating, is a stationary phase, for this specific column, C₁₈. For reversed-phase liquid chromatography, a polar mobile phase flowing through a nonpolar stationary phase, thus, C₁₈, a nonpolar species, makes for an excellent

stationary phase. As a result, when the analyte contains a more nonpolar species, the nonpolar species will have a longer retention time due to interactions with the stationary phase, as opposed to polar species which would have a quicker retention time.⁴⁴ Thus, with reversed-phase liquid chromatography, the more polar species will elute first, followed by slightly polar species, and lastly by nonpolar species.⁴⁴

After the separated analyte passes through the column, it is passed through a flow cell before going to waste. During the time in the flow cell, transmitted light from a deuterium lamp is reflected from an elliptical mirror and is passed through the flow cell.⁴⁴ The light travels through the species in the flow cell and passes through a thin slit to a second mirror that gets reflected to a grating polychromator, and finally being recorded by a photodiode array.⁴⁴

The photodiode array allows the quick analysis of a complete spectrum for the separated species as they enter the flow cell.⁴⁴ This is possible because of the current that is generated when the light that passed through the flow cell reaches the photodiode array.⁴⁴ Before the light reaches the photodiode, reverse bias is applied to each diode consisting of *p*-type and *n*-type silicon.⁴⁴ The reverse bias allows the production of a *pn* junction that acts as a capacitor that, in the absence of light, will only have a small amount of dark current present.⁴⁴ Thus, when the light hits the diodes, the *pn* junction will discharge due to the movement of free electrons and free holes to oppositely charged regions.⁴⁴

2.4.4 Objectives

The objectives for HPLC analysis was to allow the approximate determination of the quantity of species present in the degraded solution, be able to determine the concentration of the original amine species present after degradation, and then to use thermodynamic techniques to determine the rate order and the thermal degradation activation energy of each amine. Since, IC was not possible in this research, future research endeavors could use the approximate quantity of species present in the degraded solutions for the determination of what species are giving rise to the signals acquired in this research. The concentration of the original amine species present after degradation was determined using a calibration curve, which then made thermodynamic evaluations possible.

2.5 Computational Details

2.5.1 Avogadro and the Universal Force Field

The molecular models of the pure amines, CO₂, H₂O, bicarbonate, and the neutral molecule of the CO₂ captured amines (carbamates), with the exception of protonated MDEA, was constructed using Avogadro, an open source molecular editor and visualization tool.⁴⁵ After the construction, each atom making up the molecule was organized according to the Universal Force Field (UFF) developed by Rappé et al.⁴⁶ The main goal of UFF is the minimization of the potential energy of a molecule under the parameters set by UFF. To begin, the overall calculation for the potential energy of a molecule is represented by equation 2-2,

$$E = E_R + E_\theta + E_\phi + E_\omega + E_{vdw} + E_{el} \quad (2-2)$$

where E_R represents the bond stretching interactions, E_θ represents bond angle bending interactions, E_ϕ represents dihedral angle torsion, E_ω represents inversion terms, E_{vdw} represents van der Waals interactions, and E_{el} represents electrostatic interactions.⁴⁶

With the overall equation representing the potential energy calculation, the individual components that give rise to the value will be defined, beginning with the bond stretching interactions, followed by the bond angle bending interactions and then the rest following the order.⁴⁶ With the bond angle bending interactions, there are two different methods used for calculation, one is by treating the system as a harmonic oscillator (equation 2-3), and the other as a Morse function (equation 2-4).⁴⁶

$$E_R = \frac{1}{2}k_{IJ}(r - r_{IJ})^2 \quad (2-3)$$

$$E_R = D_{IJ}[e^{-\alpha(r-r_{IJ})} - 1]^2 \quad (2-4)$$

From equation 2-3, the k_{IJ} term represents the force constant, r_{IJ} is the natural bond length (described by equation 2-5 where the r_I and r_J terms are atom and bond specific, while r_{BO} [the bond order correction] and r_{EN} [the electronegativity correction] are described by equations 2-6 and 2-7 respectively), which is also present in equation 2-4.⁴⁶

$$r_{IJ} = r_I + r_J + r_{BO} + r_{EN} \quad (2-5)$$

$$r_{BO} = -\lambda(r_I + r_J) \ln(n) \quad (2-6)$$

With equation 2-6, λ represents a proportionality constant.⁴⁶

$$r_{EN} = r_I r_J \frac{(\sqrt{x_I} - \sqrt{x_J})^2}{(x_I r_I + x_J r_J)} \quad (2-7)$$

The D_{IJ} term in equation 2-4, represents the bond dissociation energy and the α term is described by equation 2-8.⁴⁶

$$\alpha = \left[\frac{k_{IJ}}{2D_{IJ}} \right]^{\frac{1}{2}} \quad (2-8)$$

It was previously stated that k_{IJ} represents a force constant, which will now be defined by equation 2-9 as,

$$k_{IJ} = \left(\frac{\partial^2 E_r}{\partial R^2} \right)_0 = 664.12 \frac{Z_I^* Z_J^*}{r_{IJ}^3} \quad (2-9)$$

where the Z^* terms represent the effective atomic charges.⁴⁶

The next interaction that will be defined is that of bond angle bending demonstrated by equation 2-10,

$$E_\theta = K_{IJK} \sum_{n=0}^m C_n \cos n\theta \quad (2-10)$$

where C_n is a boundary condition which is dependent upon the existence of a minimum at the natural bond angle ϑ_0 .⁴⁶ While there are multiple Fourier expansions that depend upon the molecule in question, only the simplest form will be demonstrated here by equation 2-11 through 2-13.⁴⁶

$$E_\theta = K_{IJ} [1 + \cos(p\theta + \Psi)] \quad (2-11)$$

$$p = \frac{\pi}{(\pi - \theta_0)} \quad (2-12)$$

$$\Psi = \pi - p\theta_0 \quad (2-13)$$

The K_{IJ} term is a force constant, and is described by equation 2-14,

$$K_{IJ} = \left(\frac{\partial^2 E}{\partial \theta^2} \right)_0 = \beta \frac{Z_I^* Z_K^*}{r_{IK}^5} r_{IJ} r_{JK} [r_{IJ}^3 r_{JK} (1 - (\cos \theta_0)^2) - r_{IK}^2 \cos \theta_0] \quad (2-14)$$

where β is an undetermined parameter that is best described by equation 2-15.⁴⁶

$$\beta = \frac{664.12}{r_{IJ}r_{JK}} \quad (2-15)$$

The dihedral angle torsion interactions are defined by equation 2-16,

$$E_{\varphi} = K_{IJKL} \sum_{n=0}^m C_n \cos n\varphi_{IJKL} \quad (2-16)$$

where K_{IJKL} and C_n are coefficients which are dependent upon V_{φ} , the equilibrium angle and the periodicity of the potential, which are defined by equation 2-17 and 2-18.⁴⁶

$$C_n = -\cos n\varphi_0 \quad (2-17)$$

$$K_{IJKL} = \frac{1}{2}V_{\varphi} \quad (2-18)$$

With equation 2-17 and 2-18, equation 2-16 could be rewritten as equation 2-19.⁴⁶

$$E_{\varphi} = \frac{1}{2}V_{\varphi}[1 - \cos n\varphi_0 \cos n\varphi] \quad (2-19)$$

The general equation for the interactions of the inversion terms can be expressed by equation 2-20,

$$E_{\omega} = K_{IJKL}(C_0 + C_1 \cos \omega_{IJKL} + C_2 \cos 2\omega_{IJKL}) \quad (2-20)$$

where K_{IJKL} is a force constant, and ω_{IJKL} represents the angle between the IL axis and IJK plane.⁴⁶ Equation 2-20 could be rewritten in terms of a normal to the IJK plane and the IL axis, however, this will not be demonstrated here.

The van der Waals interactions are defined by equation 2-21,

$$E_{vdw} = D_{IJ} \left\{ -2 \left[\frac{x_{IJ}}{x} \right]^6 + \left[\frac{x_{IJ}}{x} \right]^{12} \right\} \quad (2-21)$$

where x_{IJ} is the van der Waals bond length, with the Lennard-Jones distance being described by equation 2-22, and the crystalline van der Waals terms by equation 2-23,

and D_{IJ} is the well depth, defined by equation 2-24 where D_I represents the atomic van der Waals energy.⁴⁶

$$x_{IJ} = \frac{1}{2}(x_I + x_J) \quad (2-22)$$

$$x_{IJ} = \sqrt{x_I \times x_J} \quad (2-23)$$

$$D_{IJ} = (D_I D_J)^{\frac{1}{2}} \quad (2-24)$$

For a more in-depth analysis of the van der Waals interactions and the derived variables, reference (46) is suggested.

Finally, the electrostatic interactions are defined by equation 2-25,

$$E_{el} = 332.0637 \left(\frac{Q_i Q_j}{\epsilon R_{ij}} \right) \quad (2-25)$$

where Q represents the charge, ϵ is the dielectric constant, and R_{ij} represents the distance between the two charged particles.⁴⁶

2.5.2 Gaussian 09 with GaussView

Following the construction and organization of the molecules, each molecule file was extracted into a Gaussian 09 readable file. The calculation set up was then formed, with the basis set as 6-311++G(d,p). Density Functional Theory (DFT) with the B3LYP functional with the parameters: unrestricted, ground state, and with anharmonic corrections was used for optimization and frequency calculation for the molecules. The spin was dependent upon on the molecule, but each molecule was optimized with the solvation model Polarizable Continuum Model (PCM) and the solvent set to H₂O (CO₂ with both a solvation and gas phase model). The frequency and

optimization of each molecule, that was able to be run, was accomplished with these parameters and methods using Gaussian 09 with GaussView, like the computational methodology that was performed by Yamada, Yamada et al., and Hwang et al.^{26,32,47-48}

2.5.3 DFT, B3LYP, Basis Set, and Thermochemistry in Gaussian 09

The overarching idea of DFT is that with a known density, a Hamiltonian could be formed, and with the formation of a Hamiltonian, the Schrödinger equation could be solved giving the energy eigenvalues and the wave functions.⁴⁹ With DFT however, the B3LYP functional was utilized, which is an Adiabatic Connection Method (ACM) which connects the non-interacting Kohn-Sham (KS) reference system with an interacting system.⁴⁹ For this system, the exchange-correlation energy is calculated as demonstrated by equation 2-26,

$$E_{xc} = \int_0^1 \langle \Psi(\lambda) | V_{xc}(\lambda) | \Psi(\lambda) \rangle d\lambda \quad (2-26)$$

where the extent of the interelectronic interaction from 0 to 1 is represented by λ , and the expectation value of V_{xc} is the area under the curve for the integrated function.⁴⁹

The V_{xc} term is defined by KS methodology with equation 2-27,

$$V_{xc} = \frac{\partial E_{xc}}{\partial \rho} \quad (2-27)$$

with the Greek letter ρ representing the electron density.⁴⁹ From the evaluation of the curve produced by the integral, the total area under the curve could then be defined by equation 2-28,

$$E_{xc} = E_x^{HF} + z(E_{xc}^{DFT} - E_x^{HF}) \quad (2-28)$$

where z is a fraction of the area above the curve, and HF refers to the Hartree-Fock theory.⁴⁹ The fraction, z , is usually defined in terms of a , which is defined by $1-z$ and equation 2-28 can then be rewritten as equation 2-29, which brings the connection between the non-interacting system with the interacting system.⁴⁹

$$E_{xc} = (1 - a)E_{xc}^{DFT} + aE_x^{HF} \quad (2-29)$$

Specific to the B3LYP functional, is equation 2-30, a modified form of equation 2-29.⁴⁹

$$E_{xc}^{B3LYP} = (1 - a)E_x^{LSDA} + aE_x^{HF} + b\Delta E_x^B + (1 - c)E_c^{LSDA} + cE_c^{LYP} \quad (2-30)$$

With equation 2-30, a is 0.20, b is 0.72, c is 0.81, $LSDA$ represents local spin density approximation, LYP represents a GGA correlational functional, and B represents a GGA exchange functional that was developed by Becke.⁴⁹ For more information on DFT and DFT functionals, reference (49) is suggested.

With the basis set, a general overview on what the individual components represent will be discussed here. The basis set used was 6-311++G(d,p), which defines the contraction scheme, coefficients, and exponents for each atom of the molecule under study.⁴⁹ Since the first number is 6, there will be 6 *primitives*, which are nonlinear differential equations, used in the contracted core functions.⁴⁹ The numbers after the hyphen, 311, indicates that there is a triple valence function indicated by ζ (triple-valence- ζ), where the number of primitives applied to the valence function is indicated by the numbers after the hyphen, 311.⁴⁹ The ++ part of the basis set places diffuse functions with the operation which allows a weakly-bound electron to be more flexible in the sense that it has the ability to localize away from the remaining electron

density.⁴⁹ Finally, the G(d,p) term in the basis set indicates that the d and p orbitals are being treated as Gaussian orbitals.⁴⁹

A detailed example for how thermodynamic quantities could be calculated using Gaussian 09 is described in reference (50). For the discussion on the thermochemistry readout from the output file, the variables of interest will be discussed and how they were used for calculations. These terms include: the zero-point vibrational energy, sum of electronic and thermal free enthalpies, and sum of electronic and thermal free energies.⁵⁰ With each term, equation 2-31, 2-32, and 2-33 were used for the individual reactions to find the CO₂ binding energy (ϵ_{bind}), $\Delta_r H$, and $\Delta_r G$ respectively.⁵⁰

$$\epsilon_{bind} = \sum \epsilon_{ZPE_{products}} - \sum \epsilon_{ZPE_{reactants}} \quad (2-31)$$

$$\Delta_r H = \sum (\epsilon_0 + H_{corr})_{products} - \sum (\epsilon_0 + H_{corr})_{reactants} \quad (2-32)$$

$$\Delta_r G = \sum (\epsilon_0 + G_{corr})_{products} - \sum (\epsilon_0 + G_{corr})_{reactants} \quad (2-33)$$

With equation 2-31, ϵ_{ZPE} represents the zero-point vibrational energy and with equation 2-32 and 2-33, the terms $\epsilon_0 + H_{corr}$ and $\epsilon_0 + G_{corr}$ represent the sum of electronic and thermal enthalpy and thermal free energies respectively.⁵⁰

2.5.4 Objectives

The objectives with the computational analysis was to compute values from equation 2-31 through 2-33 for each reaction between the amines and CO₂. Also, using equation 2-31, the release of CO₂ and the regeneration of the amine was attempted. With these values, the seven amines would be compared to each other, along with the

thermal degradation activation energy and extent of degradation acquired from HPLC, to determine if any correlation could be made. This was completed to determine if computational analysis could be used to predict which amine would be more susceptible of degradation over another based on the computational model used in this work.

Chapter 3. Degraded Solutions and NMR Evaluation

“What we observe is not nature itself, but nature exposed to our method of questioning.” -Dr. Werner Karl Heisenberg

3.1 Thermal Degradation Solution Appearances and Descriptions

3.1.1 Sample Appearances

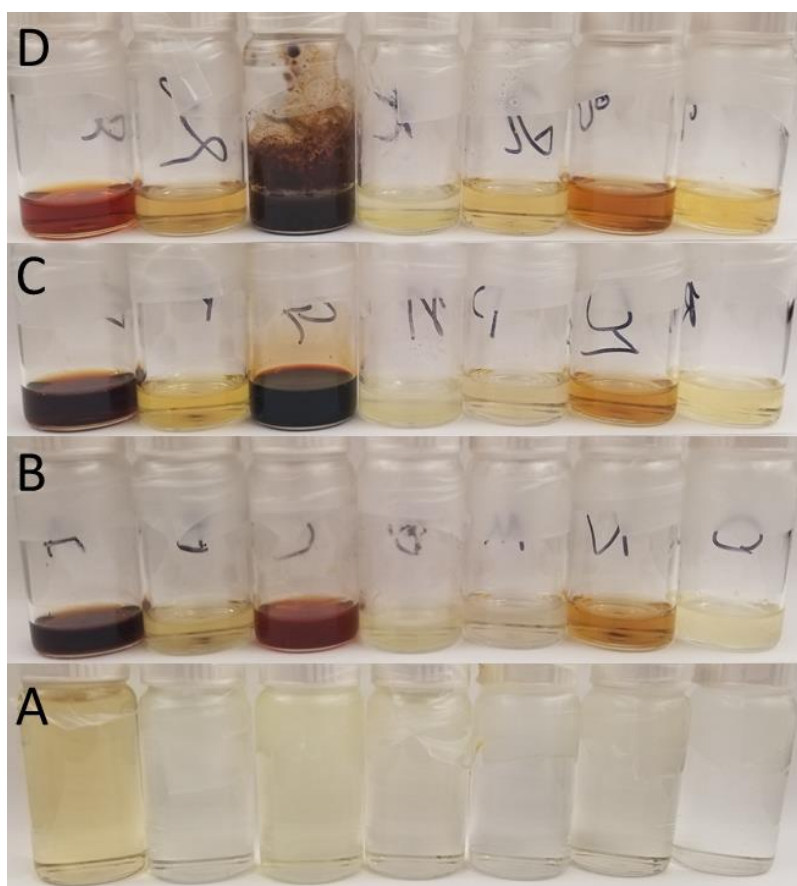


Figure 3-1. Starting on the left and going right the amines are: MEA, 1A2P, EN, 3APT, 2BAE, MDEA, PZ. A.) The stock solutions of CO₂ loaded amines before degradation. B.) Degradation at 125°C. C.) Degradation at 135°C. D.) Degradation at 145°C.

The appearances of the amines loaded with CO₂ before and after degradation at the different temperatures are demonstrated by Figure 3-1. In relation to the CO₂

loaded amines, the samples pictured are approximately two months old. It is important to note that they were all colorless solutions when they were first produced, but after being stored at room temperature in an undisturbed dark environment, slight coloration began to appear. However, MEA began to get a tint of color after one day and got darker as shown in Figure 3-1A. Also, with Figure 3-1A-D, as the temperature increased, the solution produced became darker, or stayed about the same. The only exception being with MEA, where the solution was about the same color after 125°C and 135°C, but became lighter after 145°C. With this exception, and the fact that the rest of the amines, excluding EN which showed significant degradation and is hypothesized to be the most degraded species used, other hypothesis could not be evaluated besides that most of the amines appeared to have degraded about the same degree with the others based on their appearances.

3.1.2 Sample Descriptions

With the samples pertaining to MEA (A, E, and I), the only differences between the samples was the color change and murkiness. Sample A was a red velvet, E a dark red velvet, and I a golden red-orange color. Each sample had low viscosity and a weak odor.

For the degraded samples of 1A2P, the individual samples were analyzed. Sample B and F had a faint yellow tint, a small black precipitate in the center of the solution with a faint thread-like material floating around the spot and possessed a low viscosity but had a strong odor. However, Sample L had a slight difference to it, being a

more prominent yellow, possessed no black spot, but had stray precipitates present including small black specks suspended in the solution, a low viscosity and a strong odor.

EN was an interesting case with degradation. Sample C was a blood-red color, which had some precipitates settled on the bottom of the vial, which dissipated after agitation of the solution, had a low viscosity and a low odor. Sample G was a black solution but had a red tint around the upper outer edges of the liquid surface, this sample had a sludge likeness to it, with low viscosity, and a medium odor. With sample J however, the sample was dark black, being a type of sludge that had a high viscosity and a weak odor. Upon agitation of sample J, the precipitates present were deposited upon the sides of the vial.

All the samples for 3APT possessed the sample properties, except for the slight color change from a light yellow-green tint to a more defined yellow-green color. The samples had a thick white gel-like precipitate which hovered slightly below the surface of the solution, and having a medium viscosity for each, but the viscosity increased slightly with the increasing temperatures, and a strong odor.

The samples of degraded 2BAE will be described individually as each one has a slight difference from the others. Sample M was a light yellow-green color with a low viscosity and medium odor. Sample P was a pale yellow-green color that also possessed a low viscosity but had a strong odor. The most significant difference lies within Sample T which was a clear yellow color and had a transparent oil-like

precipitate present, that would dissipate after agitation, with low viscosity and a strong odor.

MDEA samples (N, Q, and U) were nearly identical, except for a few differences which will be described. Sample U was a dark golden yellow color while samples N and Q were golden yellow. Samples N and Q also had a black spot, which was darker for N than Q, which had a precipitate thread coming off the spot. Sample U also had the black spot; however, no precipitate thread was noticed. Each sample had a low viscosity, with an increase in odor with increasing degradation temperature (N had a medium odor, Q and U had a strong odor).

Finally, the PZ samples (O, R, and V) were analyzed. Sample O was cloudy and colorless. There were shard-like precipitate present throughout the solution, which was hypothesized to have been liberated PZ due to the shards dissolving upon the warming up of the solution, much like the properties of PZ. The sample had a medium odor and was low to medium viscosity due to the precipitate and would be considered low viscosity if the precipitate was not present. Sample R was nearly identical to sample O except for being a cloudy, pale-yellow color, with a strong odor. Sample V was a near colorless pale-yellow color, which did not have a noticeable precipitate present in the solution, with a low viscosity and a strong odor.

3.2 NMR Analysis

3.2.1 Overview

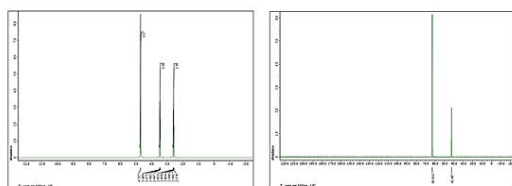
For the analysis with NMR, the ^1H and ^{13}C spectra will be used, with the DEPT-90, DEPT-135, and ^{15}N NOE spectra.* Since, structural identification could not be accomplished in this research, the hope is that these spectra could be useful for helping with the identification of the species present after degradation in future work. However, this section will present and use the ^1H and ^{13}C spectra for each species to approximate the extent of degradation for each amine at the different temperatures.

3.2.2 ^1H and ^{13}C analysis

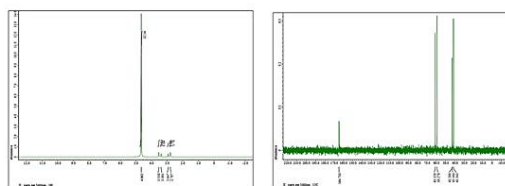
Each amine and their degraded samples will be presented in order. For example, when MEA is presented, the following data presented will be MEA degraded at 125°C , and so on. The ^1H for each sample will be positioned adjacent to the ^{13}C data of the same sample. Figure 3-2 through Figure 3-8 presents the data acquired for each of the parent amines followed by degradation at 125°C , 135°C , and 145°C .

* These spectra can be found in Appendix A-G.

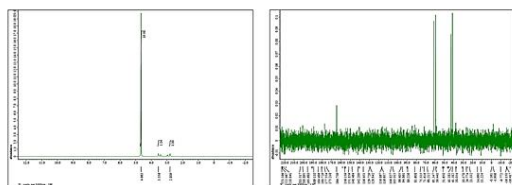
MEA



A



E



I

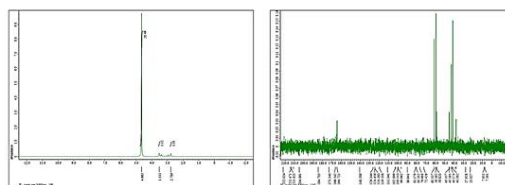
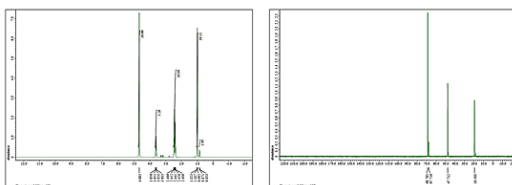
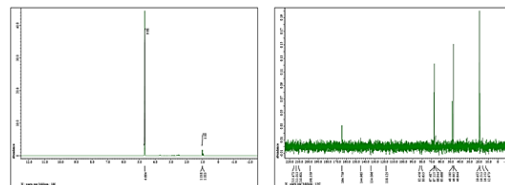


Figure 3-2. ^1H and ^{13}C NMR data acquired for MEA and its degraded samples. MEA is labelled, and the letters indicate the degraded sample.

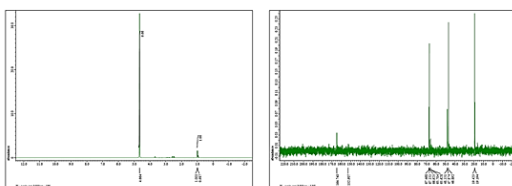
1A2P



B



F



L

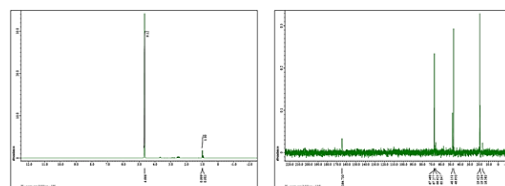
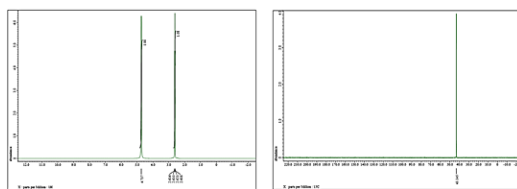
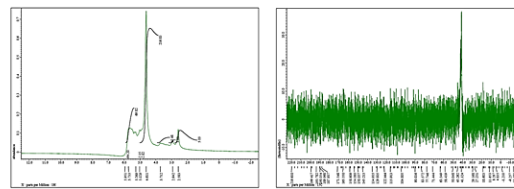


Figure 3-3. ^1H and ^{13}C NMR data acquired for 1A2P and its degraded samples. 1A2P is labelled, and the letters indicate the degraded sample.

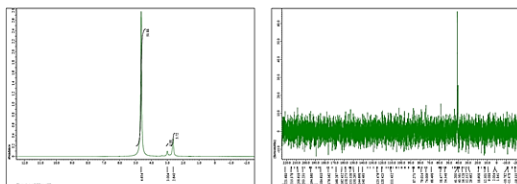
EN



C



G



J

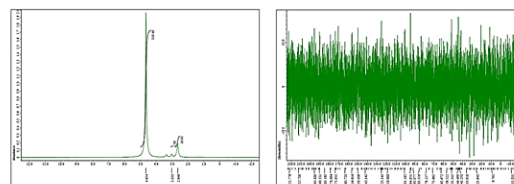
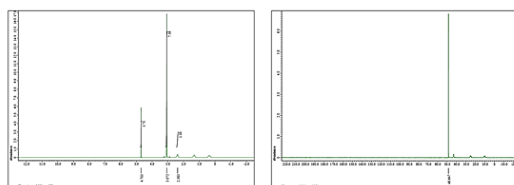
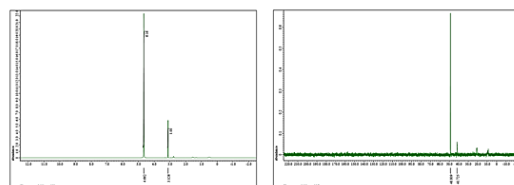


Figure 3-4. ^1H and ^{13}C NMR data acquired for EN and its degraded samples. EN is labelled, and the letters indicate the degraded sample.

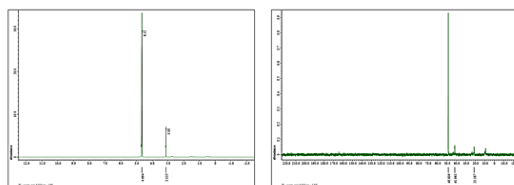
3APT



D



H



K

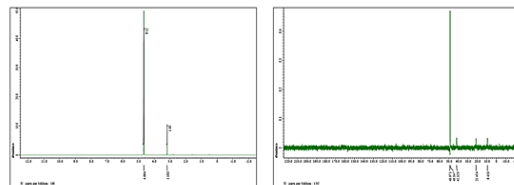
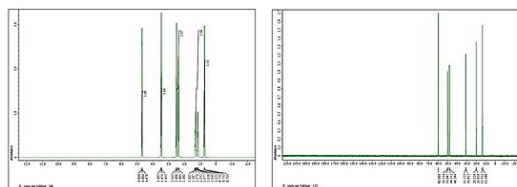
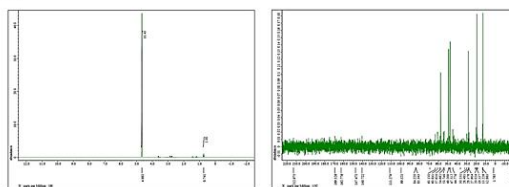


Figure 3-5. ^1H and ^{13}C NMR data acquired for 3APT and its degraded samples. 3APT is labelled, and the letters indicate the degraded sample.

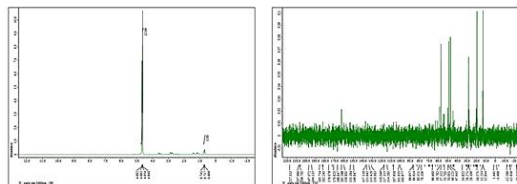
2BAE



M



P



T

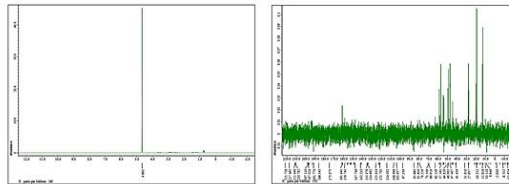
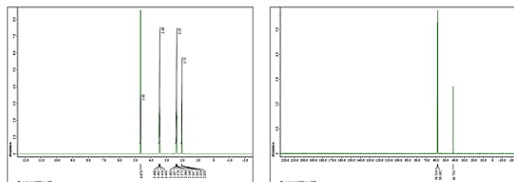
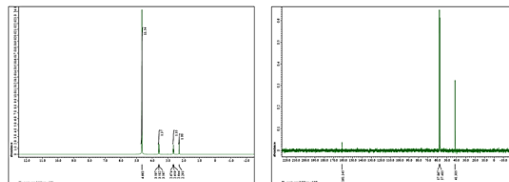


Figure 3-6. ^1H and ^{13}C NMR data acquired for 2BAE and its degraded samples. 2BAE is labelled, and the letters indicate the degraded sample.

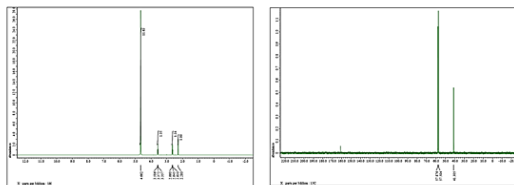
MDEA



N



Q



U

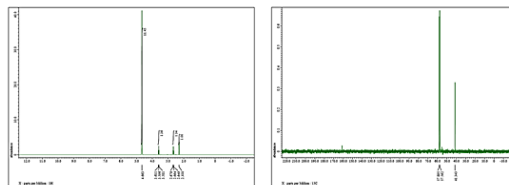


Figure 3-7. ^1H and ^{13}C NMR data acquired for MDEA and its degraded samples. MDEA is labelled, and the letters indicate the degraded sample.

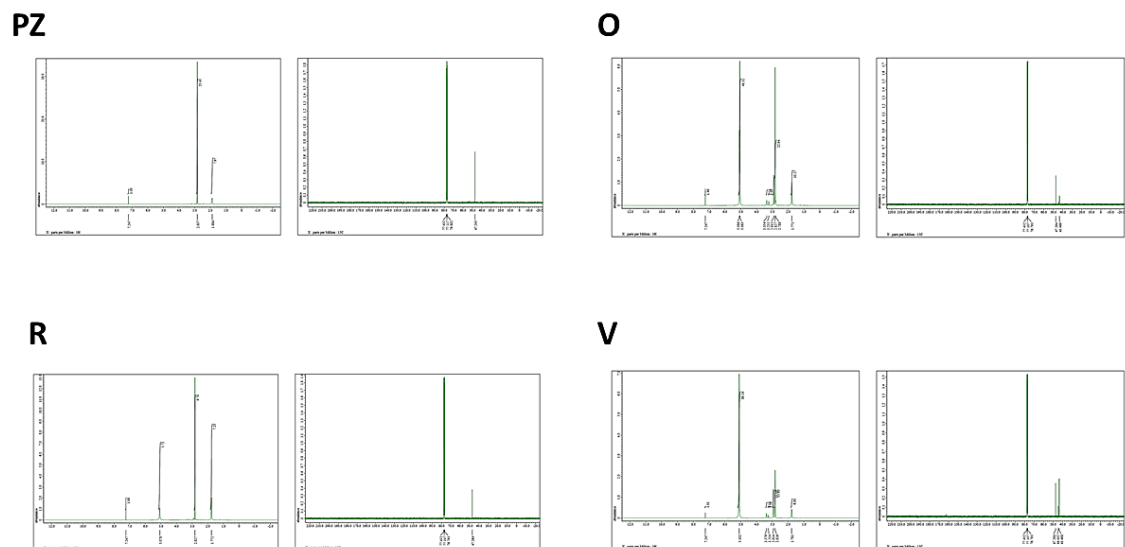


Figure 3-8. ^1H and ^{13}C NMR data acquired for PZ and its degraded samples. PZ is labelled, and the letters indicate the degraded sample.

As demonstrated by Figure 3-2 through 3-8, the ^1H spectra from each species demonstrated the hydrogens associated with the nitrogen atom to be dominant when degradation took place. In cases like 1A2P, Figure 3-3, the peaks were reduced considerably except for the N-H peak, which had clear superiority. In other cases, like PZ, Figure 3-8, the N-H peaks are still dominant, however, more hydrogen peaks emerged. These patterns were demonstrated for each amine, and since characterization of the other peaks was not possible, structural data on species produced by degradation could not be obtained.

The ^{13}C peaks however, provided more information that could be compared across the amines used in this research. This was accomplished by counting significant peaks, peaks that were distinguishable from the baseline noise, and taking the difference of the number of ^{13}C peaks from the parent amine peaks. This allowed a comparison between the ^{13}C peaks, denoted $\Delta^{13}\text{C}$, giving an idea of how many

different carbon environments arose out of degradation, and thus provide a relative approximation of how much the amine degraded at the different temperatures. This was possible for each amine, except that of EN which had indistinguishable ^{13}C peaks. With this method, the following ranking of the amines from most degraded to least was acquired: EN>2BAE>MEA>1A2P>PZ>MDEA>3APT.

3.3 Summary of Key Results

The appearance of the amines, their viscosity, and odor could be used as a possible indication of both degradation and if it would be appropriate for CO_2 . For example, EN and MEA had the most significant color change and from this, could infer that they degraded more than the amines that stayed approximately the same color. In terms of viscosity, more so for 3APT, a highly viscous amine would not be ideal as this could increase the costs of operation and be more difficult to remove from the system. Especially, since 3APT demonstrated a higher viscosity as the temperature increased, indicating the degradation species have a higher viscosity than 3APT, which would not be a good choice for post-combustion CO_2 capture. In terms of odor, if the odor becomes stronger, this could be an indication of degradation. In the case of 2BAE, the odor went from a medium odor, to a much stronger odor as the temperature increased, indicating further degradation with the production of species containing functional groups that could increase the odor, such as ureas or aldehydes.

^1H NMR results could not be distinguished for comparisons amongst the amines, possibly due to the production of polymeric compounds, however, ^{13}C was able to provide a method of comparisons. This was accomplished by calculating the

$\Delta^{13}\text{C}$ values for each amine and their respective degraded samples. Using this method provided a ranking from the most degraded to the least as:

EN>2BAE>MEA>1A2P>PZ>MDEA>3APT, which is reasonable. These findings, however, could not be deemed conclusive as this only provided different carbon environments and not concentrations. Concentrations were needed to evaluate the extent of degradation for each amine at the different temperatures.

Chapter 4. HPLC Concentrations of Each Amine and Kinetics Study on MEA, MDEA, and PZ

4.1 Introduction

The organization of this chapter begins by first demonstrating and discussing the calibration curves with the concentrations calculated as well as an approximate quantity of species present for each temperature degradation using the equation of the line produced from the calibration curves for each amine. Each amine will have its own subsection for organization and quick comparisons between the amines studied. Following this section, is the discussion of the calculated thermal degradation activation energies for MEA, MDEA, and PZ. The end of the chapter summarizes key findings from the analysis with HPLC.

For the first section, with MEA, extra information is given and can be used for each amine, and thus will not be repeated. Any information specific to the amine of interest will be discussed in that amines' subsection.

4.2 Experimental

4.2.1 Monoethanolamine

The calibration curve produced for the different diluted samples of MEA with 18.2 MΩ H₂O is demonstrated by Figure 4-1. The calibration curve demonstrated an exceptional linearity between the concentration of MEA at the specified concentration and the corresponding peak area. Using the equation of the line produced from Figure

4-1, the concentration of MEA after a one-week period of degradation at 125°C, 135°C, and 145°C was accomplished, and is demonstrated by Figure 4-2.

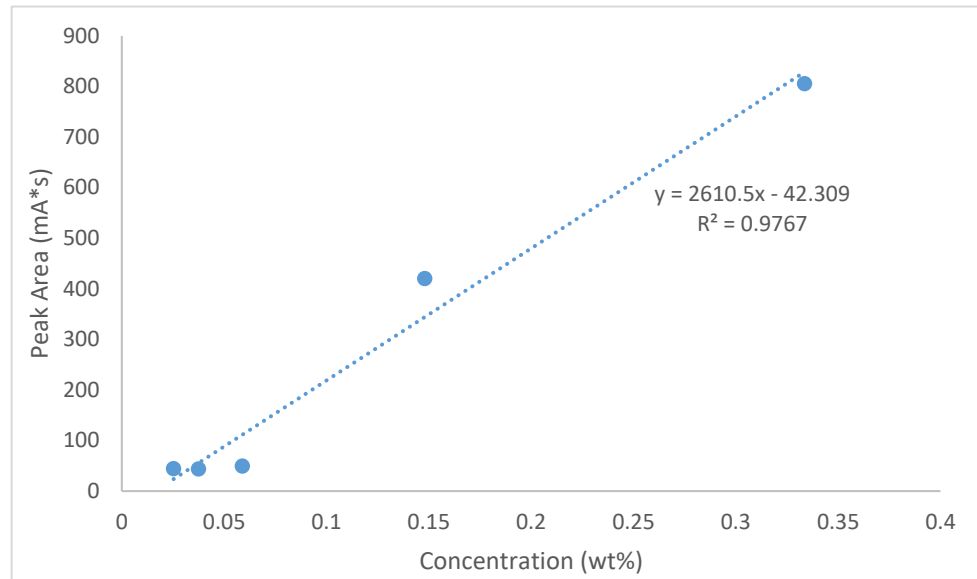


Figure 4-1. Calibration Curve for MEA.

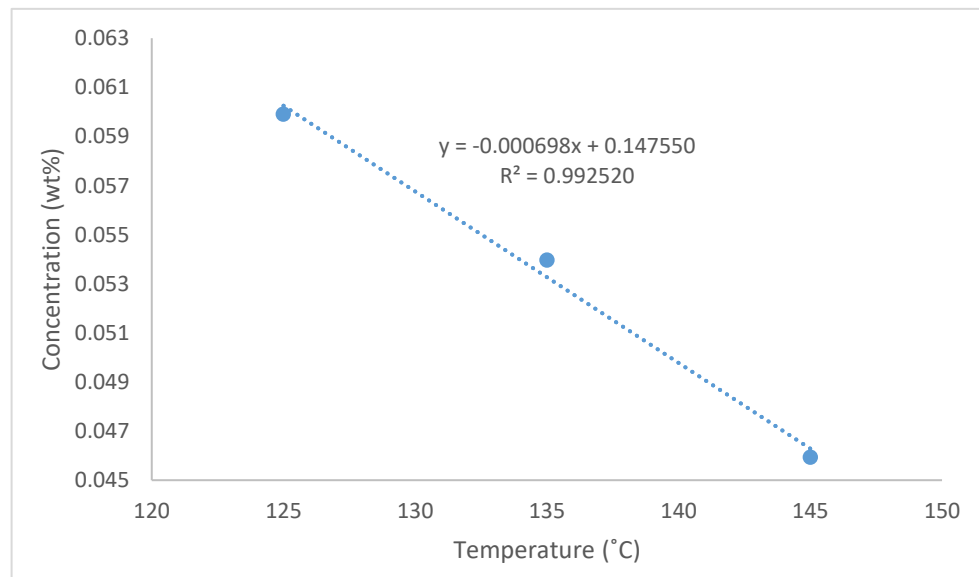


Figure 4-2. Demonstration of the concentration of MEA after degradation at different temperatures.

From Figure 4-2, the expected relationship for the concentration of MEA after degradation at the different temperatures was observed. With a higher temperature, more MEA was lost. The concentration of MEA steadily decreased at a rate of approximately -6.98×10^{-4} wt%/°C. It is important to note that each degraded sample was diluted with the same dilution factor (100x for MEA samples) to allow proper comparisons amongst the degraded samples. With this rate however, it is important to understand that this rate cannot be used as an overall statement for the decrease in MEA concentration. This rate is only for the comparison for the different concentrations after degradation at the specified temperatures. This because, the loaded amine species could have a rapid degradation within the first few days and then start to level out as demonstrated in the work by Perry et al.⁴¹ While Perry et al. studied the depletion of aminosilicone carbamates over a much longer time span than a week, the data demonstrated a rapid depletion of the amine within the first ten days using 100% carbamate loading with no additional water in the system.⁴¹ Because of this, the rate of depletion for MEA from Figure 4-2 can only be used for comparisons between 125°C, 135°C, and 145°C.

For the approximate quantity of species present after degradation, any distinguishable peak in the HPLC chromatogram was used to determine the approximation excluding the peak for MEA. For sample A and E, approximately six species are present, and for sample I, approximately eight species are present. A better approximation for the determination of the quantity of degradation products could be determined by using a more concentrated sample for HPLC analysis, however,

since no further investigation could be accomplished with the quantity of species after degradation, it is left here for future research into the matter.

4.2.2 1-Amino-2-propanol

The calibration curve for the different dilutions of 1A2P is demonstrated by Figure 4-3. Using the calibration curve, the concentrations for the degraded samples (dilution factor 100x) was accomplished and is demonstrated by Figure 4-4. As demonstrated by Figure 4-4, the approximate rate of 1A2P loss was $-0.0377 \text{ wt\%/}^\circ\text{C}$. This rate is higher than that of MEA, which upon first appearance, it may be believed that MEA degrades less than 1A2P. However, the wt% values for 1A2P are higher than that of MEA, thus demonstrating that MEA degrades more than 1A2P. This further demonstrates that the slope produced can only be used to demonstrate the relationship between the concentrations degraded at the different temperatures for the amine of interest.

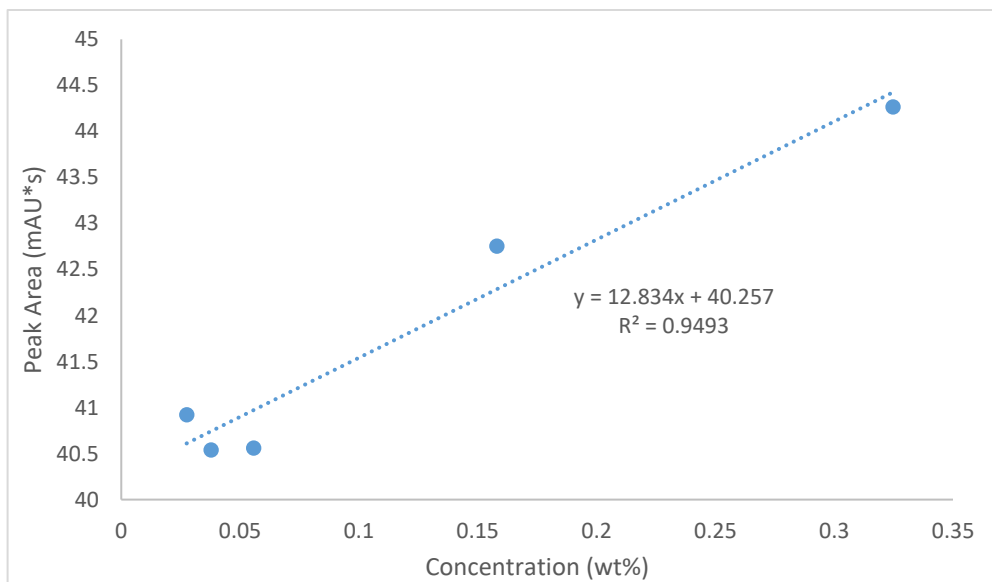


Figure 4-3. Calibration Curve for 1A2P.

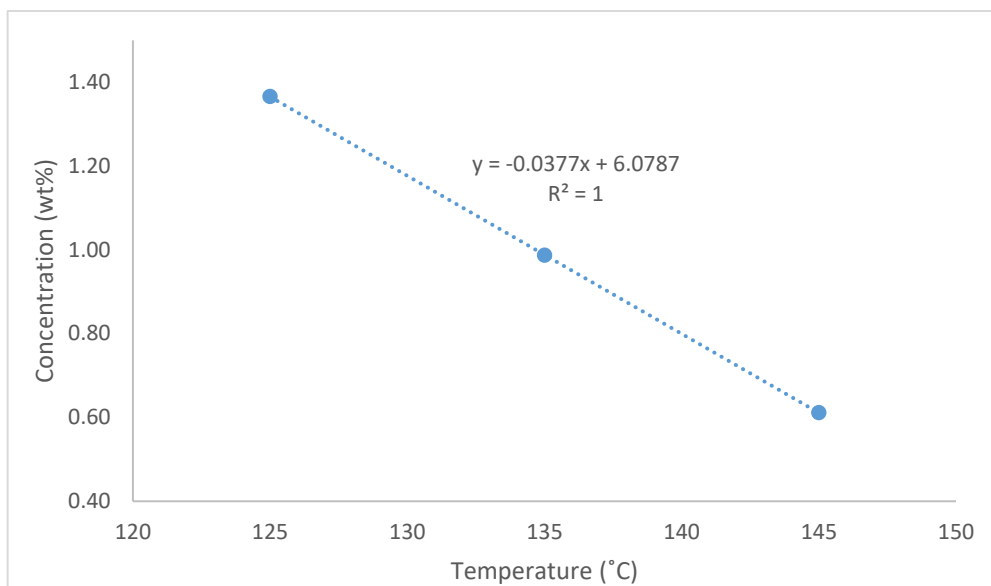


Figure 4-4. Demonstration of the concentration of 1A2P after degradation at different temperatures.

The approximate quantity of degradation products for sample B was three, sample F was five, and sample L was eleven. Note, these are all approximations based on the peaks produced from the HPLC. Further analysis would need to be carried out to determine a more accurate representation of the quantity of species and what their identity. The important point to take from this is that as the temperature increased, so did the number of species present, or, the degraded species are at a greater concentration. Since, the same dilution factor was used for each sample, the blimps observed in the chromatogram for sample L may have also been present in sample B, just not in a concentration great enough to be detected as prominently as sample L.

4.2.3 Ethylenediamine

The calibration curve for EN diluted by the different factors is demonstrated by Figure 4-5. Using the produced calibration curve, the concentrations at the different degradation temperatures was acquired and is demonstrated by Figure 4-6.

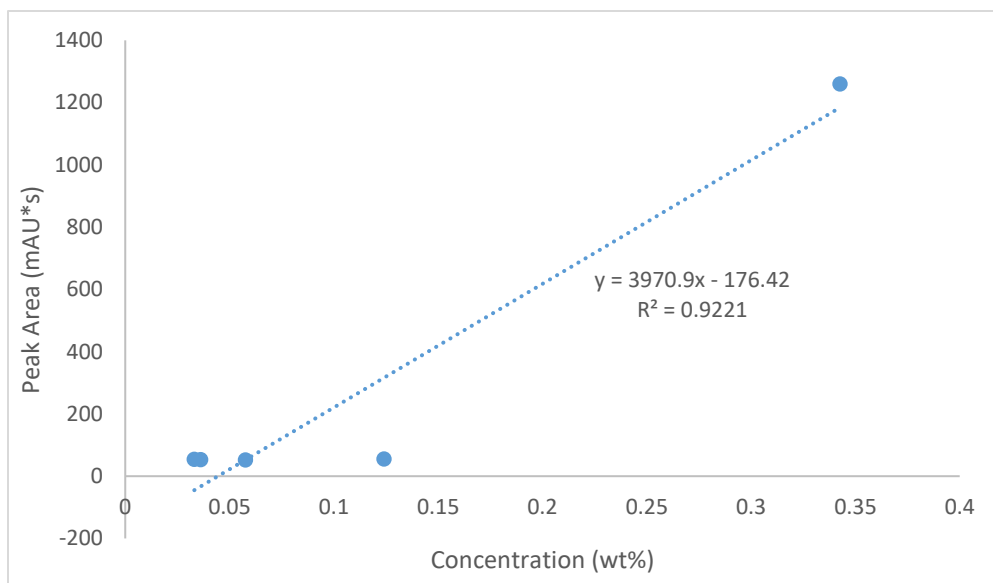


Figure 4-5. Calibration Curve for EN.

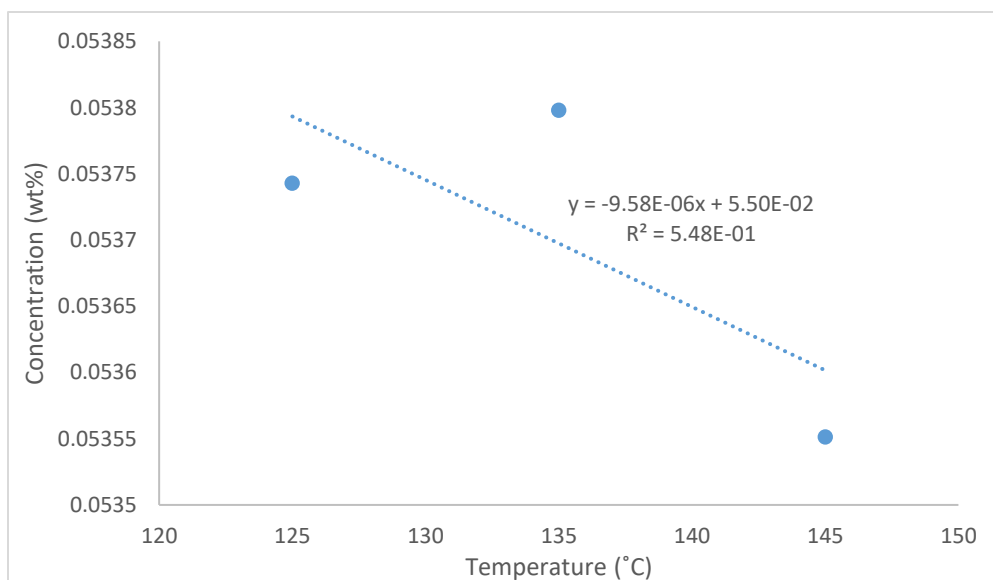


Figure 4-6. Demonstration of the concentration of EN after degradation at different temperatures.

From Figure 4-5, it was demonstrated that the resulting concentrations from degradation were incredibly close together, producing a slope of $-9.58 \times 10^{-6} \text{ wt\%/}^\circ\text{C}$. The degraded samples were diluted 100x, and then an additional dilution had to occur. Approximately, 0.1 g of each diluted samples was diluted 50x, which was the extent needed to have a clear solution. Having a more dilute sample may account for the low concentration of EN, however, all the samples were about the same concentration. This could imply that EN degrades very quickly and reaches its plateau very quickly, and no longer has any reagents for further degradation. Taking the appearance of the EN samples, the samples continued to get darker as the temperature increased, until becoming a sludge at 145°C . Since, the concentration of EN was approximately the same after each of the degradations, this could imply that the degradation species continued to degrade as opposed to EN being lost.

For the approximate quantity of degraded species present, sample C, G, and J all had approximately two peaks on either side of the EN peak. This appeared to be unlikely since the ^{13}C NMR spectra for the degraded EN samples demonstrated an indistinguishable number of peaks, implying the existence of many degraded species. The ^1H NMR spectra for each EN sample showed to be roughly the same hydrogen environments in each of the degraded species which matched up nicely with the pure EN spectrum. This phenomenon could be explained by the existence of many different polymeric compounds but at a concentration low enough to not be detected by the HPLC. The two peaks, excluding EN, could be demonstrating the existence of two other dominant degradation products present that have a concentration that could be

detected. Further evaluation of EN would need to be accomplished to understand this occurrence, however, from the results demonstrated from this research, EN was said to degrade rapidly and plateau within the week of degradation, and the degradation products were said to degraded further leading to the sludge like sample that would not be ideal for PCCC.

4.2.4 (3-aminopropyl)trimethoxysilane

Figure 4-7 represents the calibration curve for 3APT when using all the diluted samples of 3APT. The linear relationship was insufficient, producing an R^2 value of 0.3831. However, since the area of the 3APT peak from the three degraded samples resembled the area of the peaks of a higher concentration of the 3APT dilutions, another calibration curve was produced using the data for the dilutions of 100x, 200x, 500x, and 800x and is demonstrated by Figure 4-8. This new calibration curve was also produced as the concentration from 1000x was considerably different than the other values and was considered an outlier (more than 20 mAU*s difference from the average of the first four dilution peak areas). Using the calibration curve from Figure 4-7, the concentrations for the degraded samples were acquired, and is demonstrated by Figure 4-9. The concentrations acquired by using Figure 4-7 will also be mentioned, but a graphical relationship will not be demonstrated since the calibration curve was demonstrated to be insufficient.

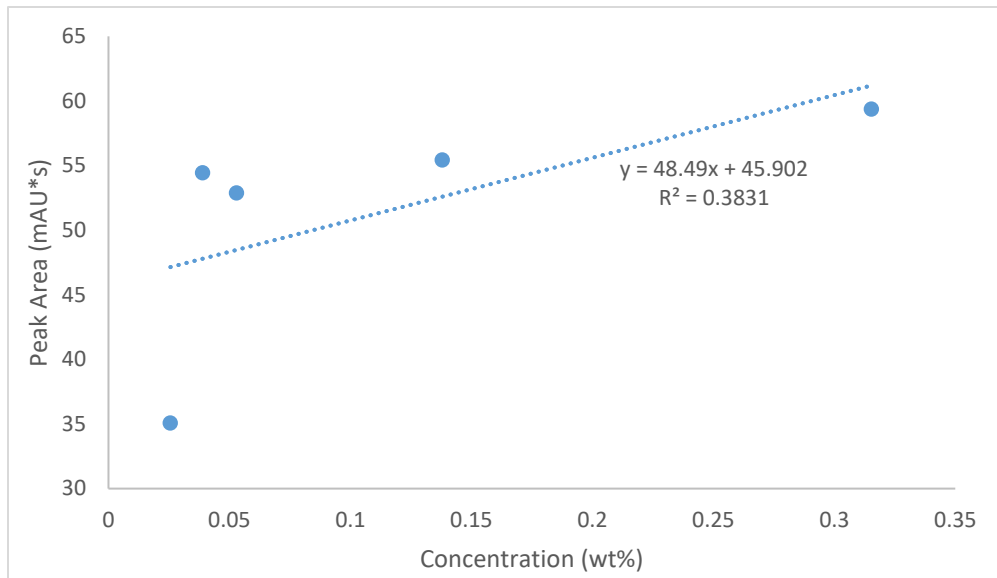


Figure 4-7. Insufficient calibration curve for 3APT.

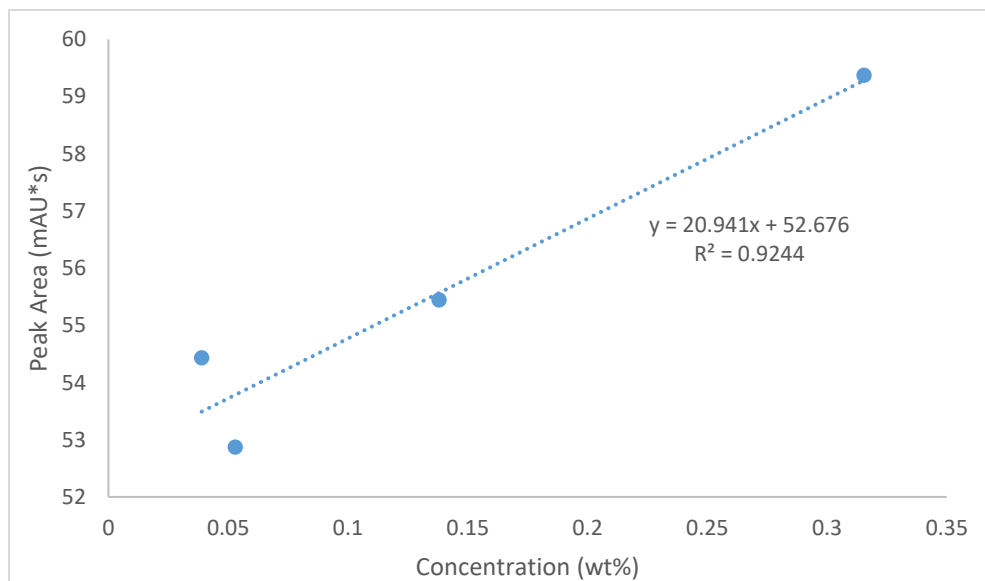


Figure 4-8. Calibration curve for 3APT.

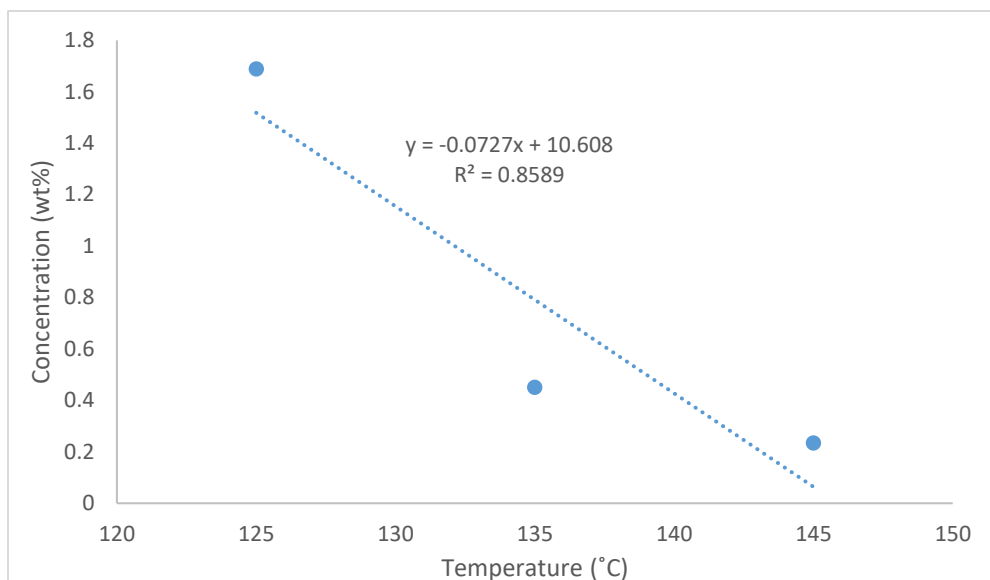


Figure 4-9. Demonstration of the concentration of 3APT after degradation at different temperatures.

Based on the concentration of 3APT after each degradation, it was observed that 3APT was the most resistive amine toward degradation of the studied amines. However, when the temperature was increased, 3APT appeared to approach a plateau demonstrated by the concentration at 135°C and 145°C. Thus, 3APT is more resistant to thermal degradation at 125°C and would be much more susceptible to degradation with an increase in temperature. This was also demonstrated by the Figure 4-9, where the slope demonstrated the loss of 3APT as -0.0727 wt%/°C. However, the difference between the concentration at 135°C from that at 145°C was only 0.217 wt%, as opposed to the difference between 125 and 135°C of 1.24 wt%. When comparing the concentration of 3APT from the calibration curve in Figure 4-8 with those from Figure 4-7 (concentration after 125°C was 0.869 wt%, 135°C was 0.334, and 145°C was 0.241) the same relationship was demonstrated, only with smaller integers.

Interestingly, when the determination of the approximate products after degradation, the results acquired produced information that was not demonstrated in the ^{13}C NMR evaluation. Sample D and H both had approximately three species present, excluding 3APT, after degradation, while sample K had approximately five. Since, the existence of new carbon environments was not demonstrated by ^{13}C NMR, the degraded products may be polymeric compounds of 3APT. The captured CO_2 may have provided a bridging between one 3APT molecule and another and was not able to be detected itself due to the much greater abundance of carbon environments given by the 3APT portions of the degraded product (see Chapter 6 for theoretical degradation products for 3APT and the other amines used in this research).

4.2.5 *2-(Butylamino)ethanol*

The calibration curve for 2BAE is demonstrated by Figure 4-10 yielding satisfactory linearity between the data collected. With the equation of the calibration curve, Figure 4-11 was produced yielding interesting and unexpected results for the concentration of 2BAE after degradation.

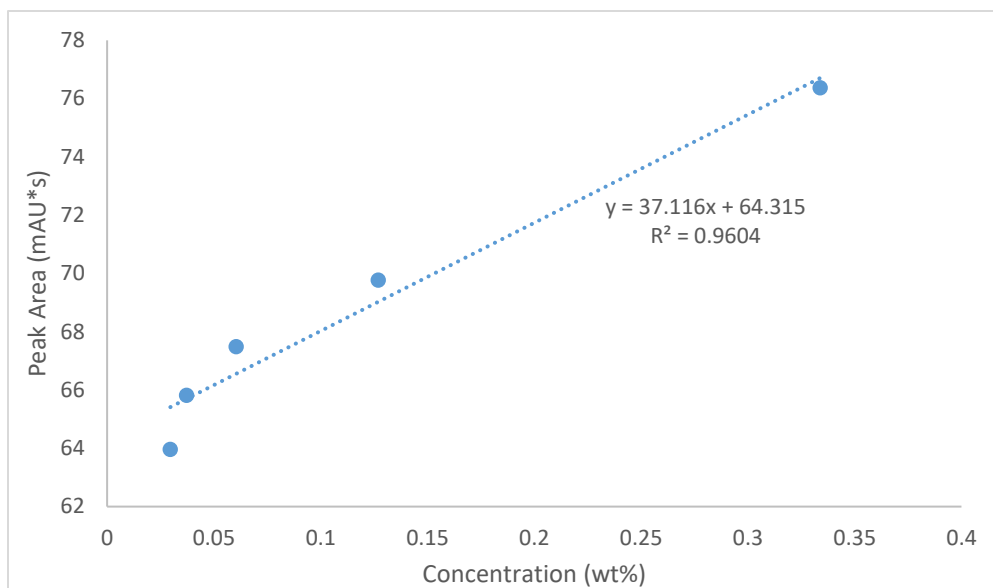


Figure 4-10. Calibration curve for 2BAE.

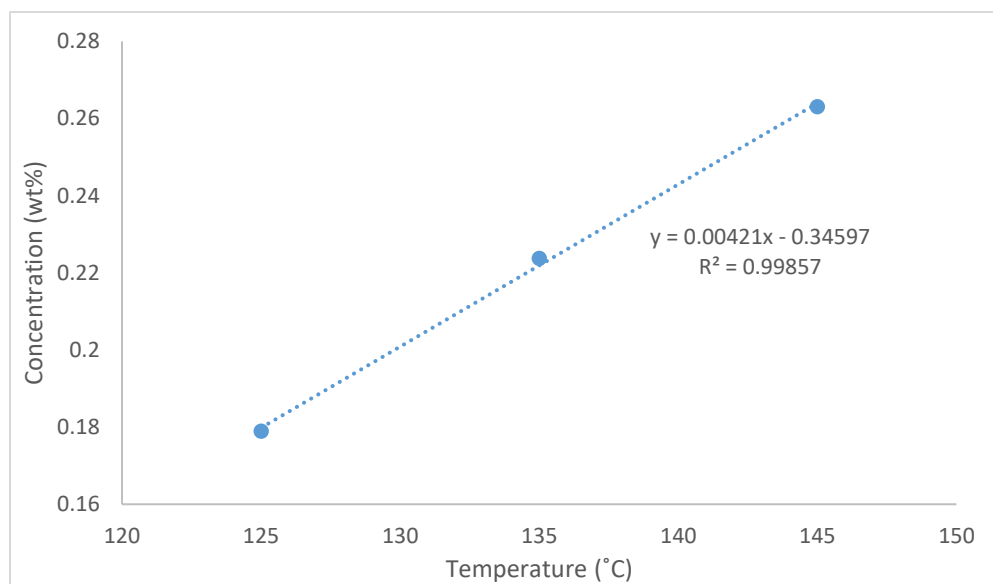


Figure 4-11. Demonstration of the concentration of 2BAE after degradation at different temperatures.

Surprisingly, 2BAE demonstrated to be more resistant to thermal degradation at higher temperatures (Figure 4-11), contrary to the expected results for more degradation to occur as the temperature was increased.^{39,41} The rate of change between the three points however was 0.00421 wt%/°C indicating that the points are relatively close in value, however, not as significant as EN, and not greater than the magnitude of the rate produced for MEA. Thus, the data was not considered as the plateau concentration. It is important to note that the degraded 2BAE samples had to be much more concentrated than the other samples (30x dilution factor for the original 2BAE degraded sample) as the 100x dilution factors led to a 2BAE concentration that produced negative concentrations. This demonstrated that 2BAE degraded tremendously at each of the temperatures, even though the concentration was higher for higher temperatures.

To explain this phenomenon, it may be possible that due to the higher temperature, different degradation species could have been formed as opposed to that at 125°C. At lower temperatures, one product is more dominant over the other, and as the temperature is increased, a new product that is more thermally stable could be produced, and thus, having less of an activating effect on 2BAE to degrade, allowing more 2BAE to be present after degradation. The degradation product could also degrade in a manner that does not affect 2BAE, and thus, allowing the concentration of the degradation product to decrease while the concentration of 2BAE remained the same or decreased at a much slower rate. This proposed explanation would occur after or as an effect of the rapid degradation of 2BAE though, due to the need for a more

concentrated sample for analysis. However, further investigation of 2BAE is required to understand this phenomenon. It may be advantageous to study the thermal degradation at various temperatures over several days, and then to evaluate the species present and how much each species is present to determine if there is a correlation between the degraded species present and the concentration of 2BAE after degradation.

When determining the approximate quantity of species present, the different peaks were much more prominent with the 2BAE due to the greater concentration of the degraded sample as opposed to the more diluted samples. This information could be used for the identification of the degradation species, as more concentrated sample could be used for a more accurate determination of the quantity of species present after degradation. Also, a longer elution time would be required, as for 2BAE, one small peak appeared just before the ten-minute mark. For sample M, approximately six species were present after degradation, excluding 2BAE. Sample P had five, and sample T had about seven species present, not including 2BAE. It is reminded that the approximation of the quantity of species should be taken lightly as many of the species present may be unable to be detected, or detected well, and thus have not been included. It should be stated however, that with each of the three samples, there are two dominant peaks. One of these peaks was 2BAE, and the other was the most abundant degradation product. However, when comparing the heights between the two peaks, a possible area of interest was formed. The difference was relatively close for sample M and P (2.31 and 1.49 mAU*s respectively), however, for sample T, the

difference jumped to 7.16. Because the concentration of 2BAE was found to be larger for sample P than for sample M, conclusive evidence that the degraded product had a direct effect on the concentration of 2BAE could not be determined, however, due to the much larger difference between the peaks for sample T, there could some kind of relationship that could explain the hypothesis for the higher 2BAE concentration with higher temperatures.

4.2.6 Methyldiethanolamine

Surprisingly, after the production of the calibration curves, demonstrated by Figure 4-12, the slope was negative. This is unlikely, since the concentration of MDEA was higher, yet it yielded a smaller peak area. This was more prominent with the dilution factor 100x when compared to the other dilution factors. Each factor was within 1.5 mAU*s of each other, except for the dilution factor at 100x, which when compared to the average peak area of the other four dilutions, produced a difference of 8.22 mAU*s. A similar occurrence appeared with PZ, that will be demonstrated in section 4.2.7. The concentration of the degraded MDEA samples calculated by using the calibration curve from Figure 4-12 is demonstrated by Figure 4-13.

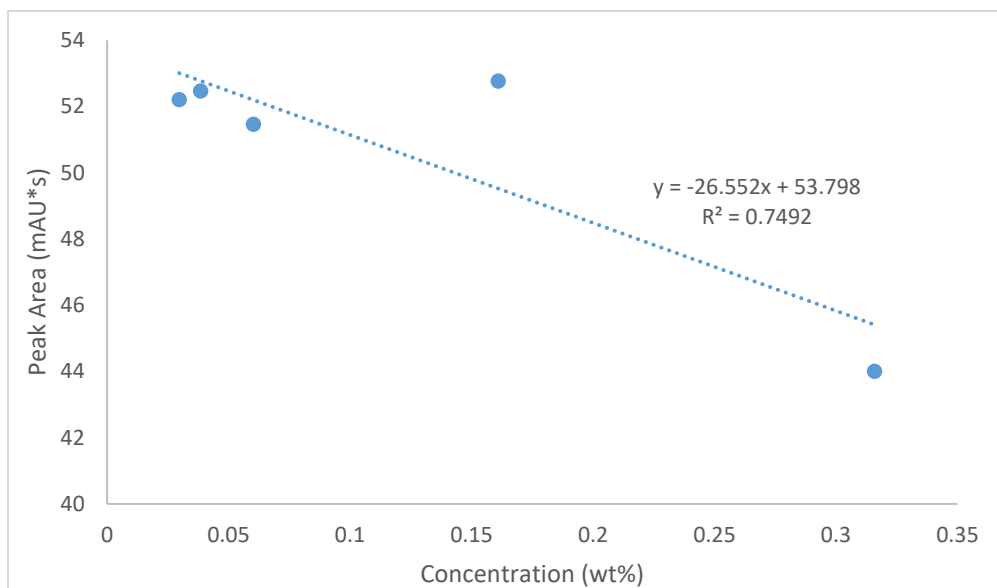


Figure 4-12. Calibration curve for MDEA.

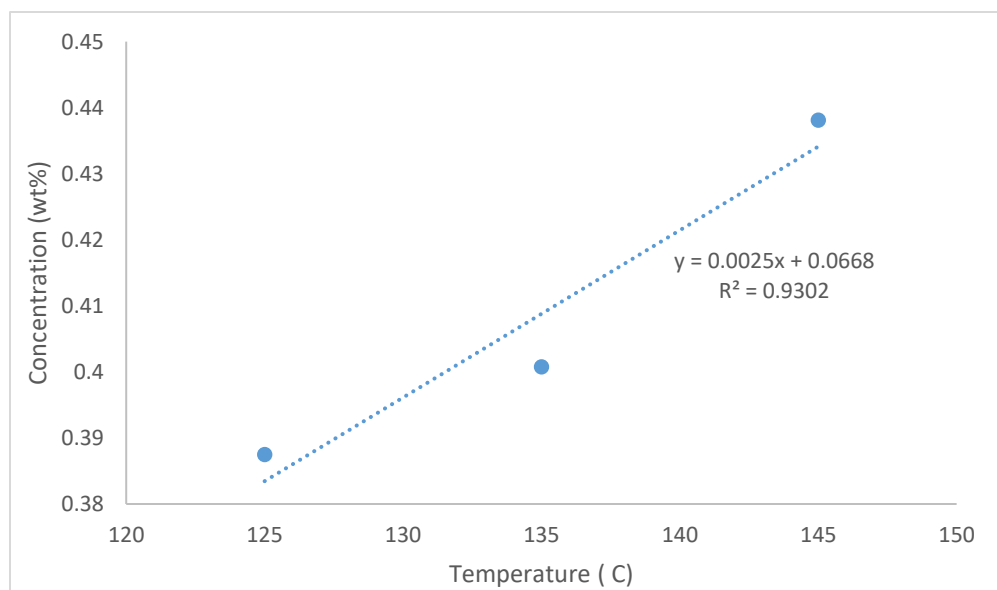


Figure 4-13. Demonstration of the concentration of MDEA after degradation at different temperatures.

The concentration of MDEA after degradation at each temperature of interest, demonstrated similar results as that of 2BAE. However, before any further analysis of the results from MDEA, it should be stated that MDEA had to be diluted further after the initial dilution factor of 100x by the dilution method used for the EN samples. This was due to the production of negative concentration values when the peak area was used for calculation with the calibration curve equation. This implied that, due to the nature of the calibration curve, more MDEA was present after degradation than that compared to how much original amine was left for the other amines in this study.

When it comes to the comparison of MDEA concentration after degradation, the positive slope of $0.0025 \text{ wt\%/}^\circ\text{C}$ indicated an increase of MDEA concentration. The peak area from each of the peaks however, resembled the peak area from the 100x dilution. Since the concentration from each temperature are close together, it could be concluded that MDEA degraded approximately the same amount for each temperature. To evaluate the increase in concentration, the production of a calibration curve with dilutions around a factor of 100x, would allow a more accurate measurement of the concentration of MDEA after degradation. This would be done since the peak area for the degraded samples were closer to the 100x dilution factor, as opposed to the higher peak area cluster from the other dilution factors. If, this was accomplished, it would be possible that the slope could be positive, thus changing the concentrations demonstrating the expecting concentration results. Time did not allow further evaluation of this phenomenon, but this would be the next step forward for future research.

For the determination of the approximate quantity of MDEA degradation products present also disagreed with the ^{13}C NMR analysis, like 3APT, as much more degraded species were present in HPLC analysis than ^{13}C environments present with the initial dilution factor of 100x. However, when the approximate quantity of degradation products for the dilution factor used for the concentration determined from Figure 4-13 was observed, results like the ^{13}C NMR analysis was observed, and will be addressed for unity, however, the quantity from the more concentrated samples will be mentioned as well. It should be recognized though, like the other amine samples, a more concentrated sample and a longer elution time would be required to determine a more accurate quantity of degradation products. Further analysis would need to be accomplished to determine why this may have been the case, however, one likely possibility is that the degraded products were present in too small of a concentration for NMR to distinguish from the more abundant MDEA. For sample N (approximately four for the more concentrated sample) and Q (four for more concentrated sample), approximately one species, excluding MDEA, was observed. For sample U (eight for more concentrated) however, two species were present (one of the species present at lower concentrations was not present at higher concentrations for all samples). The small amount of species detected at a more diluted sample indicated the high thermal stability associated with MDEA, agreeing with the expected experimental results that tertiary amines are more thermally stable due to their lower reactivity than unhindered primary and secondary amines.^{21,33-36}

4.2.7 Piperazine

The calibration curve for PZ is demonstrated by Figure 4-14, and surprisingly, had the same behavior as MDEA. The dilution factor at 100x produced a peak area significantly lower than the average cluster at the lower dilutions, a difference between the peak at 100x and the average of the cluster was 13.6 mAU*s, with the largest difference from the cluster was only 3.55 mAU*s. Using the calibration curve, the concentration of PZ from the degraded samples was accomplished and is demonstrated by Figure 4-15.

PZ behaved very similarly to MDEA, and thus, the same analysis of MDEA could be applied to PZ, including the calibration curve corrections for a more accurate determination. An exception to this, was that PZ followed more of the expected degradation results than MDEA did, producing a PZ loss rate of $-0.00161 \text{ wt\%/}^\circ\text{C}$. It should also be stated that PZ, like MDEA, was diluted further than the 100x due to the

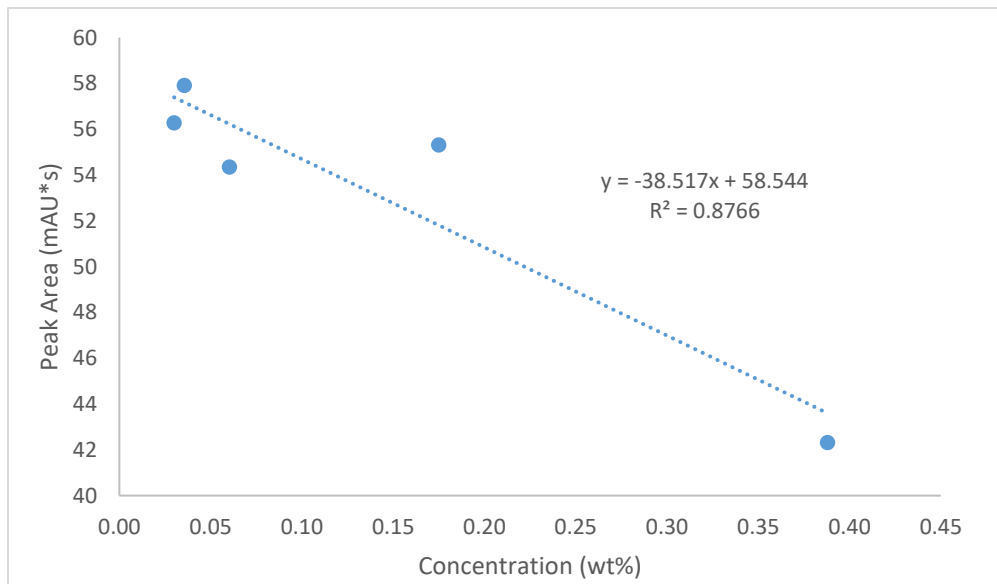


Figure 4-14. Calibration curve for PZ.

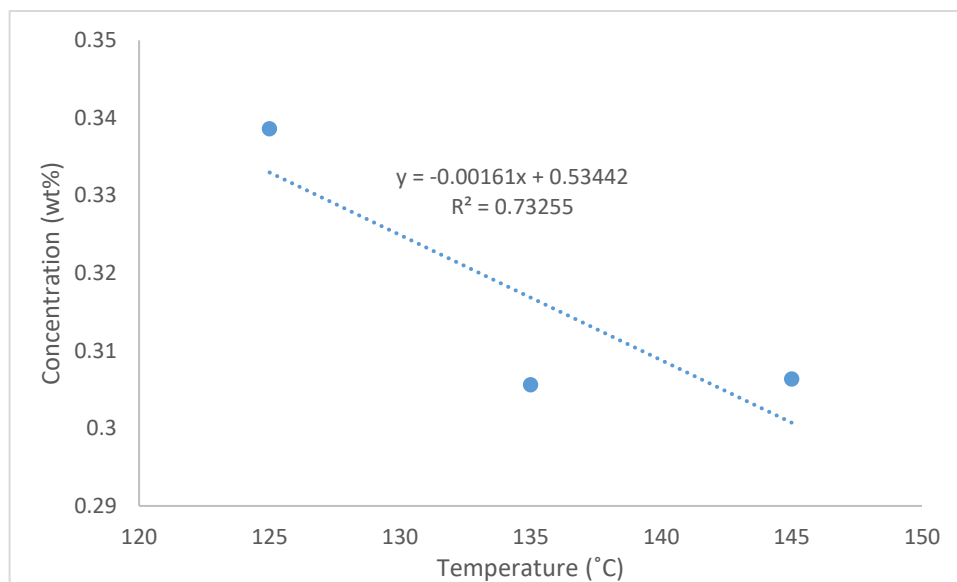


Figure 4-15. Demonstration of the concentration of PZ after degradation at different temperatures.

production of negative concentrations with the 100x peak areas. However, since MDEA and PZ were both diluted the same amount, the two amines were able to be compared to each other, and MDEA was found to have a higher concentration than PZ, however, the two were the front runners for being the most thermally stable under these experimental parameters.

Like MDEA, the approximate quantity of species of PZ will be addressed in the same manner. For sample O, R, and V, only one other species peak was present, excluding PZ, which was not observed for the more concentrated samples, like the MDEA samples. For the more concentrated samples, sample O had two, R had three, and V had four other species present with PZ after degradation.

4.3 Thermal Degradation Activation Energy

For the determination of the activation energies, stock solutions of CO₂ loaded amines were used for 125°C and 145°C over two and four days. It was important to evaluate the stock solutions used as, if the solution was darker, then reactions took place that would possibly have a different starting concentration of amine. The stock solutions had been sitting in a dark cabinet, wrapped in Parafilm, and kept at room temperature for about a month after production.

The thermal degradation activation energies were found using equation 4-1,

$$\ln \frac{k_1}{k_2} = \left(-\frac{E_A}{R} \right) \left(\frac{1}{T_1} - \frac{1}{T_2} \right) + \textit{integration constant} \quad (4-1)$$

where the rate constant k was determined by plotting the concentration of amine versus the time (two and four days) of degradation at 125°C and 145°C.⁵¹ Thus, the slope from equation 4-1 would be multiplied by the ideal gas law constant of 8.314 J/mol·K to acquire the thermal degradation activation energy.

Table 4-1 summarizes the thermal degradation activation energies and related information for MEA, MDEA, and PZ.

Table 4-1. Thermal Degradation Activation Energies as well as their Associated Slope and Reaction Order for MEA, MDEA, and PZ.

| Amine | Order | Slope (K) | Activation Energy (kJ/mol) |
|--------------|--------------|------------------|---------------------------------------|
| MEA | Zero | 2294 | 19.1 |
| | First | 20440 | 170. |
| MDEA | Zero | 1275 | 10.6 |
| | Second | -2572 | 21.4 |
| PZ | Zero | -3609 | 30.0 |

4.3.1 Monoethanolamine

All the MEA stock solutions had a slightly darker tint, some more than others, however, the solution with the least amount of tint was used, which was not far from the tint of the initial production of MEA (after being stored in darkness at room temperature for 24 h). However, this proved to be a problem and the thermal degradation activation energy was determined using the data provided after the two and four days of degradation, and by treating the reaction as a first-order that was determined from previous work.⁴ Both resulting thermal degradation activation energies will be demonstrated and discussed.

Before the discussion on the determination of the thermal degradation activation energy, the plots that gave rise to the rate constants will be discussed. Using

all three data points (two, four, and seven days) the linearity of the plot portrayed a zero-order as opposed to a first-order reaction. It is important to note that while the linearity demonstrated zero-order, the observed linear regression at 125°C was 0.0528 and for 145°C was 0.615. Not only was the linear regression below par, the slopes for each plot were positive when it should have been negative. The slopes were made positive only due to the point after seven days from the initial degraded samples being included. Thus, this phenomenon could be explained by the starting MEA concentration being lower for the data collected for the two and four days of degradation. While this demonstrated significant error for the kinetics study for seven days, it provided insightful information that after MEA has captured CO₂, it will degrade at room temperature when left alone, giving the species a relatively low amount of usage.

Table 4-1 demonstrates the data acquired for the zero-order reaction when all three points were included, and the first-order reaction for MEA when only the two- and four-day data points were included.

The thermal degradation activation energy for the zero-order reaction of MEA was found to be 19.1 kJ/mol, while that of first-order reaction was 170. kJ/mol. When comparing these results to those found by Huang, the 170. kJ/mol thermal degradation activation energy agreed with the work by Huang. Huang calculated the thermal degradation activation energy over the time intervals of 5 h, 10 h, and 14 h at 125°C, 135°C, and 145°C and found it to be 152 kJ/mol.⁴ The higher thermal degradation activation energy could be due to the lower concentration of MEA

present. Since the degradation of MEA increases with longer exposure to high temperatures, the further the degradation would take place. Had more time been available, new stock solutions would be prepared to evaluate the thermal degradation activation energy of MEA over a week for further comparisons, including analysis at 135°C.

4.3.2 Methyldiethanolamine

MDEA provided interesting results. For the data collected over the time interval at 125°C, a second-order reaction was observed (linear regression of 0.737). However, for the data 145°C, a zero-order was observed (linear regression of 0.998). The 145°C demonstrated a better fit, however, both reaction orders will be discussed here. The thermal activation energy for MDEA treating the reaction as a zero-order and as a second-order reaction is shown in Table 4-1. Unlike MEA, all three data points could be used, indicating MDEA degrades more slowly, if any, than MEA.

When treated as a zero-order reaction, the thermal degradation activation energy was demonstrated to be 10.6 kJ/mol, and with a second-order reaction, 21.4 kJ/mol. Further investigation would need to be accomplished to evaluate the true order of the thermal degradation of MDEA, including data analysis over a set time interval at 135°C. The activation energy for the thermal degradation of MDEA will be compared to MEA and PZ, however, compared to MEA, having a much lower activation would be expected as MDEA degraded much less than MEA.

4.3.3 Piperazine

PZ, like MDEA, was also able to include all three data points, indicating little to no degradation over the two months of static conditions. The linear regression fit best for the both temperatures as a zero-order reaction with the R^2 value for the data collected at different time intervals was 0.556 at 125°C, and was 0.982 for 145°C, demonstrating similar characteristics of MDEA. The thermal degradation activation energy for the zero-order reaction of PZ is demonstrated by Table 4-1.

The thermal degradation activation energy was determined to be 30.0 kJ/mol under the parameters set by this research. It is important to recognize that Freeman et al. determined an activation energy for the thermal degradation of PZ, but over much different parameters. Their research involved 8 m PZ loaded with 0.3 mol CO₂/mol alkalinity from 135°C to 175°C over the span of approximately 15 weeks.³⁸ The activation energy of thermal degradation for PZ that they determined was found to be 184 kJ/mol, which is significantly higher than that of this research.³⁸ The difference in activation energy could be explained by the different parameters set, especially with the time period. Over the 15-week interval, PZ was demonstrated to have continued to degrade at 175°C.³⁸ However, when compared to MDEA, while the activation energies were close, PZ had a higher activation energy than MDEA, which agreed with the extent of thermal degradation observed for each.

4.4 Conclusions

HPLC analysis allowed the quantification of the concentration of each amine after degradation at 125°C, 135°C, and 145°C. Based on strictly concentration, including whether a more dilute or more concentrated sample was required, the following ranking was acquired from most highest concentration to least: MDEA>PZ>1A2P>3APT>EN>MEA>2BAE. However, based on observation with concentrations, the order from highest thermal stability to least was found to be: MDEA>PZ>1A2P>3APT>MEA>2BAE,EN. The reason for 2BAE and EN being denoted as about the same in terms of thermal stability had to deal with the extreme characteristics observed for each. EN was demonstrated to degrade rapidly within a week at all three temperatures, with the degradation products producing a sludge-like substance. 2-BAE had to be in a much greater concentration than all other amines for HPLC analysis, demonstrating rapid degradation within the one-week time span.

Comparing the thermal stability ranking with that produced using the ¹³C NMR spectra, the two rankings were demonstrated to be quite similar. The difference being with the stability, or degradation, of 3APT, which was found to have no new distinguishable ¹³C peaks. After HPLC analysis was performed, 3APT was demonstrated to have degraded more than expected, being less stable than 1A2P, but more stable than MEA. This demonstrated that the methodology of using the ¹³C NMR spectra provided a starting point that provides a reasonable explanation on the thermal stability of amines, however, quantitative analysis on the concentration of each amine after degradation was still required, as demonstrated by the case with 3APT.

The thermal degradation activation energies demonstrated agreement with the expectations from the structure and with the concentrations found after degradation. MEA was found to be in excellent agreement with the results demonstrated by Huang. The thermal degradation activation energy for MEA was determined to be 170. kJ/mol over four days at 125°C and 145°C, while Huang determined the activation energy over 14 h at 125°C, 135°C, and 145°C to be 152 kJ/mol. Due to the different parameters, and the lack of data from 135°C, the activation energy would be expected to be higher for the thermal degradation set by this research, as more MEA would be expected to degrade more at 145°C with a longer time interval. With MDEA, two thermal degradation activation energies are reported, as the two different temperatures demonstrated different reaction orders. The thermal degradation activation energy for MDEA as a zero-order reaction was found to be 10.6 kJ/mol, and as a second-order reaction, 21.4 kJ/mol. With PZ, the thermal degradation activation energy was demonstrated to be 30.0 kJ/mol as a zero-order reaction. The thermal degradation activation energies demonstrated that with more degradation, the energy values would be higher. This agreed with the HPLC results, as MDEA was determined to degrade the least, and, although there were two energy values, they were both lower than PZ and MEA. The ranking from highest to lowest thermal degradation activation energy was: MEA>PZ>MDEA, which agreed with the thermal stability demonstrated by amine concentration after degradation.

Chapter 5. Computational Investigation

5.1 Introduction

Before the demonstration of computational results, the system used must be defined. Figure 5-1 demonstrates the reaction that was used for each calculation with MEA as the example. Each amine was calculated separately, with the CO₂ captured molecule being treated as that demonstrated by Figure 5-1, except for MDEA, which was unable to be completed in this computational investigation. For diamines, only a single COOH group was used for computations. Due to time restraints, only

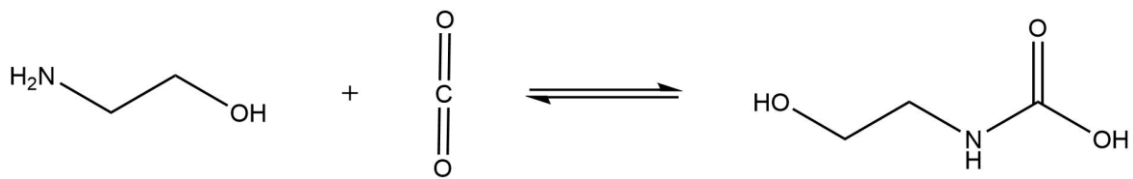


Figure 5-1. Reaction system used for the computational investigation. MEA is used as the example.

computations at 298.15 K were accomplished, and are the results demonstrated in this chapter. Also, due to there being no access to an advanced computing facility, all computations had to be run on an HP laptop with an i5 processor, which took each amine CPU days, and in many cases, CPU weeks. Thus, only four complete computations at 298.15 K for the smaller amines was able to be accomplished in this research.

5.2 Computational Analysis

5.2.1 Computational Results

The binding energy, ϵ_{bind} , Δ_rH , and Δ_rG from the computational model set by this research and calculated using equation 2-31 through 2-33, are demonstrated by Table 5-1.

Table 5-1. Summary of Computational Results for ϵ_{bind} , Δ_rH , and Δ_rG .

| Amine | ϵ_{bind} (kCal/mol) | Δ_rH (Hartrees) | Δ_rG (Hartrees) |
|-------|------------------------------|------------------------|------------------------|
| MEA | 2.03116 | -0.000885 | 0.017899 |
| 1A2P | 2.30038 | -0.000127 | 0.016918 |
| EN | 2.05758 | -0.002118 | 0.016703 |
| PZ | 1.74037 | 0.011461 | 0.027392 |

5.3 Conclusions from Computational Results

Based on the computational results for the parameters set by this research, three separate rankings for comparisons were generated. The first, being the ranking of ϵ_{bind} from greatest to least as: 1A2P>EN>MEA>PZ. It is reminded that the order of thermal stability for the amines reported are was PZ>1A2P>MEA>EN. Thus, the CO₂ binding energy did not provide any significant insights into the predictability of the thermal stability of the amines. The next ranking was with the change in enthalpy of the reaction, Δ_rH , from greatest to least: PZ>1A2P>MEA>EN. This ranking matched up

perfectly with the thermal stability ranking. Thus, at least for the amines computed under the parameters of this research, the $\Delta_r H$ values could be used as a prediction of thermal stability. Indeed, a negative enthalpy change indicates an exothermic reaction while a positive indicates an endothermic reaction, however, the ranking was based solely on comparing the numerical values.⁵¹ Further analysis would need to be conducted with these four amines, to verify that the higher the $\Delta_r H$ value for the capture of CO₂, the more thermally stable the amine. The final ranking involved the change in Gibb's energy of the reaction, $\Delta_r G$, from greatest to least: PZ>MEA>1A2P>EN. The results from the $\Delta_r G$ values did not provide any insight into the predictability of thermal stability.

Chapter 6. Theoretical Degradation Products and Reaction Pathways

6.1 Introduction

This chapter demonstrates theoretical degradation reaction pathways and degradation products using the degradation pathway demonstrated by MEA. This pathway demonstrated the production of polymeric and cyclic degradation compounds, as well as urea formations, as shown by Huang and Martin et al.^{4,40} This process was used as it demonstrated to work not only for MEA, but also for 1A2P, which will be the only amine in this chapter where the degradation pathway and products were demonstrated by a reviewed article. It is important to note that, these pathways are only possibilities, and should not be taken as fact. Some reactions have a much higher probability of occurring than others, and any discussion needed will be provided with the amine of interest. A detailed description of each reaction will not be provided, as they follow the scheme demonstrated by Figure 1-11. Also, for the proposed thermal degradation reaction pathway of PZ by Freeman et al., see Figure 1-12.³⁹

For each reaction demonstrated, the urea production will be demonstrated as the last thermal degradation reaction pathway(s), except for 3APT which had many theoretical urea formations. Each amine will be demonstrated in a separate section where any description of the amine that is necessary will be included.

6.2 Theoretical Thermal Degradation Reaction Pathways

6.2.1 1-Amino-2-propanol

Figure 6-1 demonstrates the thermal degradation pathways for 1A2P proposed

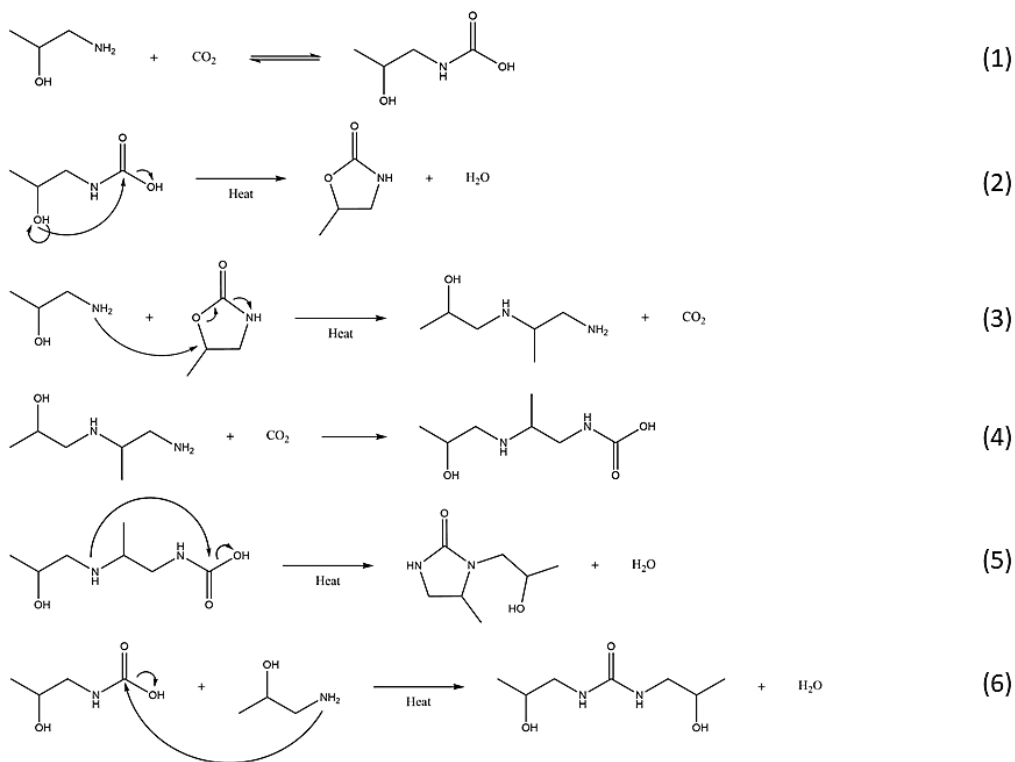


Figure 6-1. Thermal degradation reactions for 1A2P produced by reference (40).^{25,40}

by Matin et al.⁴⁰

In relation to Figure 6-1, it is important to note that the product from reaction (4) was not demonstrated by Matin et al. Matin et al. went directly from reaction (3) to reaction (5). Reaction (4) was produced to try and explain the production of 1-(2-hydroxypropyl)-5-methyl-2-imidazolidinone (HPMIZD) of reaction (5).⁴⁰ Finally, the names of each degradation product will be presented. The products of reaction (2), (3),

and (6) are: 5-methyl-2-oxazolidinone (MeOZD), 1-[(2-amino-1-methylethyl)amino]-2-propanol, and N,N'-bis(2-hydroxypropyl)urea respectively.⁴⁰

6.2.2 Ethylenediamine

Figure 6-2 and 6-3 demonstrates the theoretical thermal degradation pathways for EN.

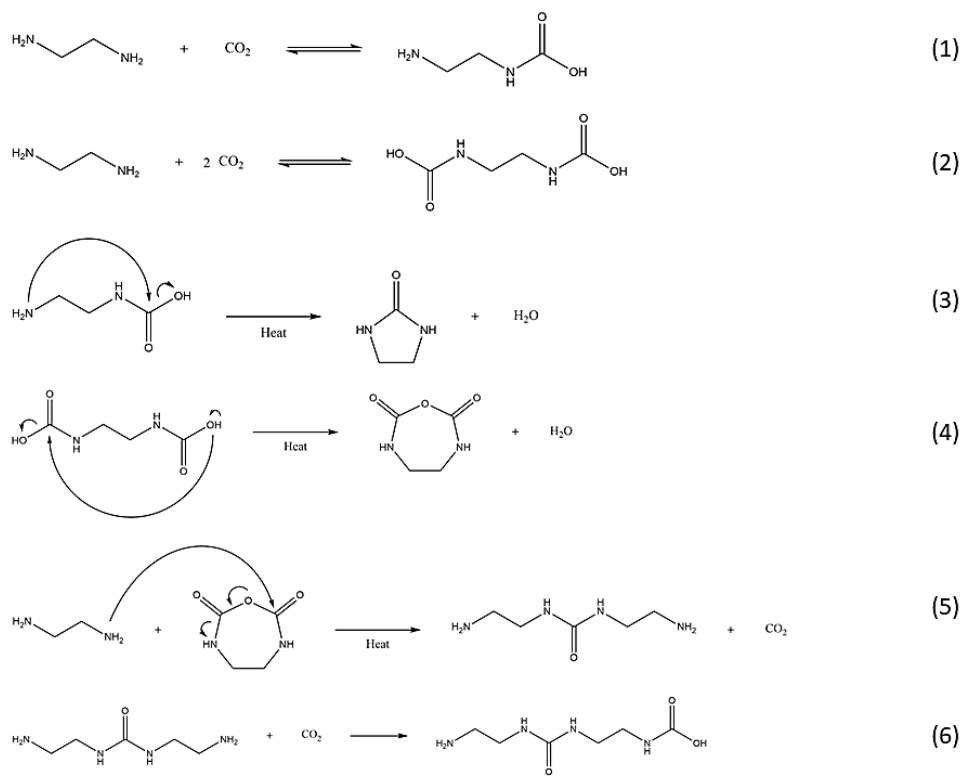


Figure 6-2. Theoretical thermal degradation reactions for EN.²⁵

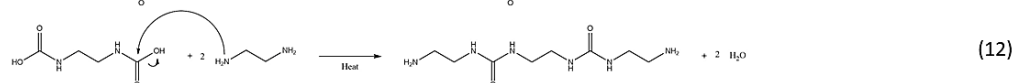
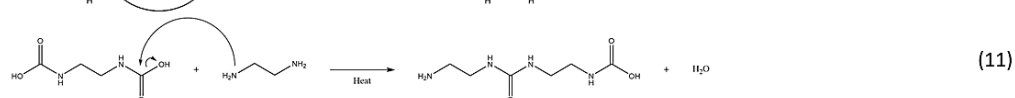
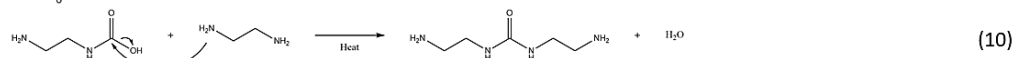
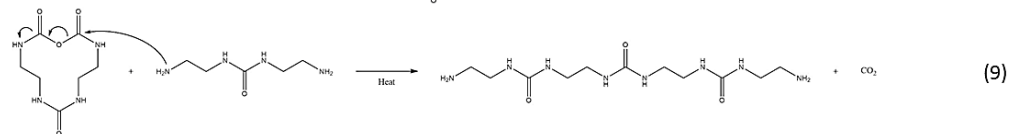
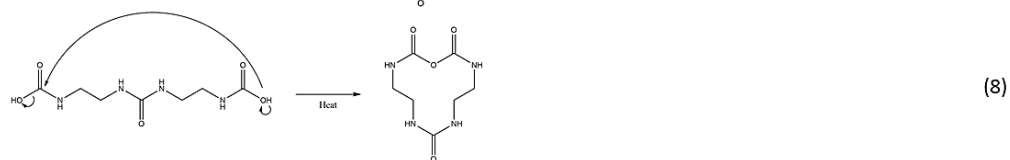
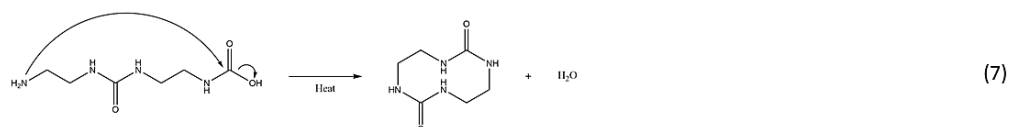


Figure 6-3. Continued theoretical thermal degradation reactions for EN.²⁵

A few comments will be made here about the theoretical thermal degradation pathway for EN. The first being that reactions are demonstrated with either one captured CO₂ molecule or with both amine groups having a captured CO₂ molecule. Because of this, there would be more options for the thermal degradation of EN. EN is also a small linear diamine, which, when coming into proximity of another degradation product, EN would have a greater chance of having an amine group react with the product, furthering the degradation of EN. Also, in terms of the large degradation rings demonstrated by reaction (4), (7), and (8), these products would have a much lower probability of being produced than, for example, the products from reaction (3) and (10-12).

6.2.3 (3-aminopropyl)trimethoxysilane

Figure 6-4 demonstrates the theoretical thermal degradation pathways for

3APT.

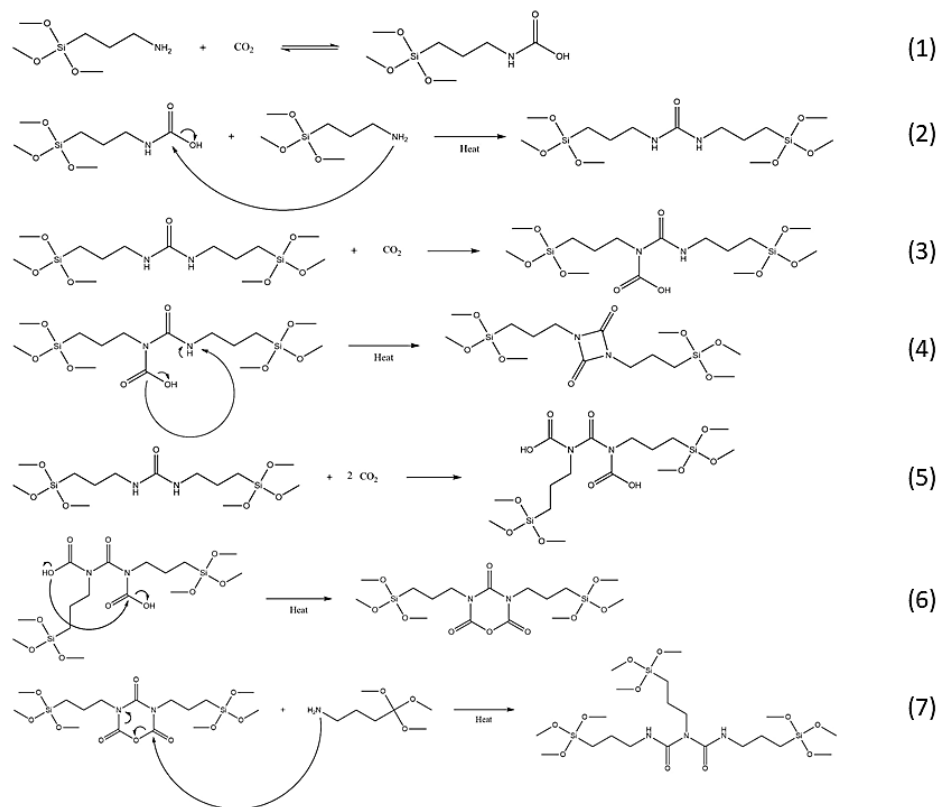


Figure 6-4. Theoretical thermal degradation reactions for 3APT.²⁵

Interestingly, with the theoretical degradation reactions of 3APT, it was demonstrated that a urea functional group was present in each product, which could be the source of the strong odor present in each degraded sample of 3APT.

6.2.4 2-(Butylamino)ethanol

Figure 6-5 and 6-6 demonstrate the theoretical thermal degradation pathways for 2BAE. For the theoretical thermal degradation reactions of 2BAE, the source of the carbonate ion can be demonstrated by Figure 1-6.

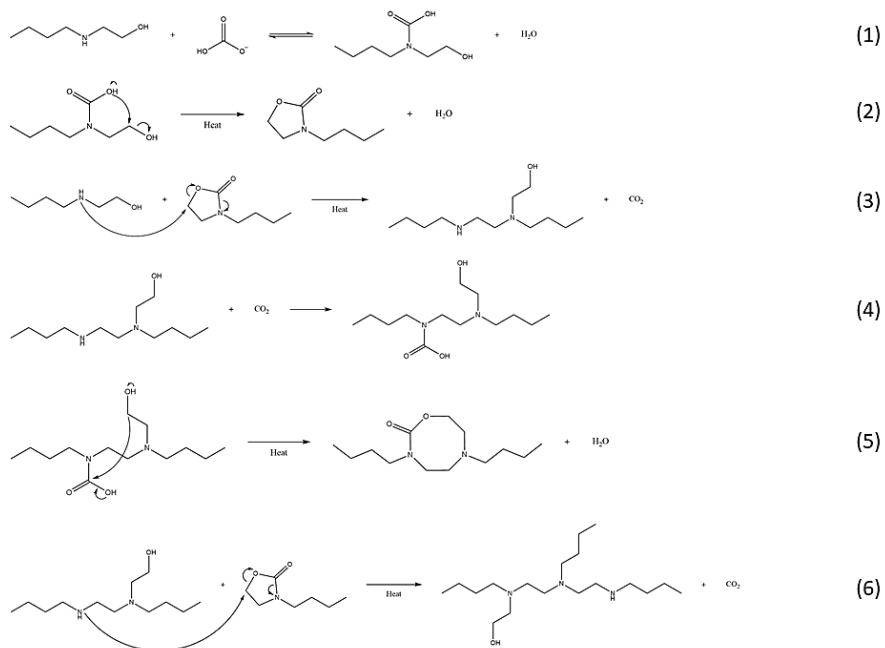


Figure 6-5. Theoretical thermal degradation reactions for 2BAE.²⁵

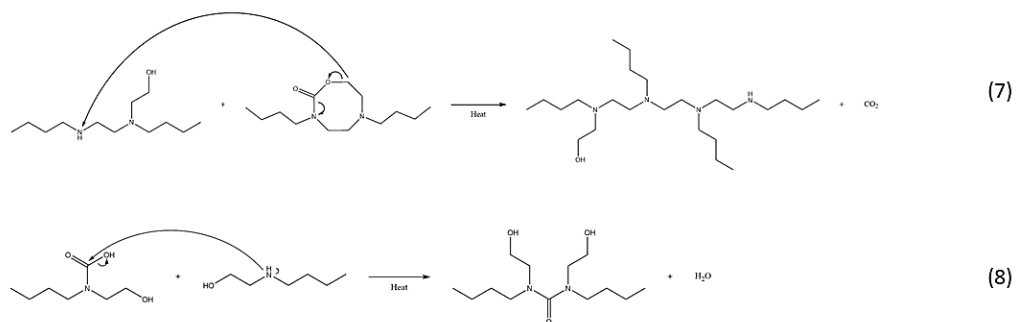


Figure 6-6. Continued theoretical thermal degradation reactions for 2BAE.²⁵

Like EN, the large ring formation from reaction (5) in Figure 6-5, would be unlikely to happen, however, is still included as it has a slight probability to occur and be a possible intermediate for the formation of the product demonstrated by reaction (7) in Figure 6-6.

6.2.5 Methyldiethanolamine

The theoretical thermal degradation pathways for MDEA is demonstrated by Figure 6-7.

The ring formations of reaction (5) and (6) have a low probability of occurring, however, they are interesting possibilities. Knowing MDEA was the least degrading amine out of the seven in this study, reaction (3) and (4) would be the most probable reactions if MDEA follows this mechanism of degradation. If, however, MDEA follows a nonpredictive path as PZ, completely different products could be the result of MDEA

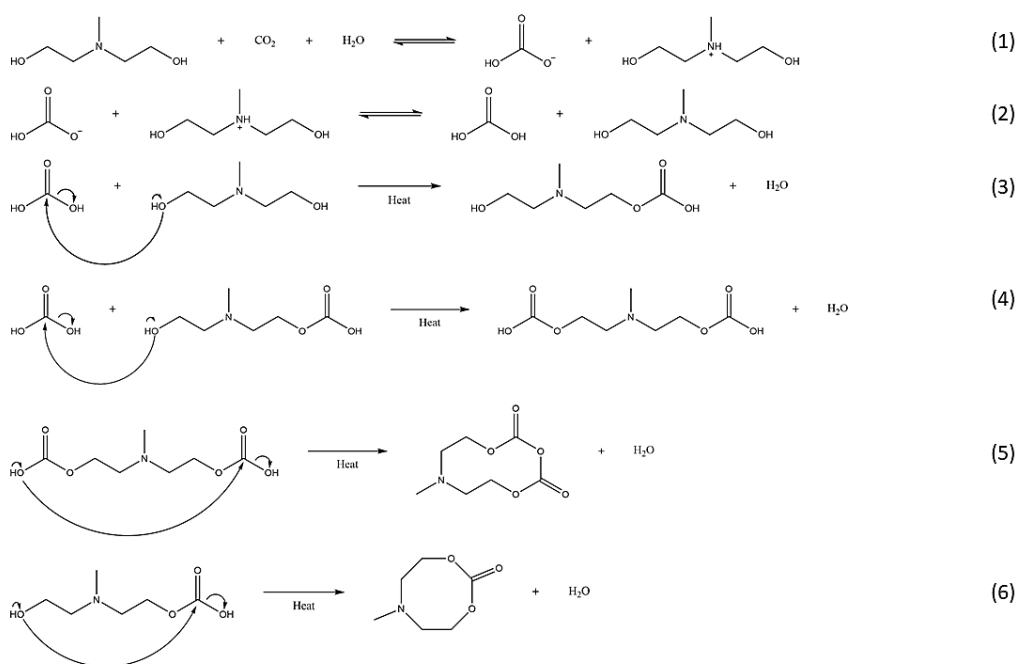


Figure 6-7. Theoretical thermal degradation reactions for MDEA.²⁵

thermal degradation. Regardless, further investigation on the thermal degradation products for MDEA, as well as the other amines, is required.

6.3 Conclusions

The proposed theoretical degradation reaction pathways were proposed based on the results from Huang and Matin et al.^{4,40} The degradation pathways could be tested as they not only provide an understanding of the degradation mechanism of different amines, but also some degradation products could serve as a potential function in different fields.

Each theoretical thermal degradation pathway could serve as a guideline for future investigations on the thermal degradation pathway and kinetics. Instrumental methods, such as IC, could justify the existence of these degradation products and the proposed theoretical pathways. Kinetically, with the proposed reaction pathways, a better correlation between the reaction rate and the change in concentrations could be acquired, which could result in the reactions being optimized to avoid degradation.

Chapter 7. Conclusions and Future Directions

7.1 Summary of Key Results from this Study

It was demonstrated that several factors used in determining the thermal stability of an amine. While, concentration values demonstrated how much of the parent amine was left after degradation, it does not portray the full picture. The solutions required attention as the properties of the solutions would play a major role in whether the amine would be a good candidate to use for CO₂ capture.

¹³C NMR analysis proved to be a useful technique in the approximate determination of the extent of degradation for each sample. By analyzing the number of new, distinguishable, ¹³C peaks, the difference between the peaks demonstrated for the pure amine versus the degraded samples ($\Delta^{13}\text{C}$) provided a ranking from greatest $\Delta^{13}\text{C}$ to least as: EN>2BAE>MEA>1A2P>PZ>MDEA>3APT.

Further analysis of the samples using HPLC provided quantitative information on the concentration of the parent amine after degradation. When only the concentration of each amine was observed, the ranking from highest concentration to least after degradation was found to be: MDEA>PZ>1A2P>3APT>EN>MEA>2BAE. It is reminded that MDEA, PZ, and EN had to have further dilutions, while 2BAE required a more concentrated sample for analysis.

The thermal degradation activation energy of MEA, PZ, and MDEA demonstrated a correlation with the thermal stability of each amine. MEA was shown to have a large thermal degradation activation energy over 4 days, with PZ and MDEA

have a much smaller energy value. However, the thermal degradation activation energy of PZ was demonstrated to be higher than MDEA, supporting the ranking of amines.

Computational modelling on the CO₂ binding to an amine molecule was unable to provide much insight into how the capture of CO₂ could predict the thermal degradation extent of the amine of interest. However, while the ϵ_{bind} and Δ_rG did not provide any correlation with the experimental results, Δ_rH did provide results that matched with the HPLC results. When only the numerical values, and not physical meaning, of Δ_rH for each amine, the ranking from greatest to least was PZ>1A2P>MEA>EN, which agreed with experimental results, PZ being the most thermally stable, and EN being the least.

Combining the information provided by sample observation, ¹³C NMR, and HPLC analysis, an overall thermal stability ranking was produced from highest stability to least, under the conditions set by this experiment as:

MDEA>PZ>1A2P>3APT>MEA>2BAE,EN. A representation of this ranking using the amine structures is demonstrated by Figure 7-1. EN dropped in ranking since, even though it did not have the lowest concentration, EN reached its plateau concentration rapidly and had an uncountable number of ¹³C peaks for each sample for analysis. EN also demonstrated to have tremendous degradation of its degradation products as, at 135°C and 145°C, the sample became a sludge-like solution.

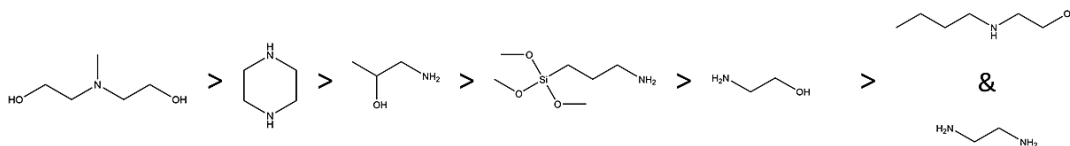


Figure 7-1. Structural representation for the thermal stability of the amines used in this study.²⁵

MEA was low on the thermal stability ranking, and by comparing the structures, interesting results were demonstrated. When the hydroxyl group is removed from MEA and replaced by an amine group (EN), the amine is less stable. Interestingly, when a long carbon chain (2BAE) was attached to the amine group of MEA, the amine was also less stable. 3APT, which had a silane group in place of a hydroxyl group in MEA, the amine was shown to be more stable, however, 3APT and its degraded samples were shown to be highly viscous, making it another poor choice for CO₂ capture. In the case of 1A2P, the amine was found to be much more stable than MEA thermally, which could be attributed to the greater steric hindrance of the amine group. Likewise, MDEA which was a tertiary amine was shown to have the least amount of degradation which could also be attributed to the hindrance about the nitrogen atom. Interestingly, PZ was shown to be second to MDEA in terms of degradation. Considering the nature of EN, it could be easy to assume that PZ would not perform as well as was demonstrated. The ring structure of PZ restricts the flexibility of the molecule, which could help explain the thermal degradation pathways of PZ and the higher thermal stability than MEA and EN.

Thus, amines with more shielding associated with the amine group were demonstrated to have a higher thermal stability. Also, the ring structure of PZ, a

secondary amine, was demonstrated to have a higher thermal stability than the secondary amine 2BAE.

7.2 Future Directions

Using the parameters set by this study, further investigations on the thermal degradation activation energy for each amine could provide more details on the rate of thermal degradation over a set time period. Thus, it is suggested that further research on the kinetics of each amine used in this study be investigated. Along with the kinetics, a degradation mechanism for these amines should be conducted. This would provide a more in-depth study as to why and how the amines degrade. Knowing how the amines degrade would allow a profound understanding of the thermal stability of each amine. With the thermal degradation mechanisms, a more detailed description with the kinetics of each amine could be accomplished, much like that done by Huang with MEA.⁴

To help with the determination of the mechanisms and degradation products, IC, liquid chromatography-mass spectrometry (LC-MS), and two-dimensional (2-D) NMR analysis is suggested. The results from the 2-D NMR could be used alongside of the NMR data collected in this study to help with the identification of degradation products, if distinguishable results are acquired.

Computational models could also be used to evaluate the amines in this that were unable to be calculated in this study. This would determine if $\Delta_r H$ agrees with the other amines in this study, or if it only applied to the ones accomplished. Also,

computational modelling of the degradation pathways could be accomplished to try and determine if a correlation could be made. An investigation into the computational modelling of the degradation system could help describe the energetics of the reaction to provide further understanding on the thermal degradation reactions involved with amines used for PCCC.

References

- (1) GISTEMP Team, 2019: *GISS Surface Temperature Analysis (GISTEMP), version 4*. NASA Goddard Institute for Space Studies. Dataset accessed 2019-12-29 at <https://data.giss.nasa.gov/gistemp/>.
- (2) Lenssen, N., G. Schmidt, J. Hansen, M. Menne, A. Persin, R. Ruedy, and D. Zyss, 2019: Improvements in the GISTEMP uncertainty model. *J. Geophys. Res. Atmos.* **124**, 12, 6307-6326.
- (3) Girard, J. E. *Principles of Environmental Chemistry*, 3rd ed.; Jones & Bartlett Learning: Burlington, 2014.
- (4) Huang, Q., Thermal Degradation of Amines for CO₂ Capture. Ph.D. Dissertation, the University of Kentucky, Lexington, KY, 2015.
- (5) Photo courtesy of Barb Deluise, NOAA, Boulder, Colorado, USA (<http://esrl.noaa.gov/gmd/>).
- (6) Data provided by NOAA ESRL Global Monitoring Division, Boulder, Colorado, USA (<http://esrl.noaa.gov/gmd/>).
- (7) Ed Dlugokencky, NOAA/ESRL (www.esrl.noaa.gov/gmd/ccgg/trends_ch4/).
- (8) Ed Dlugokencky, NOAA/ESRL (www.esrl.noaa.gov/gmd/ccgg/trends_n2o/).
- (9) Ed Dlugokencky, NOAA/ESRL (www.esrl.noaa.gov/gmd/ccgg/trends_sf6/).
- (10) Vitillo, J.; Smit, B.; Gagliardi, L. Introduction: Carbon Capture and Separation. *Chem. Rev.* **2017**, *117*, 9521-9523.
- (11) Stowe, H. M.; Hwang, G. S. Fundamental Understanding of CO₂ Capture and Regeneration in Aqueous Amines from First-Principles Studies: Recent Progress and Remaining Challenges. *Ind. Eng. Chem. Res.* **2017**, *56*, 6887-6899.
- (12) Hwang, S. J.; Kim, J.; Kim, H.; Lee, K. S. Solubility of Carbon Dioxide in Aqueous Solutions of Three Secondary Amines: 2-(Butylamino)ethanol, 2-(Isopropylamino)ethanol, and 2-(Ethylamino)ethanol Secondary Alkanolamine Solutions. *J. Chem. Eng. Data* **2017**, *62*, 2428-2435.
- (13) Lv, B.; Guo, B.; Zhou, Z.; Jing, G. Mechanisms of CO₂ Capture into Monoethanolamine Solution with Different CO₂ Loading during the Absorption/Desorption Processes. *Environ. Sci. Technol.* **2015**, *49*, 10728-10735.
- (14) Conway, W.; Beyad, Y.; Maeder, M.; Burns, R.; Feron, P.; Puxty, G. CO₂ Absorption into Aqueous Solutions Containing 3-Piperidinemethanol: CO₂ Mass Transfer, Stopped-Flow Kinetics, ¹H/¹³C NMR, and Vapor-Liquid Equilibrium Investigations. *Ind. Eng. Chem. Res.* **2014**, *53*, 16715-16724.
- (15) Liu, F.; Jing, G.; Zhou, X.; Lv, B.; Zhou, Z. Performance and Mechanisms of Triethylene Tetramine (TETA) and 2-Amino-2-methyl-1propanol (AMP) in Aqueous and

- Nonaqueous Solutions for CO₂ Capture. *ACS Sustainable Chem. Eng.* **2018**, *6*, 1352-1361.
- (16) Pieter Tans and Kirk Thoning, NOAA Earth System Research Laboratory, Boulder, Colorado September 2008. Updated December 2016; March 2018.
- (17) Oyenekan, B. A.; Rochelle, G. T. Energy Performance of Stripper Configurations for CO₂ Capture by Aqueous Amines. *Ind. Eng. Chem. Res.* **2006**, *45*, 2457-2464.
- (18) Heischkamp, E.; Varlik, M.; Korkmaz, Ö.; Oeljeklaus, G.; Görner, K. Analysis of Operating Conditions of a Flue Gas Scrubbing Process for CO₂ Separation in a Coal-Fired Power Plant. *Energy Procedia* **2011**, *4*, 1377-1384.
- (19) Rochelle, G. T. Amine Scrubbing for CO₂ Capture. *Science* **2009**, *325*, 1652-1654.
- (20) Carey, F. A.; Giuliano, R. M. *Organic Chemistry*, 9th ed.; McGraw-Hill: New York, 2014.
- (21) Amann, J.-M. G.; Bouallou, C. Kinetics of the Absorption of CO₂ in Aqueous Solutions of N-Methyldiethanolamine + Triethylene Tetramine. *Ind. Eng. Chem. Res.* **2009**, *48*, 3761-3770.
- (22) Hsu, C. H.; Chu, H.; Cho, C. M. Absorption and Reaction Kinetics of Amines and Ammonia Solutions with Carbon Dioxide in Flue Gas. *J. Air & Waste Manage. Assoc.* **2003**, *53*, 246-252.
- (23) Bonenfant, D.; Mimeault, M.; Hausler, R. Determination of the Structural Features of Distinct Amines Important for the Absorption of CO₂ and Regeneration in Aqueous Solution. *Ind. Eng. Chem. Res.* **2003**, *42*, 3179-3184.
- (24) Richner, G.; Puxty, G. Assessing the Chemical Speciation during CO₂ Absorption by Aqueous Amines Using *in Situ* FTIR. *Ind. Eng. Chem. Res.* **2012**, *51*, 14317-14324.
- (25) Chemdraw, version 18.2; PerkinElmer; 1998-2019.
- (26) Hwang, G. S.; Stowe, H. M.; Paek, E.; Manogaran, D. Reaction Mechanisms of Aqueous Monoethanolamine with Carbon Dioxide: a Combined Quantum Chemical and Molecular Dynamics Study. *Phys. Chem. Chem. Phys.* **2015**, *17*, 831-839.
- (27) Mukherjee, S.; Bandyopadhyay, S. S.; Samanta, A. N. Kinetic Study of CO₂ Absorption in Aqueous Benzylamine Solvent Using a Stirred Cell Reaction Calorimeter. *Energy Fuels* **2018**, *32*, 3668-3680.
- (28) Matsuzaki, Y.; Yamada, H.; Chowdhury, F. A.; Higashii, T.; Onoda, M. Ab Initio Study of CO₂ Capture Mechanisms in Aqueous Monoethanolamine: Reaction Pathways for the Direct Interconversion of Carbamate and Bicarbonate. *J. Phys. Chem. A* **2013**, *117*, 9274-9281.
- (29) Perinu, C.; Arstad, B.; Bouzga, A. M.; Jens, K. J. ¹³C and ¹⁵N NMR Characterization of Amine Reactivity and Solvent Effects in CO₂ Capture. *J. Phys. Chem. B* **2014**, *118*, 10167-10174.

- (30) Puxty, G.; Rowland, R.; Allport, A.; Yang, Q.; Bown, M.; Burns, R.; Maeder, M.; Attalla, M. Carbon Dioxide Postcombustion Capture: A Novel Screening Study of the Carbon Dioxide Absorption Performance of 76 Amines. *Environ. Sci. Technol.* **2009**, *43*, 6427-6433.
- (31) Huertas, J. I.; Gomez, M. D.; Giraldo, N.; Garzón, J. CO₂ Absorbing Capacity of MEA. *J. Chem.* **2015**.
- (32) Yamada, H.; Matsuzaki, Y.; Higashii, T.; Kazama, S. Density Functional Theory Study on Carbon Dioxide Absorption into Aqueous Solutions of 2-Amino-2-methyl-1-propanol Using a Continuum Solvation Model. *J. Phys. Chem. A* **2011**, *115*, 3079-3086.
- (33) Chowdhury, F. A.; Yamada, H.; Higashii, T.; Goto, K.; Onoda, M. CO₂ Capture by Tertiary Amine Absorbents: A Performance Comparison Study. *Ind. Eng. Chem. Res.* **2013**, *52*, 8323-8331.
- (34) Gao, H.; Wu, Z.; Liu, H.; Luo, X.; Liang, Z. Experimental Studies on the Effect of Tertiary Amine Promoters in Aqueous Monoethanolamine (MEA) Solutions on the Absorption/Stripping Performances in Post-combustion CO₂ Capture. *Energy Fuels* **2017**, *31*, 13883-13891.
- (35) Zhang, X.; Zhang, C.-F.; Liu, Y. Kinetics of Absorption of CO₂ into Aqueous Solution of MDEA Blended with DEA. *Ind. Eng. Chem. Res.* **2002**, *41*, 1135-1141.
- (36) Zhang, Y.; Chen, C.-C. Thermodynamic Modeling for CO₂ Absorption in Aqueous MDEA Solution with Electrolyte NRTL Model. *Ind. Eng. Chem. Res.* **2011**, *50*, 163-175.
- (37) Huang, Q.; Thompson, J.; Bhatnagar, S.; Chandan, P.; Remias, J.; Selegue, J. P.; Liu, K. Impact of Flue Gas Contaminants on Monoethanolamine Thermal Degradation. *Ind. Eng. Chem. Res.* **2014**, *53*, 553-563.
- (38) Freeman, S. A.; Rochelle, G. T. Thermal Degradation of Aqueous Piperazine for CO₂ Capture: 1. Effect of Process Conditions and Comparison of Thermal Stability of CO₂ Capture Amines. *Ind. Eng. Chem. Res.* **2012**, *51*, 7719-7725.
- (39) Freeman, S. A.; Rochelle, G. T. Thermal Degradation of Aqueous Piperazine for CO₂ Capture: 2. Product Types and Generation Rates. *Ind. Eng. Chem. Res.* **2012**, *51*, 7726-7735.
- (40) Matin, N. S.; Thompson, J.; Abad, K.; Bhatnagar, S.; Liu, K. Thermal Degradation Rate and Kinetic Modeling of CO₂-Loaded Amine Solvent Blends of 2-Amino-2-methyl-1-propanol and 1-Amino-2-propanol. *Ind. Eng. Chem. Res.* **2019**, A-H.
- (41) Perry, R. J.; Rainka, M. P.; Doherty, M. D.; Wood, B. R.; Namjoshi, O.; Hatchell, D.; Liu, H.; Rochelle, G. T. Thermal Degradation of Aminosilicone Carbamates. *Energy Fuels* **2016**, *30*, 10671-10678.
- (42) Ge, X.; Shaw, S. L.; Zhang, Q. Toward Understanding Amines and Their Degradation Products from Postcombustion CO₂ Capture Processes with Aerosol Mass Spectrometry. *Environ. Sci. Technol.* **2014**, *48*, 5066-5075.

- (43) Silverstein, R. M.; Webster, F. X.; Kiemle, D. J.; Bryce, D. L. *Spectrometric Identification of Organic Compounds*, 8th edition; John Wiley & Sons, Inc.: Hoboken, 2015.
- (44) Harris, D. C. *Quantitative Chemical Analysis*, 9th edition; W. H. Freeman and Company: New York, 2016.
- (45) Avogadro: an open-source molecular builder and visualization tool. Version 1.2.0. <http://Avogadro.cc/>.
- (46) Rappé, A. K.; Casewit, C. J.; Colwell, K. S.; Goddard III, W. A.; Skiff, W. M. UFF, a Full Periodic Table Force Field for Molecular Mechanics and Molecular Dynamics Simulations. *J. Am. Chem. Soc.* **1992**, *114*, 10024-10035.
- (47) Yamada, H. Comparison of Solvation Effects on CO₂ Capture with Aqueous Amine Solutions and Amine-Functionalized Ionic Liquids. *J. Phys. Chem. B* **2016**, *120*, 10563-10568.
- (48) Gaussian 09, Revision B.01; Gaussian, Inc.: Wallingford, CT, 2016.
- (49) Cramer, C. J. *Essentials of Computational Chemistry Theories and Models*, 2nd edition, John Wiley & Sons Ltd: West Sussex, 2004.
- (50) Ochterski, J. W. *Thermochemistry in Gaussian*; Gaussian, Inc.: Wallingford, CT, 2000; pp 1-19.
- (51) Ball, D. W. *Physical Chemistry*, 2nd ed.; Cengage Learning: Stamford, 2015.

APPENDICES

Appendix A. NMR Spectra for MEA

Figure A-1 through Figure A-3 demonstrate the DEPT-90, DEPT-135, and ^{15}N NOE NMR spectra for MEA and the degraded MEA samples, respectively.

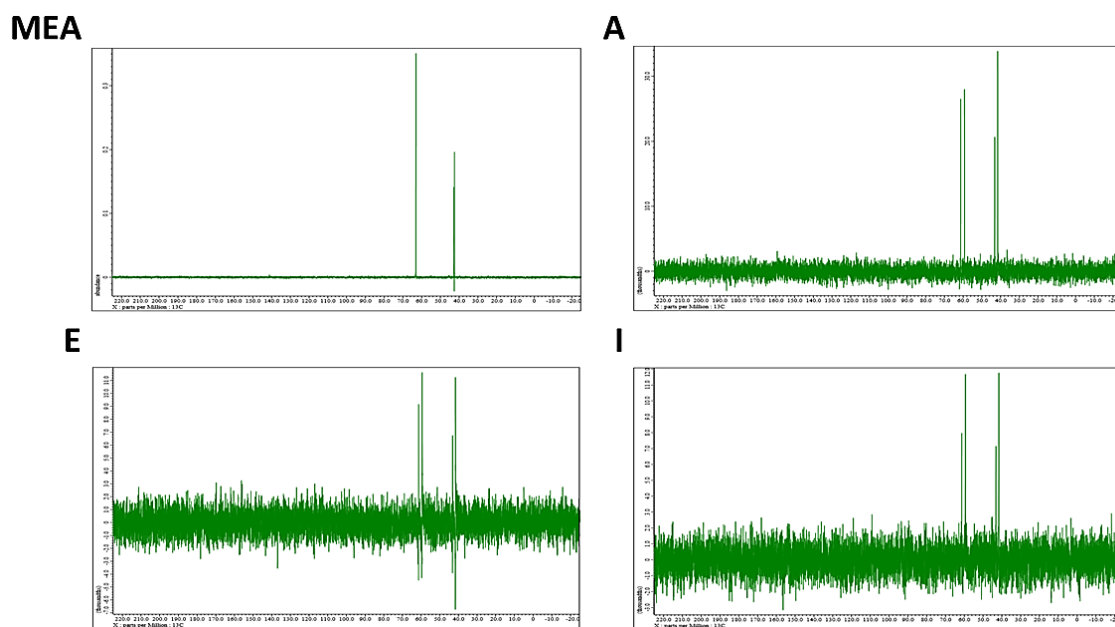


Figure A-1. DEPT-90 NMR data acquired for MEA and its degraded samples. MEA is labelled, and the letters indicate the degraded sample.

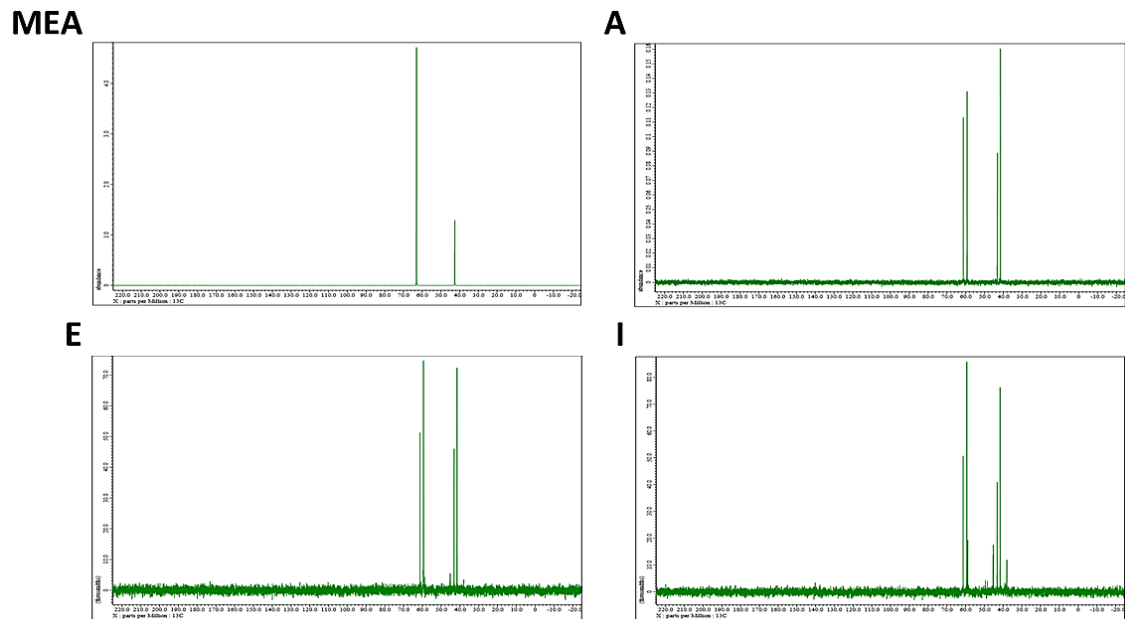


Figure A-2. DEPT-135 NMR data acquired for MEA and its degraded samples. MEA is labelled, and the letters indicate the degraded sample.

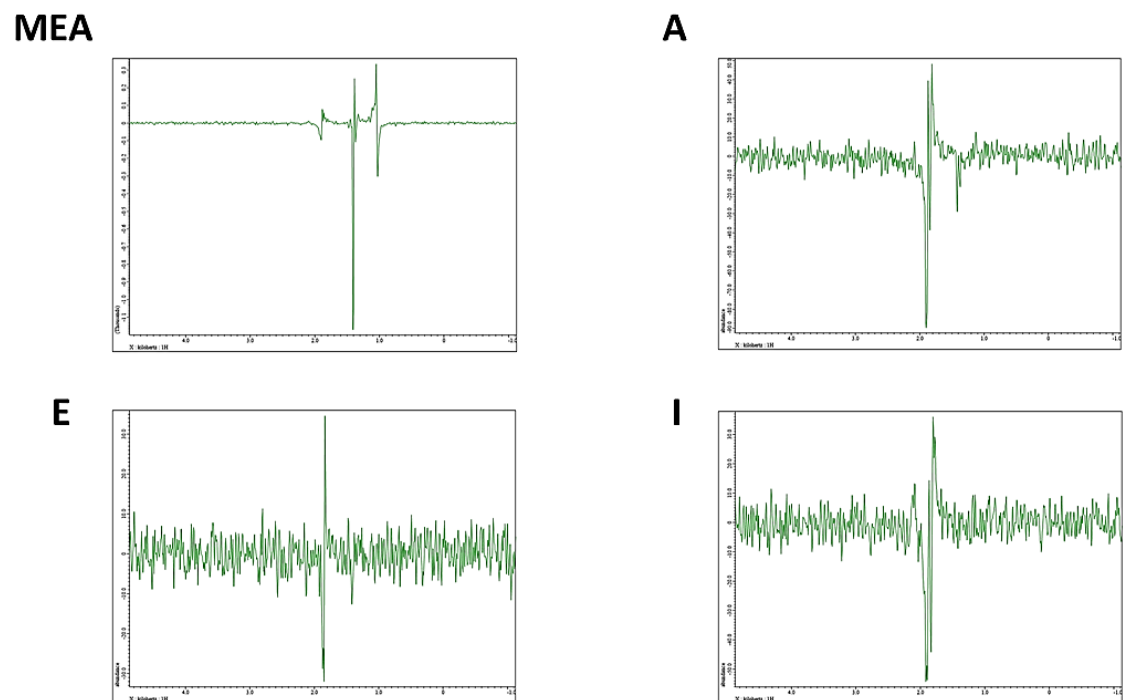
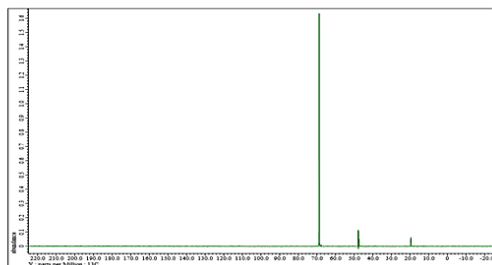


Figure A-3. ^{15}N NOE NMR data acquired for MEA and its degraded samples. MEA is labelled, and the letters indicate the degraded sample.

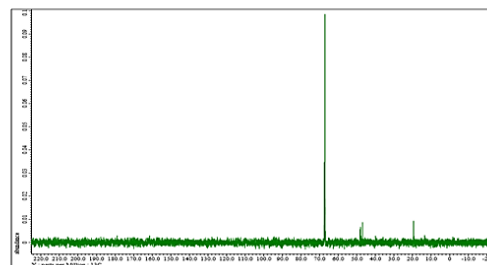
Appendix B. NMR Spectra for 1A2P

Figure B-1 through B-3 demonstrate the DEPT-90, DEPT-135, and ^{15}N NOE NMR spectra for 1A2P and the degraded 1A2P samples, respectively.

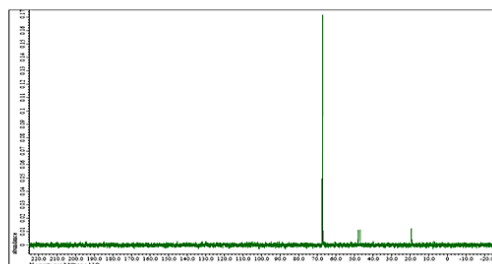
1A2P



B



F



L

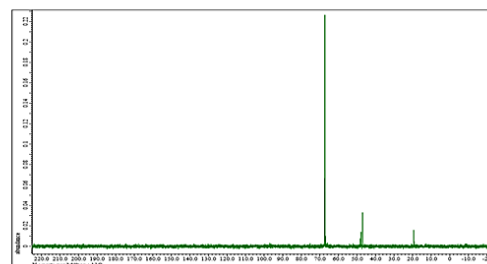
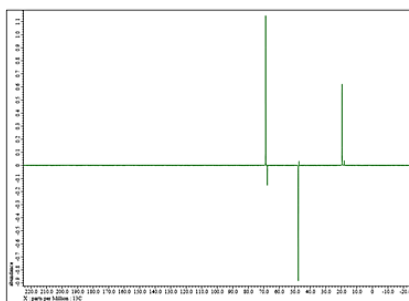
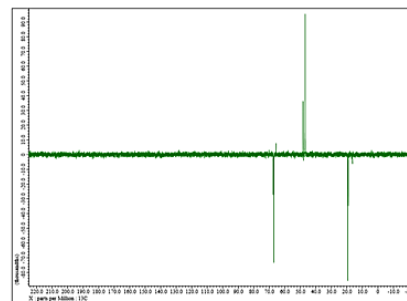


Figure B-1. DEPT-90 NMR data acquired for 1A2P and its degraded samples. 1A2P is labelled, and the letters indicate the degraded sample.

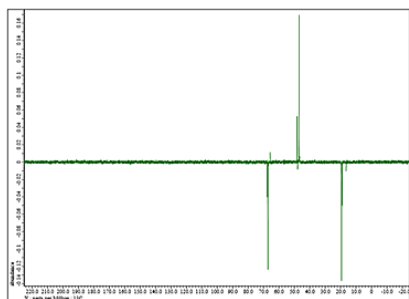
1A2P



B



F



L

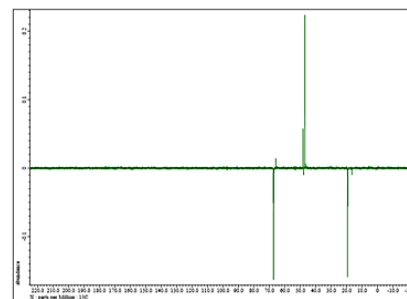
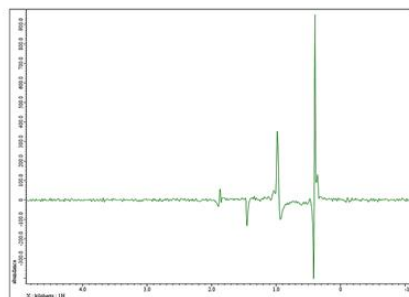
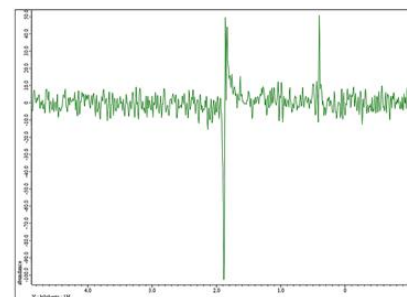


Figure B-2. DEPT-135 NMR data acquired for 1A2P and its degraded samples. 1A2P is labelled, and the letters indicate the degraded sample.

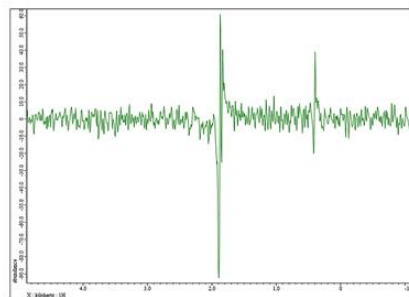
1A2P



B



F



L

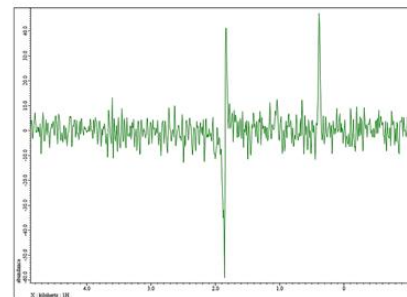


Figure B-3. ^{15}N NOE NMR data acquired for 1A2P and its degraded samples. 1A2P is labelled, and the letters indicate the degraded sample.

Appendix C. NMR Spectra for EN

Figure C-1 through C-3 demonstrate the DEPT-90, DEPT-135, and ^{15}N NOE NMR spectra for EN and the degraded EN samples, respectively.

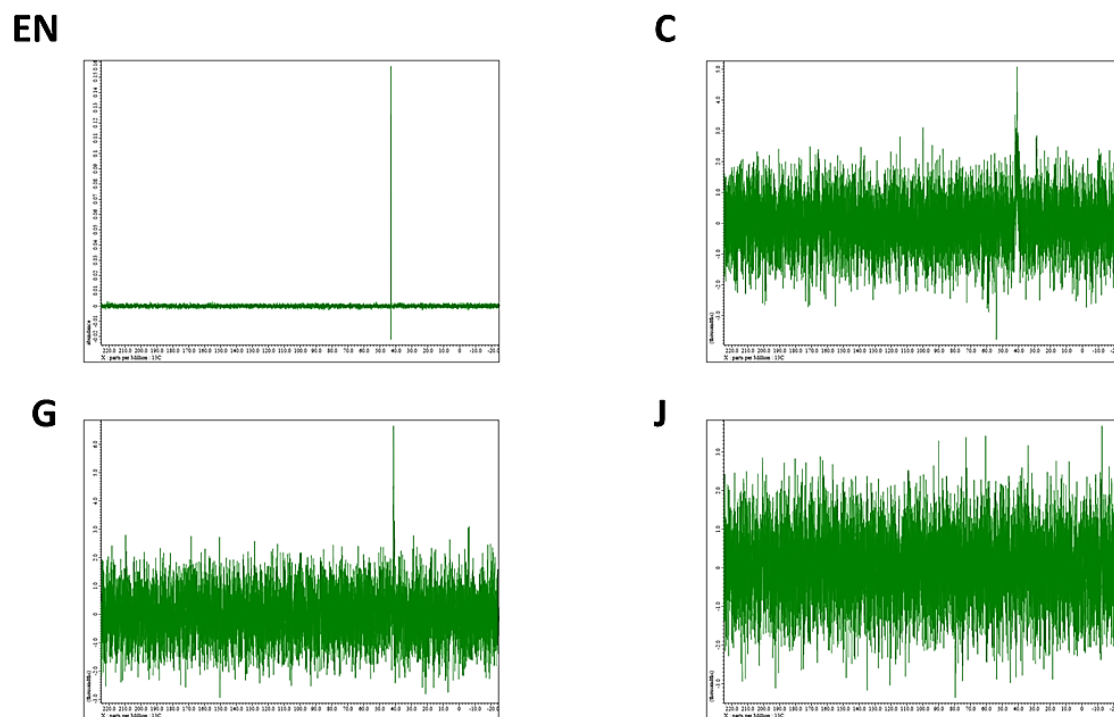
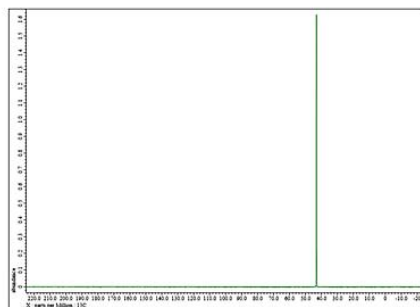
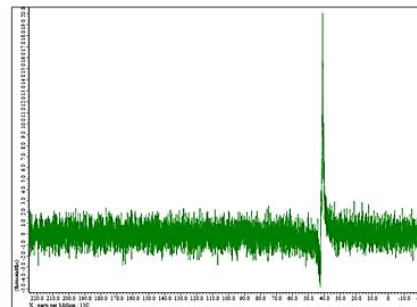


Figure C-1. DEPT-90 NMR data acquired for EN and its degraded samples. EN is labelled, and the letters indicate the degraded sample.

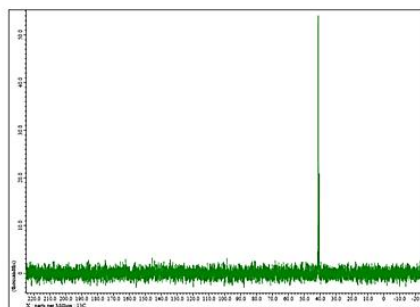
EN



C



G



J

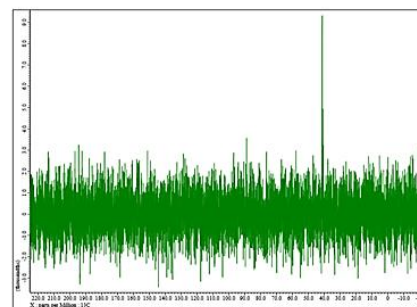
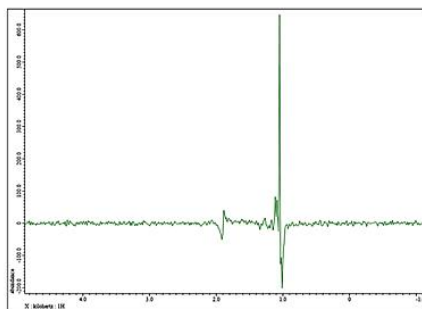
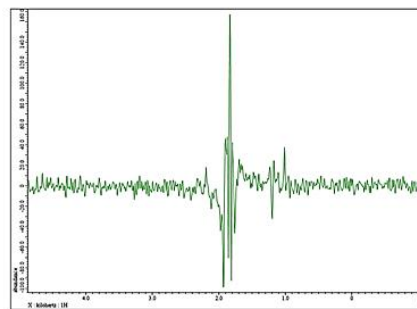


Figure C-2. DEPT-135 NMR data acquired for EN and its degraded samples. EN is labelled, and the letters indicate the degraded sample.

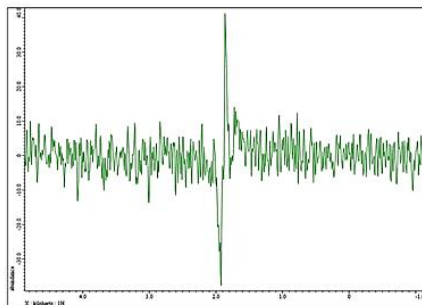
EN



C



G



J

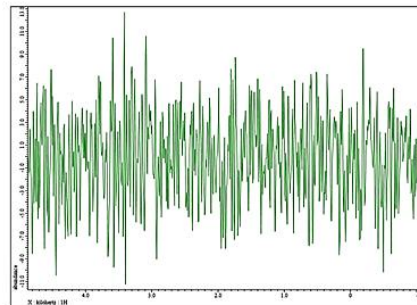


Figure C-3. ^{15}N NOE NMR data acquired for EN and its degraded samples. EN is labelled, and the letters indicate the degraded sample.

Appendix D. NMR Spectra for 3APT

Figure D-1 through D-3 demonstrate the DEPT-90, DEPT-135, and ^{15}N NOE NMR spectra for 3APT and the degraded 3APT samples, respectively.

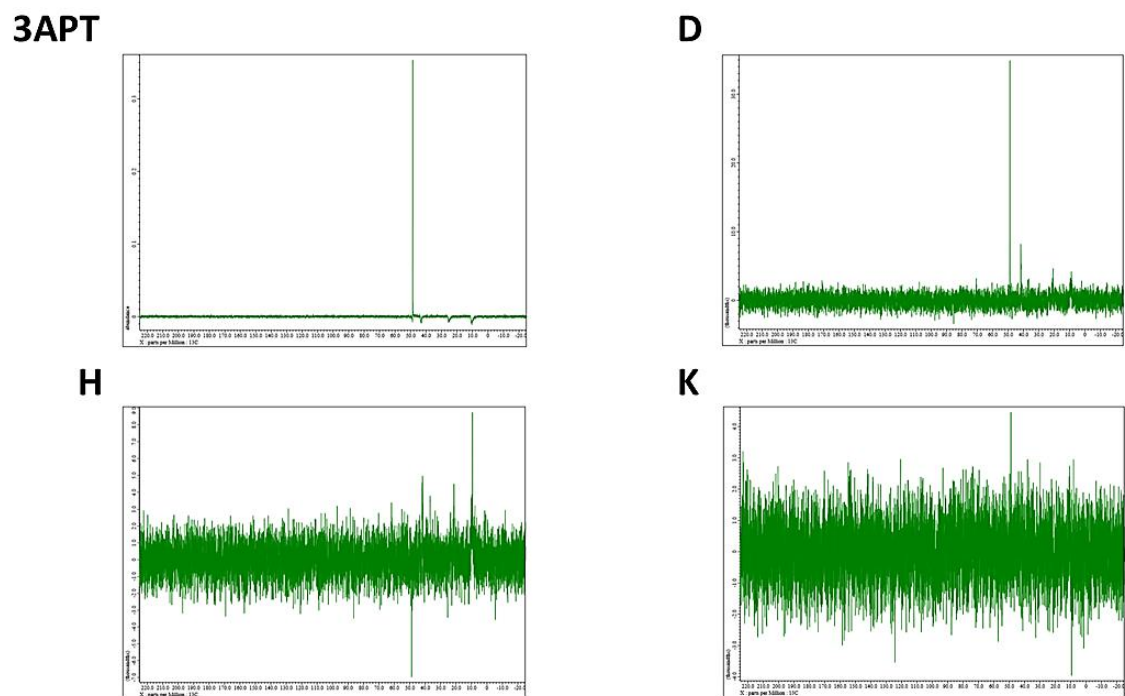
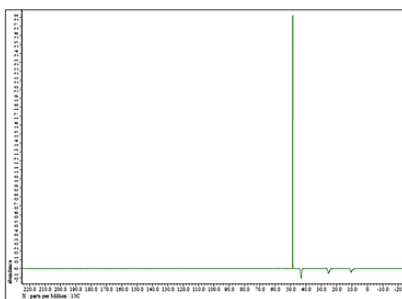
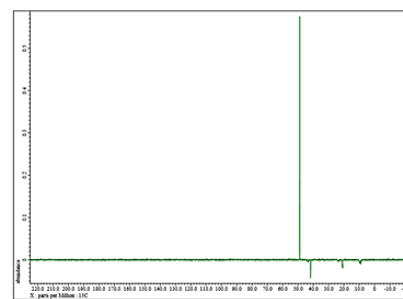


Figure D-1. DEPT-90 NMR data acquired for 3APT and its degraded samples. 3APT is labelled, and the letters indicate the degraded sample.

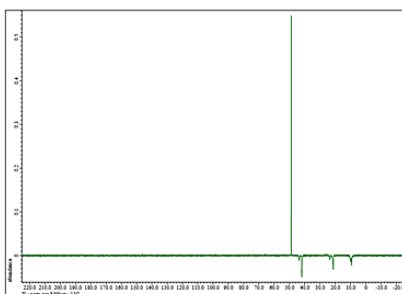
3APT



D



H



K

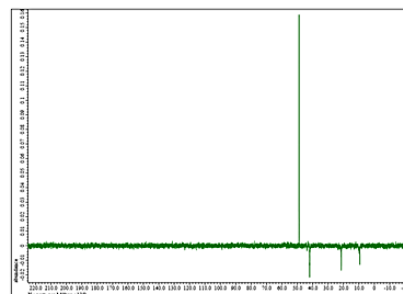
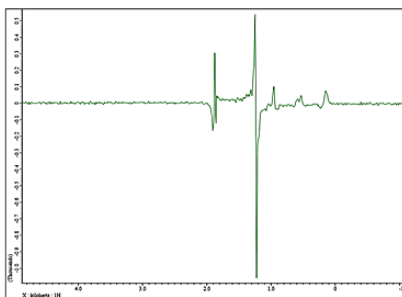
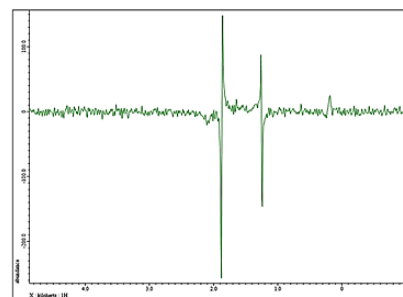


Figure D-2. DEPT-135 NMR data acquired for 3APT and its degraded samples. 3APT is labelled, and the letters indicate the degraded sample.

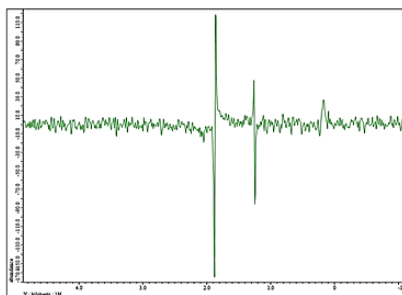
3APT



D



H



K

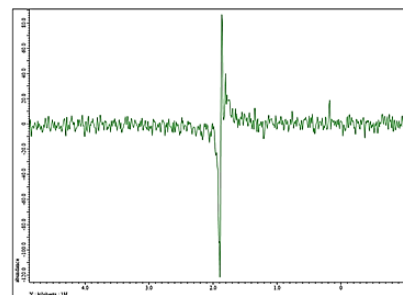


Figure D-3. ^{15}N NOE NMR data acquired for 3APT and its degraded samples. 3APT is labelled, and the letters indicate the degraded sample.

Appendix E. NMR Spectra for 2BAE

Figure E-1 through E-3 demonstrate the DEPT-90, DEPT-135, and ^{15}N NOE NMR spectra for 2BAE and the degraded 2BAE samples, respectively.

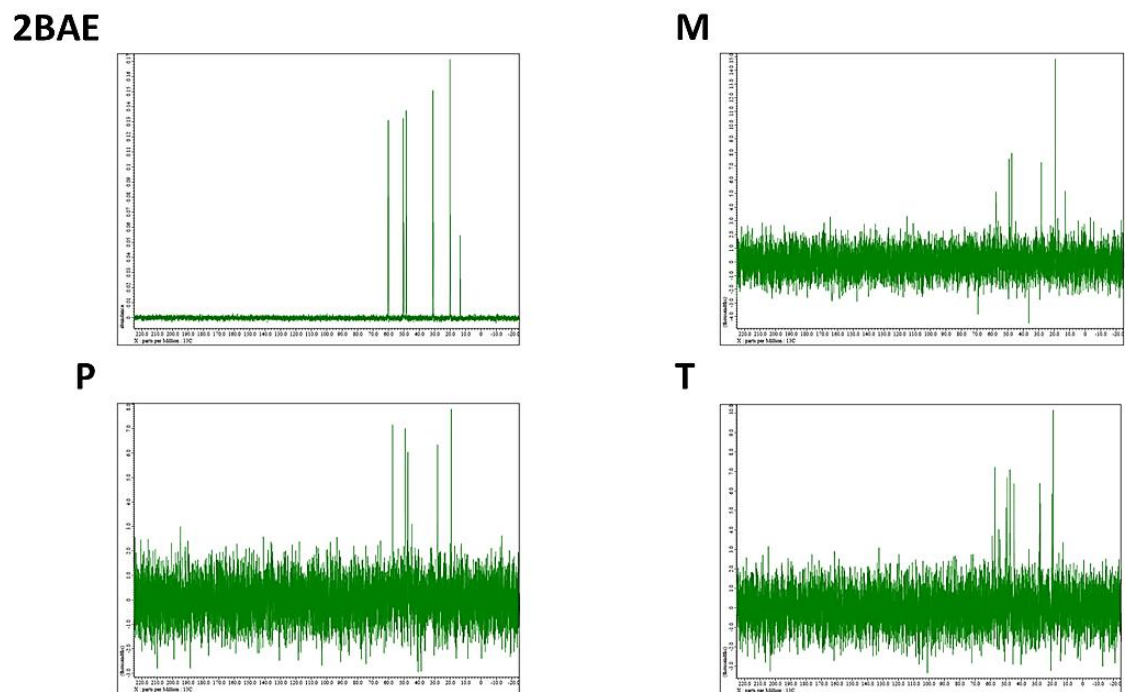
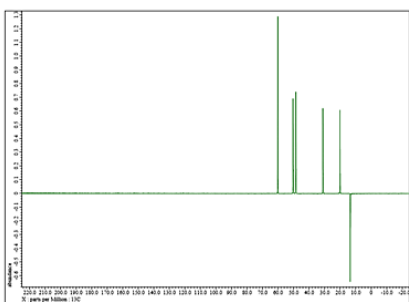
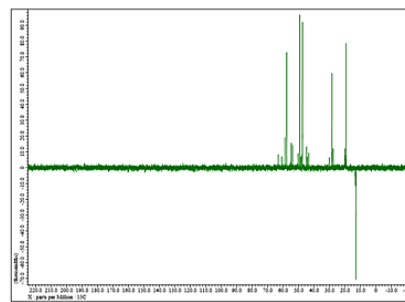


Figure E-1. DEPT-90 NMR data acquired for 2BAE and its degraded samples. 2BAE is labelled, and the letters indicate the degraded sample.

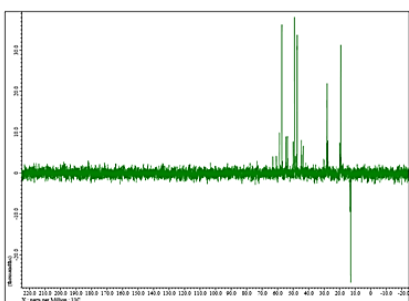
2BAE



M



P



T

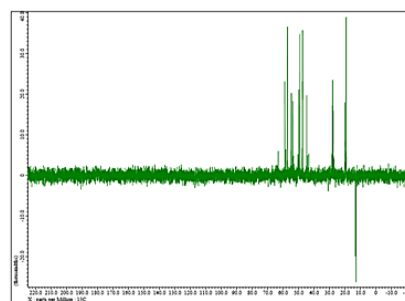
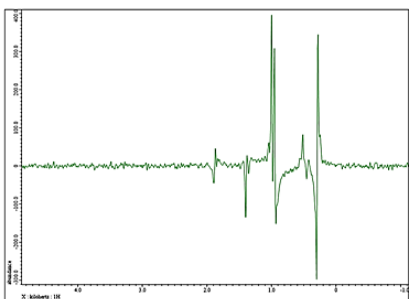
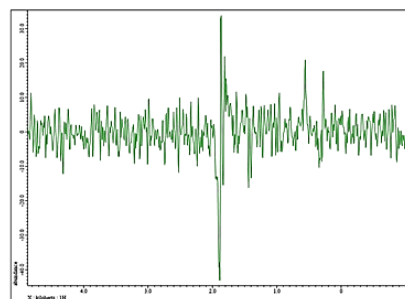


Figure E-2. DEPT-135 NMR data acquired for 2BAE and its degraded samples. 2BAE is labelled, and the letters indicate the degraded sample.

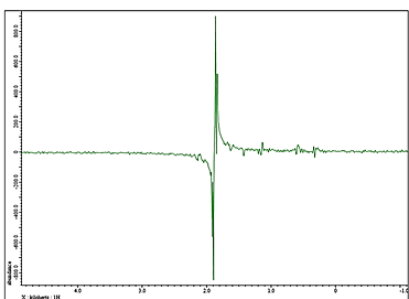
2BAE



M



P



T

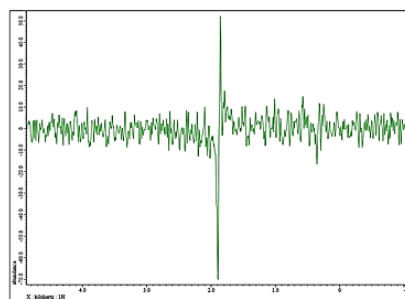


Figure E-3. ^{15}N NOE NMR data acquired for 2BAE and its degraded samples. 2BAE is labelled, and the letters indicate the degraded sample.

Appendix F. NMR Spectra for MDEA

Figure F-1 through F-3 demonstrate the DEPT-90, DEPT-135, and ^{15}N NOE NMR spectra for MDEA and the degraded MDEA samples, respectively.

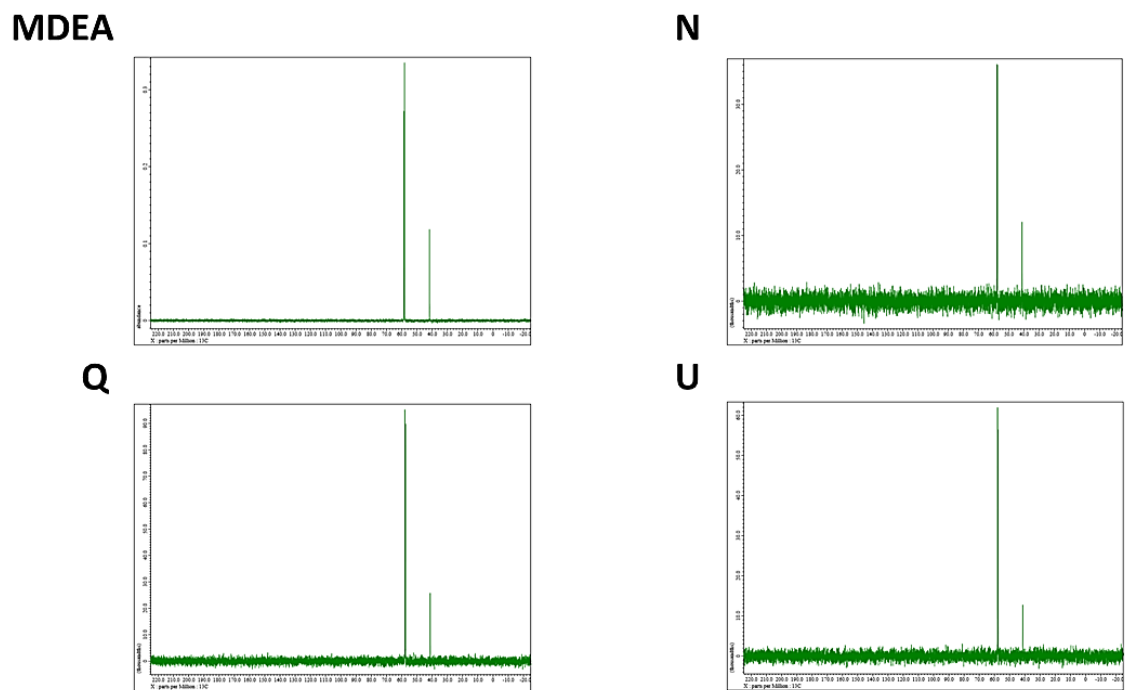
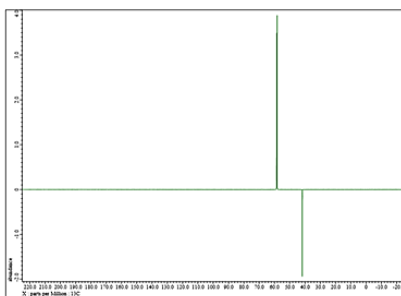
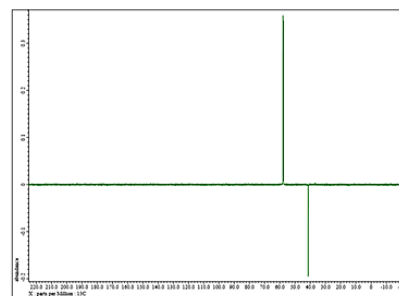


Figure F-1. DEPT-90 NMR data acquired for MDEA and its degraded samples. MDEA is labelled, and the letters indicate the degraded sample.

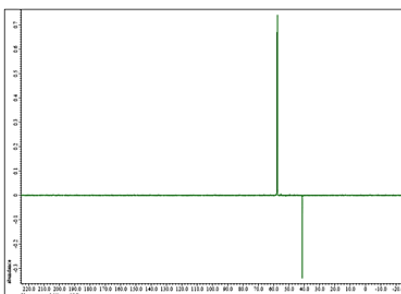
MDEA



N



Q



U

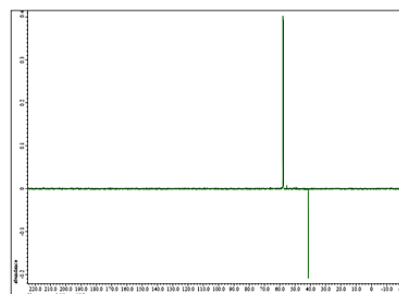
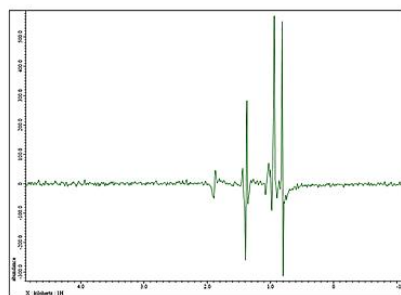
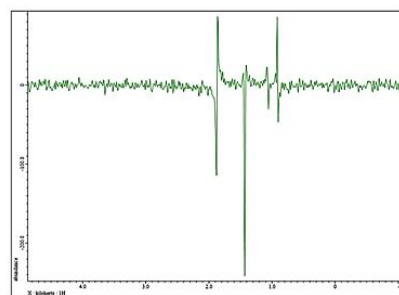


Figure F-2. DEPT-135 NMR data acquired for MDEA and its degraded samples. MDEA is labelled, and the letters indicate the degraded sample.

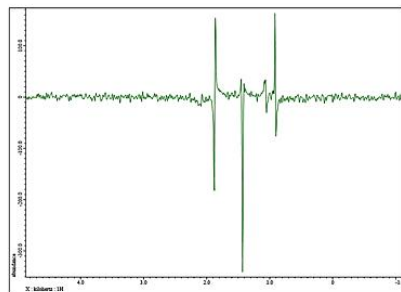
MDEA



N



Q



U

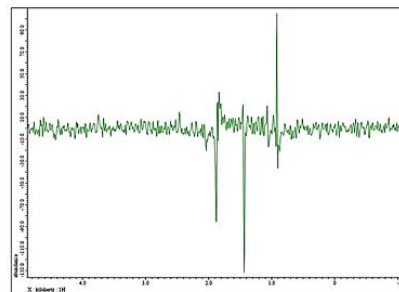


Figure F-3. ^{15}N NOE NMR data acquired for MDEA and its degraded samples. MDEA is labelled, and the letters indicate the degraded sample.

Appendix G. NMR Spectra for PZ

Figure G-1 through G-3 demonstrate the DEPT-90, DEPT-135, and ^{15}N NOE NMR spectra for PZ and the degraded PZ samples, respectively.

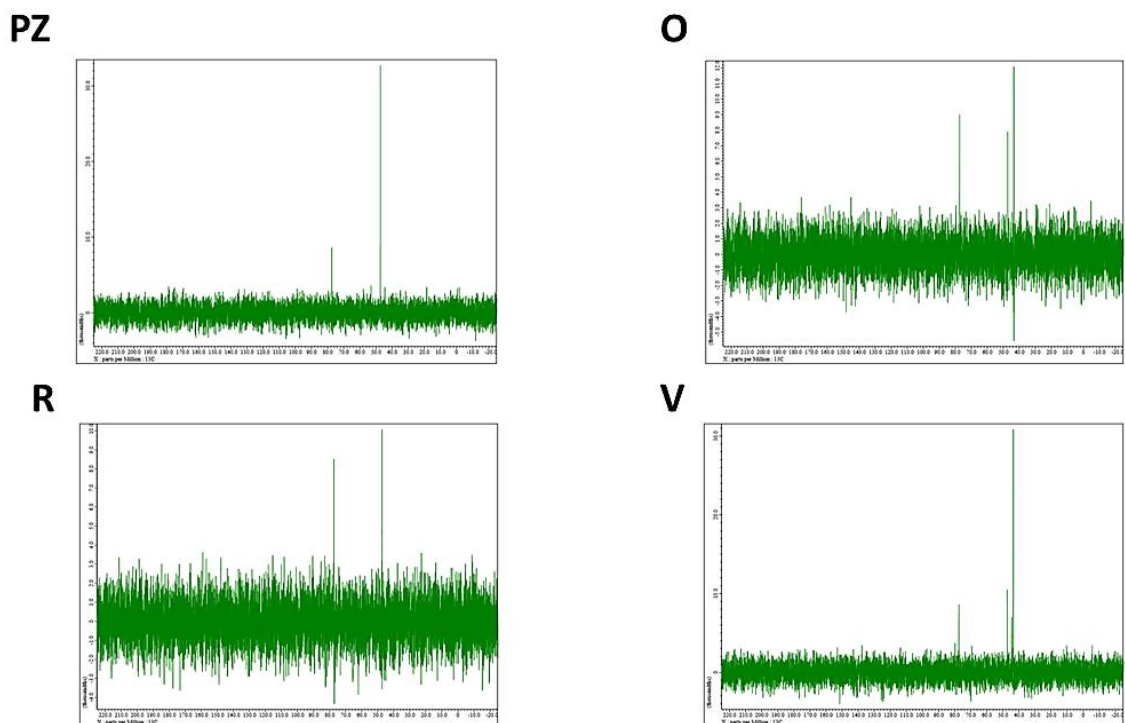
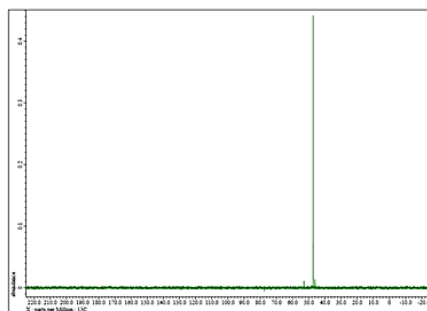
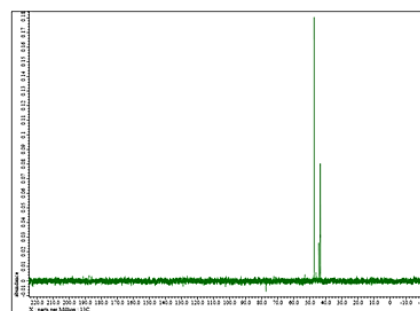


Figure G-1. DEPT-90 NMR data acquired for PZ and its degraded samples. PZ is labelled, and the letters indicate the degraded sample.

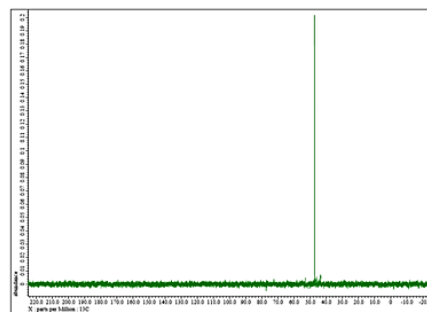
PZ



O



R



V

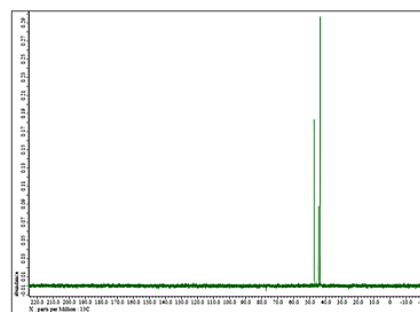
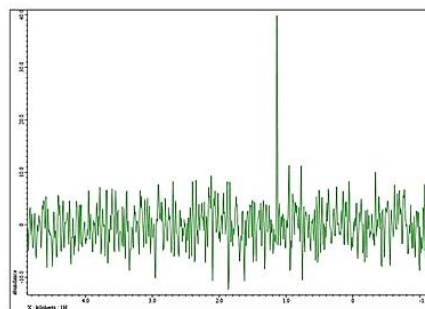
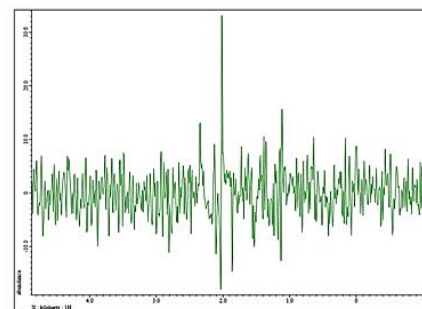


Figure G-2. DEPT-135 NMR data acquired for PZ and its degraded samples. PZ is labelled, and the letters indicate the degraded sample.

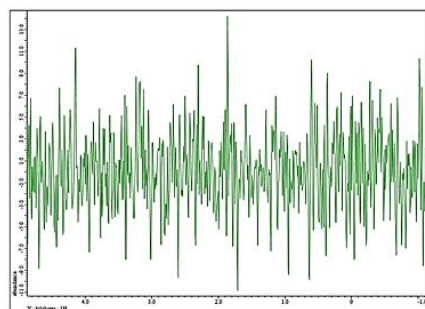
PZ



O



R



V

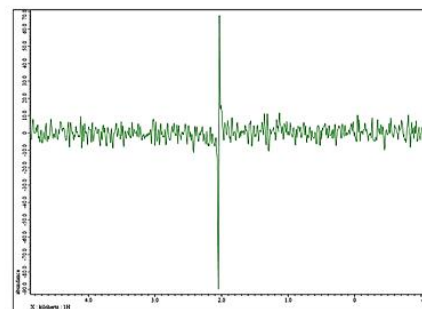


Figure G-3. DEPT-135 NMR data acquired for PZ and its degraded samples. PZ is labelled, and the letters indicate the degraded sample.